Annual Report
Jahresbericht

2019

Walther–Meißner–Institut
für Tieftemperaturforschung

Bayerische Akademie der Wissenschaften

Contact:

Prof. Dr. Rudolf Gross
Walther–Meißner–Institut für Tieftemperaturforschung
Bayerische Akademie der Wissenschaften
and
Lehrstuhl für Technische Physik – E23
Technische Universität München

Address:

Walther–Meißner–Str. 8
D - 85748 Garching
GERMANY

Phone: +49 – (0)89 289 14201
Fax: +49 – (0)89 289 14206
e–mail: Rudolf.Gross@wmi.badw.de
www: http://www.wmi.badw.de

Secretary's Office and Administration:

Emel Dönertas
Phone: +49 – (0)89 289 14202
Fax: +49 – (0)89 289 14206
e–mail: Emel.Doenertas@wmi.badw.de
Sekretariat@wmi.badw.de

Andrea Hamitaga
Phone: +49 – (0)89 289 14205
Fax: +49 – (0)89 289 14206
e–mail: Andrea.Hamitaga@wmi.badw.de
Verwaltung@wmi.badw.de

Preface

Dear colleagues, friends, partners, and alumni of the Walther-Meißner-Institute (WMI),

an eventful and very successful year 2019 came to an end. Our ***Annual Report 2019*** provides you with a summary of the activities at the Walther-Meißner-Institute during the year 2019. It also contains relevant statistical data, an overview of our teaching and public engagement activities, and information on recent developments in infrastructure and experimental facilities.

The year 2019 was characterized by starting up important long-term projects, after we have been highly successful with proposals in both Germany's ***«Excellence Strategy»*** and the ***«European Quantum Flagship»*** in 2018. First, WMI is a key partner of the Munich Universities in the new Cluster of Excellence ***«Munich Center for Quantum Science and Technology» (MCQST)***, which started in January 2019 (see report on page 17 – 21). Together with Immanuel Bloch and Ignacio Circac, Rudolf Gross of WMI is one of the spokespersons of MCQST. Second, WMI coordinates the EU Quantum Flagship project ***«Quantum Microwave Communication and Sensing» (QMiCS)***, which started in October 2018 (see report on page 22 – 23). QMiCS is a project in the basic science pillar of the «European Quantum Flagship» and is coordinated by Frank Deppe of WMI. The strong involvement of WMI in MCQST and QMiCS is a natural continuation of its strong research focus on solid-state quantum systems and its active participation in several projects related to quantum science & technology (see page 25). The new projects will give the research efforts of WMI a further boost.

The technological infrastructure of WMI could be considerably improved via third party funding also in 2019. In particular, we could acquire substantial microwave equipment and set up new optical cryostats. Moreover, a new UHV thin film deposition system for qubit fabrication and a dry dilution refrigerator for the study of quantum systems already have been ordered and will be delivered in 2020. To this end, we gratefully acknowledge financial support from the German Research Foundation, the Bavarian Ministry for Science and Arts, the BMBF and the EU.

In 2019, we finally could reap the benefits of the major reconstruction measures with a total budget of more than 6 million euro, which fortunately could be completed in 2019, although with long and nerve-shattering delays (see page 13). Despite some unfavorable circumstances, our research activities have been successfully continued and resulted in a number of high level publications (see page 91). The high impact of our research work is documented by more than 2 000 citations of WMI publications in 2019 (ISI Web of Science) and a large number of invited conference, colloquium and seminar talks (see page 113). As in previous years, WMI was active in organizing symposia, workshops and conferences to increase its international visibility (see page 105). I would like to thank the scientific, technical and administrative staff of WMI for its outstanding performance! Only due to the strong commitment and persistence of everybody our ambitious research programs could be implemented.

An important key to our success is the training of students and the recruitment of outstanding, scientifically independent group leaders with complementary research interests and technical expertise. This process is monitored by the Scientific Advisory Board of WMI which has a strong commitment to support and promote young scientists in their career. Attracting the best students and young scientists is only possible due to the extensive teaching efforts of the WMI scientists as well as the inspiring and collaborative atmosphere offered by WMI to young talents. Of course, we are committed to diversity and the promotion of women and to mutual respect regardless of nationality, skin color, religion and personal life plans. In 2019, 12 bachelor, 9 master and 3 PhD theses were completed at WMI, while 10 master and 18 PhD students as well as 3 habilitation candidates are still ongoing with their work (see page 95).

Successful recruitment is also of key relevance at the director's level. Fortunately, the appointment procedure for a new WMI director could be finished in 2019 with great success. The premature appointment of a new director not only guarantees sufficient temporal overlap with the present director of WMI, but also was used to change the governance structure of WMI. Due to the strong increase of staff, number and breadth of research projects, and administrative tasks over the past two decades, the present director proposed to change the governance structure of WMI from a single director to a board of up to three directors headed by a managing director. This change of governance structure has been supported by the Scientific Advisory Board of WMI and the decision-making bodies of BAdW. Meanwhile, it is implemented in the new rules of order of WMI valid since 18th October 2019.

Finally, I would like to express my deep thanks and gratitude to all colleagues, guests, students, postdocs and cooperating partners, who contributed to our research and teaching activities within the past year, and last but not least to all our friends and sponsors for their interest, trust and continuous support. I hope that our Annual Report 2019 inspires your interest in WMI.

Garching, December 2019

Rudolf Gross

Contents

The Walther–Meißner–Institute

General Information

The ***Walther-Meißner-Institute for Low Temperature Research (WMI)*** was originally operated by the Commission for Low Temperature Research of the ***Bavarian Academy of Sciences and Humanities (BAdW)***. Between 2013 and 2015, the Bavarian Academy of Sciences and Humanities with its more than 300 employees was reorganized. With the passing of the new statutes in October 2015, the 36 Commissions (Research Groups) of the Academy — they were originally set up in order to carry out long-term projects, which are too ambitious for the lifetime or capacity of any single researcher, or which require the collaboration of specialists in various disciplines — were abolished. The research program of BAdW is now implemented in Academy Institutes (such as the Walther-Meißner-Institute or the Leibniz Supercomputing Center) and Academy Projects. The Academy Institutes and Projects are managed by the Institute and Project Committees and supervised by the Institute and Project Advisory Boards, respectively. In this way a clear separation between the managing bodies of the institutes/projects (responsible for the implementation of the research programs) and the corresponding supervisory bodies (responsible for the quality control) was established. To this end, also the Commission for Low Temperature Research was dissolved and replaced by the WMI Committee and the WMI Advisory Board in 2015.

The historical roots of WMI go back to ***Walther Meißner***. He founded the Commission for Low Temperature Research in 1946 when he was president of BAdW (1946 – 1950). The first research activities then were started in 1946 in the Herrsching barracks. After the retirement of Walther Meißner in 1952, Heinz Maier-Leibnitz, who followed Walther Meißner on the Chair for Technical Physics of the Technical University of Munich (TUM), became the new head of the Commission for Low Temperature Research. In 1967, the commission moved to the Garching research campus after the construction of the new *«Zentralinstitut für Tieftemperaturforschung»* (ZTTF) was completed (director: Prof. Heinz Maier-Leibnitz, technical director: Prof. Franz Xaver Eder). Until 1972, the theory group of the Institute Laue Langevin was hosted at the ZTTF with prominent members such as Peter Fulde. In 1980, Prof. Dr. Klaus Andres became the new director of the ZTTF again associated with the Chair for Technical Physics (E23) at TUM, followed by Prof. Dr. Rudolf Gross in 2000. In 1982, the ZTTF was renamed into Walther-Meißner-Institute for Low Temperature Research (WMI) on the occasion of the 100. anniversary of Walther Meißner's birth.

Starting from 2000, the so far unused basement of the WMI building was made available for technical infrastructure (airconditioning, particulate airfilters, pure water system etc. for clean room) and additional laboratory space. Fortunately, in 2008 WMI succeeded in getting extra money from the state government within the so-called *«Konjunkturpaket II»*. This money has been used to establish the new *«WMI Quantum Science Laboratory»* in the basement of the building, providing about 150 m^2 additional laboratory space particularly suited for low temperature facilities and ultra-sensitive studies on solid state quantum systems. The WMI Quantum Science Laboratory was fully operational early in 2011 and meanwhile hosts three new mK systems and sophisticated experimental techniques for the study of solid state based quantum systems and circuits. In 2016, the Bavarian Ministry for Science and Arts granted more than 6 Mio. Euro for redevelopment measures regarding the technical infrastructure, safety requirements and energy efficiency. An important part of the building project implemented in 2017/18 was the reconstruction of the entrance area and the main staircase, providing now direct access to the new WMI Quantum Laboratories in the basement of the WMI building as well as additional communication areas and meeting rooms in the ground floor. Moreover, it included the replacement of all windows and doors, the upgrade of the technical infrastructure for cooling water, air conditioning, liquid nitrogen and helium storage, as well as the complete redevelopment of the mechanical workshop and various safety measures.

With the availability of additional laboratory space and the success of the WMI in Germany's Excellence Initiative (2006-2018), Excellence Strategy (starting from 2019), and other third-party funded research projects, the research activities, the number of staff and obviously the related administrative tasks at WMI were strongly growing. Therefore, Rudolf Gross proposed in 2017 to start the appointment procedure for his successor at an early stage to guarantee sufficient temporal overlap. Moreover, due to the strong increase of staff, research projects and administrative tasks he proposed to change the governance structure of WMI from a single director to a board of up to three directors headed by a managing director. This change of governance structure has been supported by the Scientific Advisory Board of WMI and the decision-making bodies of BAdW. Meanwhile, it is implemented in the new rules of order of WMI valid since 18th October 2019.

As already mentioned, it is a long tradition that WMI hosts the Chair for Technical Physics (E 23) of TUM with the director of the WMI being a full professor at the Faculty of Physics of TUM. In general, WMI has established tight links to research groups of both Munich universities, joining technological and human resources in the fields of experimental and theoretical solid-state and condensed matter physics, low temperature techniques, materials science as well as thin film and nanotechnology. Noteworthy, the WMI supplies liquid helium to more than 25 research groups at both Munich universities and provides the technological basis for low temperature research.

Important Discoveries

The WMI looks back on a long history of successful research in low temperature physics. In the following we list some important discoveries as well as experimental and technical developments made at WMI:

- **1961: discovery of flux quantization in multiply connected superconductors**

  (R. Doll, M. Näbauer, *Experimental Proof of Magnetic Flux Quantization in a Superconducting Ring*, Phys. Rev. Lett. **7**, 51-52 (1961)).
- **1986: discovery of an anomalous temperature dependence of the penetration depth in UBe_{13}**

  (F. Gross, B.S. Chandrasekhar, D. Einzel, K. Andres, P.J. Hirschfeld, H.R. Ott, J. Beuers, Z. Fisk, J.L. Smith, *Anomalous Temperature Dependence of the Magnetic Field Penetration Depth in Superconducting UBe_{13}*, Z. Physik B - Condensed Matter **64**, 175-188 (1986)).
- **1992: discovery the intrinsic Josephson effect**

  (R. Kleiner, F. Steinmeyer, G. Kunkel, and P. Müller, *Intrinsic Josephson Effects in $Bi_2Sr_2CaCu_2O_8$ Single Crystals*, Phys. Rev. Lett. **68**, 2394-2397 (1992)).
- **2002: development of dilution refrigerators with pulse tube refrigerator precooling**

  (K. Uhlig, *$^3He/^4He$ Dilution Refrigerator with Pulse Tube Precooling*, Cryogenics **42**, 73-77 (2002)).
- **2010: first demonstration of ultrastrong light-matter interaction**

  (T. Niemczyk, F. Deppe, H. Huebl, E. P. Menzel, F. Hocke, M. J. Schwarz, J. J. Garcia-Ripoll, D. Zueco, T. Hümmer, E. Solano, A. Marx, R. Gross, *Circuit Quantum Electrodynamics in the Ultrastrong-Coupling Regime*, Nature Physics **6**, 772-776 (2010)).
- **2010: development of dual path method for state tomography of propagating quantum microwaves**

  (E.P. Menzel, M. Mariantoni, F. Deppe, M.A. Araque Caballero, A. Baust, T. Niemczyk, E. Hoffmann, A. Marx, E. Solano, R. Gross, *Dual-Path State Reconstruction Scheme for Propagating Quantum Microwaves and Detector Noise Tomography* , Phys. Rev. Lett. **105**, 100401 (2010)).

- **2012: first realization of path entanglement of propagating quantum microwaves**

  (E. P. Menzel, R. Di Candia, F. Deppe, P. Eder, L. Zhong, M. Ihmig, M. Haeberlein, A. Baust, E. Hoffmann, D. Ballester, K. Inomata, T. Yamamoto, Y. Nakamura, E. Solano, A. Marx, R. Gross, *Path Entanglement of Continuous-Variable Quantum Microwaves*, Phys. Rev. Lett. **109**, 250502 (2012)).
- **2013: discovery of the spin Hall magnetoresistance** (jointly with partners at Tohoku University and TU Delft)

  (H. Nakayama, M. Althammer, Y.-T. Chen, K. Uchida, Y. Kajiwara, D. Kikuchi, T. Ohtani, S. Geprägs, M. Opel, S. Takahashi, R. Gross, G. E. W. Bauer, S. T. B. Goennenwein, E. Saitoh, *Spin Hall Magnetoresistance Induced by a Non-Equilibrium Proximity Effect*, Phys. Rev. Lett. **110**, 206601 (2013)).
- **2013: first demonstration of strong magnon-photon coupling**

  (H. Huebl, Ch. Zollitsch, J. Lotze, F. Hocke, M. Greifenstein, A. Marx, R. Gross, S.T.B. Goennenwein, *High Cooperativity in Coupled Microwave Resonator Ferrimagnetic Insulator Hybrids*, Phys. Rev. Lett. **111**, 127003 (2013)).
- **2017: first experimental observation of the spin Nernst effect**

  (S. Meyer, Yan-Ting Chen, S. Wimmer, M. Althammer, S. Geprägs, H. Huebl, D. Ködderitzsch, H. Ebert, G.E.W. Bauer, R. Gross, S.T.B. Goennenwein, *Observation of the spin Nernst effect*, Nature Materials **16**, 977-981 (2017)).
- **2019: first demonstration of remote state preparation in the microwave regime**

  (S. Pogorzalek, K. G. Fedorov, M. Xu, A. Parra-Rodriguez, M. Sanz, M. Fischer, E. Xie, K. Inomata, Y. Nakamura, E. Solano, A. Marx, F. Deppe, R. Gross, *Secure Quantum Remote State Preparation of Squeezed Microwave States*, Nature Communications **10**, 2604 (2019)).

Present Research Activities

The research activities of the Walther-Meißner-Institute are focused on low temperature condensed matter and quantum physics (see reports below). The research program is devoted to both **fundamental** and **applied research** and also addresses **materials science, thin film and nanotechnology** aspects. With respect to **basic research** the main focus of the WMI is on

- quantum phenomena and quantum coherence in solid state systems,
- superconductivity and superfluidity,
- magnetism, including spin transport, spin dynamics, spin mechanics and spin caloritronics,
- circuit quantum electrodynamics and circuit electro-nanomechanics,
- ordering and emergent phenomena in correlated quantum matter,
- and the general properties of metallic systems at low and very low temperatures.

The WMI also conducts **applied research** in the fields of

- solid-state quantum information processing and quantum communication systems,
- superconducting and spin-based devices,
- multi-functional and multiferroic materials,
- and the development of low and ultra-low temperature systems and techniques.

With respect to **materials science, thin film and nanotechnology** the research program is focused on

- the synthesis of superconducting and magnetic materials,
- the single crystal growth of oxide materials,
- the thin film technology of complex superconducting and magnetic heterostructures, including multi-functional and multi-ferroic material systems,
- and the fabrication of superconducting, magnetic and hybrid nanostructures.

The WMI also develops and operates systems and techniques for low and ultra–low temperature experiments. A successful development have been dry mK-systems that can be operated without liquid helium by using a pulse-tube refrigerator for precooling. In the early 2000s, these systems have been successfully commercialized by the company VeriCold Technologies GmbH at Ismaning, Germany, which was taken over by Oxford Instruments in 2007. As a further typical example we mention very flexible dilution refrigerator inserts for temperatures down to about 20 mK fitting into a 2 inch bore. These systems have been engineered and fabricated at WMI and also provided to other research groups for various low temperature experiments. WMI also operates a helium liquifier with an annual capacity of above 180.000 liters and supplies both Munich universities with liquid helium. To optimize the transfer of liquid helium into transport containers, WMI has developed a pumping system for liquid helium that is commercialized in collaboration with a company.

To a large extent the research activities of WMI are integrated into national and international research projects such as Clusters of Excellence, Collaborative Research Centers, Research Units, or EU projects. The individual research groups of WMI offer a wide range of attractive research opportunities for bachelor and master students, Ph.D. students and postdoctoral fellows.

Experimental Facilities and Resources

The WMI is equipped with state of the art facilities for the preparation and characterization of superconducting and magnetic materials as well as for various low and ultra–low temperature experiments. The main experimental and technological resources of WMI are listed in the following.

Materials Preparation and Fabrication of Nanostructures

- Laser Molecular Beam Epitaxy (L-MBE) system for oxide heterostructures (equipped with in–situ RHEED, Omicron AFM/STM system, atomic oxygen/nitrogen source, infrared-laser heating system, metallization). The L-MBE systems is connected to a UHV magnetron sputtering systems for metals (e.g. Nb, Al, NiPd, ...) and an electron beam deposition system via a UHV transfer chamber
- molecular beam epitaxy (MBE) system for metals
- UHV cluster tool consisting of two magnetron sputter deposition systems for superconducting and magnetic heterostructures, respectively, and a load lock
- UHV magnetron sputtering system for large-area deposition of superconducting thin films and heterostructures
- reactive ion etching (RIE) system, Plasmalab 80 Plus with ICP plasma source, Oxford Instruments Plasma Technology
- ion beam etching (IBE) system equipped with a LN_2 cooled sample holder
- automated critical point dryer Leica EM CPD 300
- polishing machine for substrate preparation
- ultrasonic bonding machine
- 50 m^2 class 1000 clean room facility
- maskless lithography UV Direct Laser Writer, PicoMaster 200 UV of the company 4PICO, The Netherlands
- 100 kV nB5 Electron Beam Lithography System by NanoBeam Limited, UK, with 6 inch laser stage
- optical lithography (Süss maskaligner MJB 3 and projection lithography)
- four-mirror image furnace for crystal growth

Characterization

- 2–circle x–ray diffractometer (Bruker D8 Advance, sample temperature up to 1 600°C)
- high resolution 4–circle x–ray diffractometer with Göbel mirror and Ge monochromator (Bruker D8 Discover)
- Philips XL 30 SFEG scanning electron microscope with EDX analysis
- UHV room temperature AFM/STM system
- two Raman spectroscopy systems (1.5 to 300 K, in-situ sample preparation)
- tip-enhanced Raman spectroscopy (TERS) system
- SQUID magnetometer (Quantum Design, 1.5 to 700 K, up to 7 T)
- several high field magnet systems (up to 17 T Tesla) with variable temperature inserts
- 7 T split coil magnet systems with optical access and variable temperature insert
- 3D vector magnet (2/2/6 Tesla) with variable temperature inserts
- experimental set–ups for the measurement of noise including low noise SQUID amplifiers and signal analyzers
- high-frequency network analyzers (up to 40 GHz) and various microwave components (sources, mixers, circulators, attenuators) for the determination of high frequency parameters
- ultra-sensitive microwave receiver for state tomography of quantum microwaves (dual path method with FPGA signal processing)
- high-frequency cryogenic probing station (up to 20 GHz, $T > 4\,\mathrm{K}$)
- magnetooptical Kerr effect (MOKE) system
- broadband ferromagnetic resonance (FMR) system

Low temperature systems and techniques

- several ^{3}He/^{4}He dilution refrigerator inserts for temperatures down to 10 mK
- "dry" mK-cooler based on a dilution refrigerator with pulse-tube precooling and equipped with a large number of microwave lines and cold electronics (e.g. amplifiers, circulators, attenuators, directional couplers) for ultra-sensitive experiments on solid state quantum systems
- "dry" dilution refrigerator with a base temperature of about 10 mK equipped with a 3D vector magnet (1/1/6 Tesla)
- "wet" mK-cooler based on a dilution refrigerator liquid helium precooling and equipped with a large number of microwave lines and cold electronics (e.g. amplifiers, circulators, attenuators, beam splitters) for time-domain microwave experiments on solid state quantum systems
- experimental set–ups for the measurement of specific heat, magnetization, thermal expansion as well as electrical and thermal transport properties as a function of temperature, magnetic field and pressure

Building Projects

WMI Building and Infrastructure

Rudolf Gross, Achim Marx

Figure 1: View on the northern cross-aisle and new main staircase of the WMI building as seen from the inner courtyard.

The staff of WMI is extremely happy that the general redevelopment measures regarding the technical infrastructure, safety requirements and energy efficiency have been finally completed in 2019. As the last step, the installation of a new transformer station for increasing the power handling capability of the WMI electric power system has been completed late in 2019. The change from a low to medium voltage connection reduces the required cross-sectional area of the underground cables considerably and removed the problem of missing space in the cable duct.

The building project included the following specific measures:

- extension of the main staircase of the WMI building to the basement and redesignment of the front entrance
- replacement of all windows and office/laboratory doors
- equipping the WMI laboratories with air conditioning systems, including the installation of a central refrigeration unit in the basement
- installation of a new chemical laboratory
- redevelopment and replacement of the helium recovery system and the liquid nitrogen tank
- installation of a new transformer station to increase the power handling capability of the electric power system.

The fact that the completion of the whole building project took more than three years and finally much more than expected was very unfortunate for the WMI research activities. Laboratory rooms could not be used for an extended period of time and experiments have been often perturbed by the ongoing construction work. This was nerve-shattering and perturbing for everybody. However, meanwhile it is also clearly visible that the redevelopment measure has been a large success and will have a large future benefit for WMI.

Although the perturbing general redevelopment measures have been just finished, new building activities have already been started in 2019. On the one hand, they are necessary to accommodate new equipment ordered within the new Cluster of Excellence MCQST. On the other hand, a new WMI director has been appointed in 2019 and will start in April 2020. Therefore, several laboratories in the southern cross-aisle of the WMI-building have to be rearranged according to his needs. This means that building activities will unfortunately perturb the scientific work of the WMI team also within the next years.

Joint Research Projects

Clusters of Excellence

Rudolf Gross

A. The «Nanosystems Initiative Munich» (NIM)

The WMI has been a founding member and one of the key institutions of the Cluster of Excellence ***«Nanosystems Initiative Munich» (NIM)*** since it was established in 2006. NIM was funded as a Cluster of Excellence by the Deutsche Forschungsgemeinschaft (DFG) under Germany's *Excellence Initiative* between November 2006 and October 2019. The Cluster brought together more than 60 research groups in the Munich area and merged their interdisciplinary expertise in physics, chemistry, electrical engineering, biology, pharmacy and medicine into a coherent nanoscience cluster. The second funding period of NIM ended in October 2019 after 13 highly successful years. NIM had a big impact on nano-related research in Munich and provided an inspiring atmosphere. It was a lot of fun working in NIM!

The overarching vision of NIM was to realize and achieve control of a broad range of multi-functional nanoscale systems and to unlock their potential for applications in fields as diverse as information and energy technologies and the life sciences. Research efforts focussing on nanosystems included single-electron and -spin behavior at ultra-low temperatures, nano-photonic systems, and the investigation of practical strategies for quantum computation. These were complemented by research areas that addressed the realization of extremely sensitive nanosensors, artificial and natural molecular machines, nanoscale objects and vehicles in live cells, and drug delivery nanosystems. In the second funding period of NIM, the original research areas were complemented by "Nanosystems for Energy Conversion", focusing on nanotechnological solutions for the conversion of light into other forms of energy.

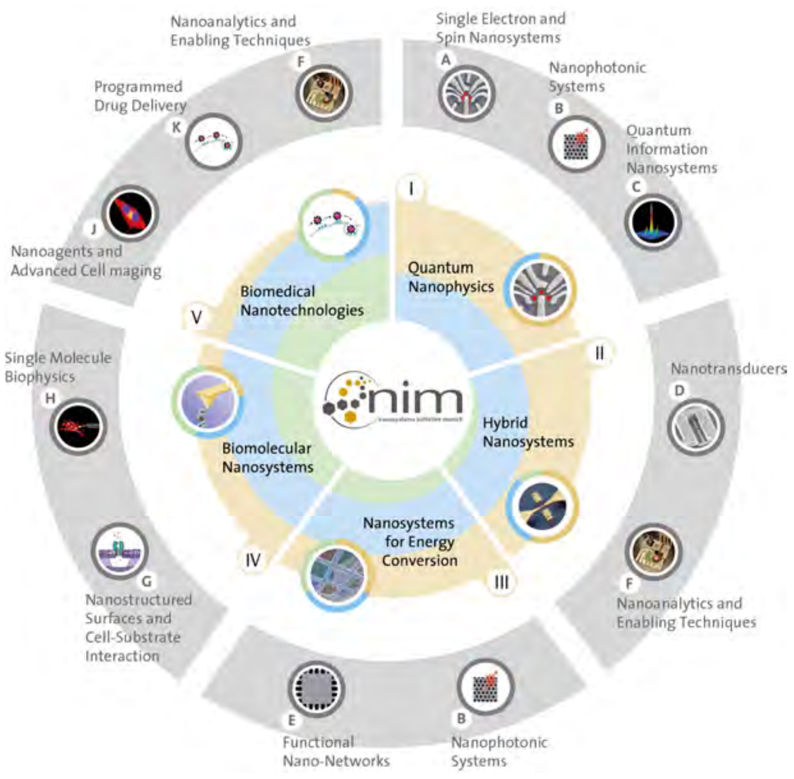

Figure 1: NIM started with 10 Research Areas in 2006 (outer circle), which have been reorganized into five in 2010 (inner circle): I) Quantum Nanophysics, II) Hybrid Nanosystems, III) Nanosystems for Energy Conversion, IV) Biomolecular Nanosystems, and V) Biomedical Nanotechnologies.

The highly interdisciplinary nature of the NIM cluster ensured the efficient utilization of synergies and an internationally competitive research program, generated a stimulating environment for graduate education, and provided ideal conditions for technological innovations. As one of the main structural goals, NIM succeeded to establish a world-leading nanoscience research site in Germany, attracting the most gifted young scientists in the field. Special emphasis was put on early independence of junior scientists, offering them competitive start-up packages, seed-funding and tenure-track professorships to provide a long-term career perspective.

Within the 13-year funding period, NIM scientists published more than 2500 articles with many of them in the most highly ranked scientific journals. In addition, the cluster generated numerous patents, awards, prizes and grants from the European Research Council (ERC) as well as a series of globally successful spin-off companies. NIM also gained world-wide visibility by initiating active partnerships with leading nano-centers such as the California NanoSystems Institute (CNSI), by running a Graduate Program, by effective outreach activities, and by organizing a series of international conferences. Most importantly, NIM has set the ground for a number of new initiatives such as the successful new clusters of excellence ***«Munich Center for Quantum Science and Technology» (MCQST)*** and ***«Fundamentals of Energy Conversion Processes» (e-conversion)***, both funded since January 2019. The nanoscience facilities (e.g. the Center for Nanoscience and Nanotechnology at TUM, the Nano-Institute Munich at LMU or the Quantum Science Laboratories at WMI) and the state-of-the-art instrumentation established by NIM represent a key infrastructure for these new clusters. Therefore, without any doubt the Munich area will continue to act as a leading hub for nanoscience oriented research with worldwide visibility. At all institutions participating in NIM the core research activities on nanoscience and nanotechnology will be continued and the key research facilities of NIM will be maintained.

The WMI was continuously contributing to the highly successful NIM cluster mainly in the NIM Research Areas on *«Quantum Nanophysics»* and *«Hybrid Nanosystems»*. Hans Hübl and Sebastian Gönnenwein of WMI were Principal Investigators and Frank Deppe was an Associate Member. Rudolf Gross was both member of the NIM Executive Board and coordinator of the Research Area 1 on *«Quantum Nanophysics»* over the full funding period of NIM.

The WMI was not only providing valuable input to the scientific program of NIM, but also was receiving continuous support from NIM for its research projects and technological infrastructure. For example, the new electron beam lithography system at WMI only could be acquired due to substantial support of NIM. The same is true for thin film technology as well as low temperature and microwave equipment. Three junior group leaders (Sebastian Gönnenwein, Hans Hübl, Frank Deppe) obtained generous support as PIs and by many seed funding projects. They could finish their habilitation theses within the funding period of NIM and, in the case of Sebastian Gönnenwein, could acquire a full professor position at TU Dresden. Finally, more than 25 PhD and 60 master students of WMI were supported by NIM with most of them having started a successful career in science or industry. Also in this respect NIM was a big success: Many thanks you NIM!

B. The «Munich Center for Quantum Science and Technology» (MCQST)

The new Cluster of Excellence ***«Munich Center for Quantum Science and Technology» (MCQST)*** has been granted on 27th September 2018 within Germany's ***Excellence Strategy***. The first seven-year funding period started on 1st January 2019. The cluster joins groups from the Ludwig-Maximilians University Munich (LMU), the Technical University of Munich (TUM), the Max Planck Institute of Quantum

Optics (MPQ), the Walther-Meißner-Institute (WMI) and the German Science Museum (DM). It is coordinated by the three spokespersons Immanuel Bloch (LMU Munich and MPQ), Ignacio Cirac (MPQ and TUM) and Rudolf Gross (TUM and BAdW). The acquisition of the new Cluster of Excellence has been a great success and allows Munich to become an internationally leading center in one of the most exciting research and technology fields.

Meanwhile, MCQST combines more than 50 Principal Investigators and more than 300 scientists in the Munich research area working across the different disciplines of Quantum Science and Technology (QST), including Physics, Computer Science, Mathematics, Materials Science, Electrical Engineering and Chemistry. MCQST aims at discovering and understanding the novel and unifying concepts in the vibrant interdisciplinary research fields of QST. It will make them tangible and practical, in order to develop the extraordinary applications being in reach through next generation quantum devices. MCQST is structured in seven interconnected Research Units covering the entire range from fundamental science, through technology and material development to applications (see Fig. 2).

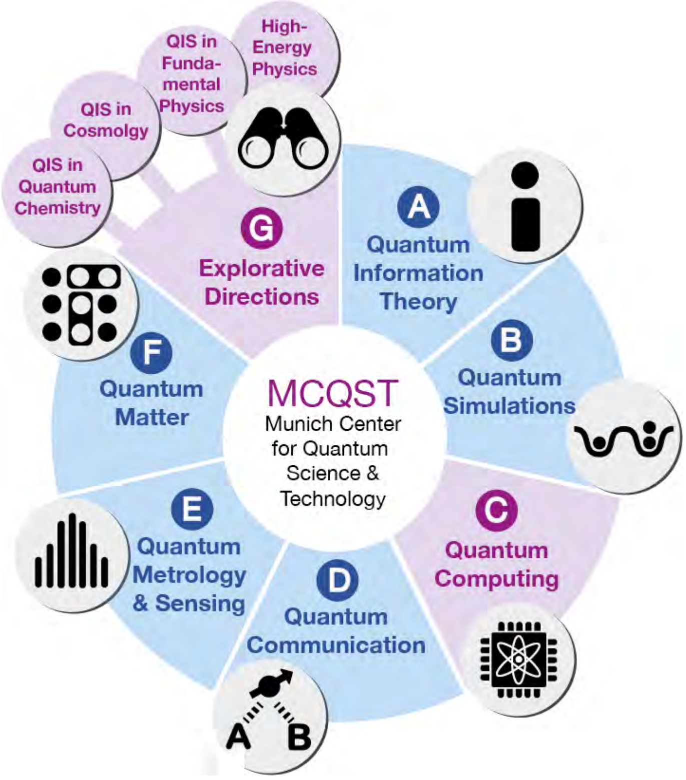

Figure 2: Schematic of the focus Research Units A-G of MCQST, connecting fundamental science and technological applications. Purple fields/circles indicate either topics to be strengthened (RU-C) or new, explorative fields of research (RU-G) that will significantly extend the reach of the MCQST and connect Quantum Information Science (QIS) to other fields of science.

Based on the broad and complementary competence available in the Munich research landscape, MCQST researchers exhibit proven core expertise, with many pioneering and foundational contributions to each of the core fields. This is a unique aspect of MCQST compared to other national and international centers focusing on related research. In addition, Munich researchers are among the forefront of paving the way to establish QST also in other fields of science and identifying new explorative topics and applications.

Research Rationale

After quantum mechanics has revolutionized our understanding of nature and has enabled the development of ground-breaking new technologies during the last century, we are witnessing a «*second quantum revolution*» today: information theory and quantum physics are uniting, thereby providing radically new ways of communication and computation as well as a general new framework for our understanding of nature. The research strategy of MCQST is guided by the expectation that this second quantum revolution will have a transformative impact on science, technology and ultimately on society. Quantum computers are expected to solve problems that could never be addressed even by the most powerful supercomputers. This opens up unforeseen possibilities of designing and developing new materials with unparalleled properties, of discovering chemical compounds for materials science and drug design, or powerful algorithms that will transform machine learning and artificial intelligence. Quantum communication will eventually replace the way we interact remotely in the future. Finally, quantum technologies will lead to ultraprecise sensors and clocks, with impact in medicine, biology and transportation.

MCQST Start-up Phase

MCQST officially started in January 2019 and already was very active within the first year. This included a lot of administrative work (e.g. finalizing the statutes and legal contracts among the participating institutions, hiring the people for the MCQST office, etc.) but fortunately also a lot of research-related activities. An overview of the MCQST scientific activities and programs including outreach and equal opportunity measures, press releases, etc. can be found at www.mcqst.de.

To start-up interdisciplinary research projects as soon as possible, MCQST asked twice for the submission of seed-funding proposals and already granted more than 10 projects in a competitive selection procedure. Not only the PIs of MCQST but also all associate members are eligible for seed applications. The MCQST Executive Committee together with an international Advisory Board also granted the first Junior Researcher START Fellowships to support young talents on their transition from postdocs to independent researchers. With a total budget of 300.000 € for a funding period of two years, the fellows have the opportunity to start their own scientific project in one of the Research Units of MCQST. The next candidates already have been invited for an interview in Munich on 19th February 2020. Selection criteria are scientific excellence and an original research proposal.

MCQST organized already several conferences and workshops. Most notably are the ***Munich Conference on Quantum Science and Technology*** at the Center for New Technologies (ZNT) of the German Science Museum and the ***MCQST-Technion Symposium on QST*** at the Max Planck Institute of Quantum Optics. MCQST also started the ***MCQST Colloquium*** with prominent speakers such as Hartmut Neven, John Preskill, Erez Berg or Atac Imamoglu, attracting a broad audience. As Distinguished Lecturer, John Preskill gave three different presentations during his visit to MCQST, each specially targeted to a different audience: a talk at the Ehrensaal of the Deutsches Museum for the public interested in scientific discoveries and developments, a Colloquium for the local scientific community, as well as a more specialized seminar for researchers working in the same field.

Strong public engagement is of key interest for MCQST to raise the awareness for the specific QST research in Munich. This is achieved by a dedicated public relations office and through our partner Deutsches Museum, one of the most prominent science and technology museums worldwide. In collaboration with this partner MCQST develops joint outreach activities such as a series of temporary and permanent exhibitions on QST to make the public aware of QST and introduce them to this new and fascinating research field.

MCQST Graduate Education and Master's Program

An important educational component of MCQST is a dedicated Master's program on Quantum Science and Technology for top students from all over the world. Such a program is urgently required to make the new generation of scientists, engineers and entrepreneurs well trained for the QST revolution to come. Therefore, MCQST made a considerable effort to establish the new Master's program on QST as soon as possible. Despite the fact that the new Master's program is a joint program between two universities (TUM, LMU) and involves several faculties, MCQST succeeded in getting the new Master's program accepted within less than a year. MCQST owes in particular Alex Holleitner a great debt of gratitude for his patience and persistence with all the administrative and coordination work. The new program will start in WS 2020/21. It will link students in physics, mathematics, chemistry, information science and engineering to the MCQST graduate program. It will thus provide a broad education in QST, foster interdisciplinary collaboration from an early stage and provide students skill sets in QST of relevance for both academia and industry.

LMU TUM

Studiengangsdokumentation
Masterstudiengang Quantum
Science & Technology

Teil A
Fakultät für Physik, Technische Universität München
und
Fakultät für Physik, Ludwig-Maximilians-Universität München

Figure 3: A dedicated Master's program in Quantum Science and Technology co-organized by both LMU and TUM will provide an advanced education in QST starting from WS 2020/21. Shown is the title page of the «Studiengangsdokumentation» with the key players setting up the program.

The PhD program of MCQST will build on the existing excellence graduate schools (*Ph.D. School of Excellence «Exploring Quantum Matter» (ExQM)* and *International Max Planck Research School «Quantum Science and Technology» (IMPRS-QST)*), providing PhD students with a rich variety of research topics, while engaging them directly in a unique environment.

Recent progress in the EU Quantum Flagship project QMiCS

F. Deppe, K. G. Fedorov, A. Marx, M. Partanen, M. Renger, R. Gross [1]

Since 2018, the European Union (EU) fosters the development of quantum technologies via the *Quantum Flagship* program. One of the 20 projects funded in the first call is *«Quantum Microwave Communication and Sensing» (QMiCS)*. It is coordinated by Frank Deppe of WMI. The project logo together with the logos of the Quantum Flagship and the European Union are shown on the right. Scientific project partners are Aalto University (Finland), École Normale Superieure der Lyon (ENSL, France), Instituto de Telecomunicações (Portugal), Universidad del País Vasco / Euskal Herriko Unibertsitatea (UPV/EHU, Spain), and VTT (Finland). Active industry partners are Oxford Instruments Nanotechnology Ltd. (OINT, United Kingdom) and TTI Norte S.L. (Spain).

Figure 1: The new tailset of Alice-fridge including two connection ports.

After establishing the project governance and starting up, the year 2019 has been dedicated to pushing on the first scientific and technological achievements. With respect to science, WMI has experimentally realized secure remote state preparation (RSP) for the first time in the microwave regime [1]. The distance between the two parties of this fundamental communication protocol has been 36 cm. Additional insights regarding the quantum Fisher information in RSP, a series connection of two Josephson parametric amplifiers, and FPGA-based data processing in the tomography of propagating quantum microwaves can be found in the reports by M. Renger (page 67-68), S. Pogorzalek (page 37-38), and K. G. Fedorov (page 65-66), respectively.

Regarding technology, one of the core developments in QMiCS is the microwave quantum local area network (QLAN) cable, a 6.6 m long superconducting link at millikelvin temperatures between two cryostats. This link will connect a homemade dilution refrigerator from WMI ("Alice-fridge") with another one ("Bob-fridge") provided by our industrial partner OINT. OINT also develops the cryotechnological aspects of the link. The two fridges will be located in separate labs and the link will pass through an intermediate utility room. So far, WMI and OINT have defined a scope of work document and ordered all required parts. In particular, the Alice-fridge has to be equipped with a new tailset (see Fig. 1), which has safely arrived at WMI and will be tested early in 2020.

The superconducting microwave cable, which is to be mounted inside the cryolink for a functional QLAN cable falls within the responsibility of WMI. Although superconducting coaxial cables are typically fabricated only in lengths smaller than 2 m, the external company KEYCOM Corp. developed a low-loss and low-reflectivity joint to provide NbTi superconducting

---

[1] We acknowledge support by the Germany's Excellence Strategy EXC-2111-390814868, Elite Network of Bavaria through the program ExQM, and the European Union via the Quantum Flagship project QMiCS (Grant No. 820505).

coaxial cables of the required length. The successful test of this connection is described in the report by M. Partanen (see page 69), and as a result, two 7 m sections with two joints each were purchased.

Of course, QMiCS also has an educational aspect, since it brings together partners with complementary backgrounds and knowhow. Therefore, a series of teleconference colloquia has been established. So far, UPV/EHU has introduced the theory of quantum microwave teleportation and ENSL the experimental approaches to Josephson parametric converters and qubit-based microwave photodetection. In addition, there have been several bi- and multilateral meetings between the partners, such as the WMI-theory meeting in January 2019 or the joint design of parametric devices between WMI, ENSL, and VTT.

In conclusion, QMiCS is well on track and, at WMI, exciting action such as the installation and testing of the cryolink and the QLAN cable are scheduled for the next year.

References

[1] S. Pogorzalek, K. G. Fedorov, M. Xu, A. Parra-Rodriguez, M. Sanz, M. Fischer, E. Xie, K. Inomata, Y. Nakamura, E. Solano, A. Marx, F. Deppe, and R. Gross, Nat. Commun. **10**, 2604 (2019).

The EU Project «Magnetomechanical Platforms for Quantum Experiments and Quantum Enabled Sensing Technologies» (MaQSens)

Hans Hübl, Rudolf Gross [1]

The EU Project *«MaQSens»* (coordinator: Markus Aspelmeyer, University of Vienna) started in January 2017. Within this project, WMI collaborates with partners from the University of Vienna, the Technical University of Vienna, the Austrian Academy of Sciences, and the Universitat Autonòma de Barcelona as well as the industry partners Airbus DS GmbH and attocube systems AG. The project got a nine month extension and will come to an end in autumn 2020.

MaQSens seeks to establish a radically new technology platform for experiments in macroscopic quantum physics and for quantum enabled sensing. It exploits magnetic coupling between superconducting quantum circuits and superconducting mechanical resonators – both levitated and suspended – to enter a hitherto inaccessible parameter regime of both unprecedented force sensitivity and full quantum control of massive, macroscopic objects. The technology developed in MaQSens will enable quantum experiments of otherwise unachievable coherence times and masses, which has immediate implications for testing fundamental physical questions, for performing hybrid quantum information processing and, on the applied side, for ultrasensitive force sensing applications.

Within the MagQSens project, we could demonstrate that inductive electromechanical coupling schemes have the potential to reach the vacuum strong-coupling regime. This was achieved by integrating a partly suspended superconducting quantum interference device (SQUID) into a microwave resonator. We could demonstrate a sideband-resolved electromechanical system with a tunable vacuum coupling rate of up to 1.62 kHz, allowing to reach sub-aN/$\sqrt{\mathrm{Hz}}$ force sensitivity. Our coupling scheme showed the high potential of SQUID-based electromechanics for targeting the full wealth of the intrinsically nonlinear optomechanics Hamiltonian. Further details are given in the report of Schmidt *et al.* (see page 59–61).

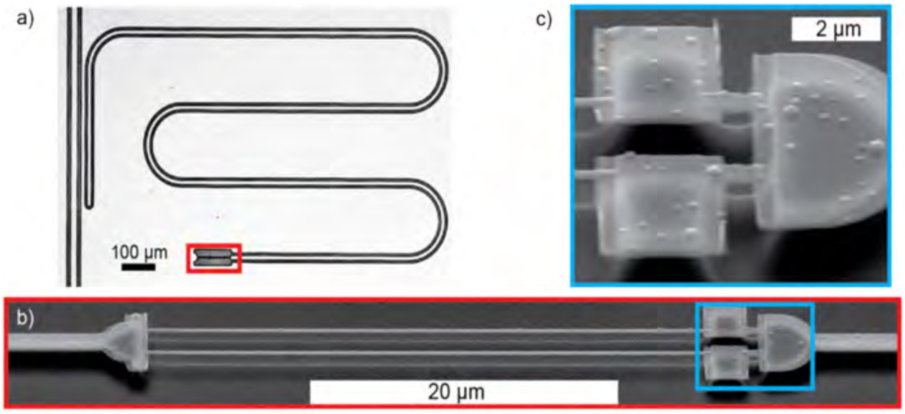

Figure 1: (a) Microscopic image of a flux tunable microwave resonator, consisting of a coplanar waveguide and a dc-SQUID shunting the center conductor to ground. (b) SEM image of the suspended SQUID with the two nanomechanical strings. (c) Magnified view of the area with the two Josephson junctions.

References

[1] Philip Schmidt, Mohammad T. Amawi, Stefan Pogorzalek, Frank Deppe, Achim Marx, Rudolf Gross, and Hans Huebl. Sideband-resolved resonator electromechanics on the single-photon level based on a nonlinear Josephson inductance. `arXiv:1912.08731` (2019).

---

[1] Supported by the EU Horizon 2020 research and innovation programme under grant agreement No. 736943 and from the ERC under grant agreement No. 649008.

Coordinated Projects in Quantum Science and Technology

Rudolf Gross

The Walther-Meißner-Institute (WMI) participates in several coordinated research programs, centers, graduate schools and initiatives in the field of Quantum Science and Technology (QST). Besides the Clusters of Excellence (see page 17–21)

- *«Nanosystems Initiative Munich»* (11/2006 – 10/2019)
- *«Munich Center for Quantum Science and Technology»* (01/2019 – 12/2025)

and the EU projects

- *«Quantum Microwave Communication and Sensing» (QMiCS)* (see page 22–23)
- *«Magnetomechanical Platforms for Quantum Experiments and Quantum Enabled Sensing Technologies» (MaQSens)* (see page 24)

these are the graduate programs

- **Ph.D. School of Excellence «Exploring Quantum Matter» (ExQM)** and
- **International Max Planck Research School «Quantum Science and Technology» (IMPRS-QST)**

as well as the

- **Munich Quantum Center (MQC)**.

We would like to emphasize that beside the clusters and the EU projects both MQC and the graduate schools ExQM and IMPRS-QST are important for WMI to continue its ambitious research program in QST, which started already in 2003 within the Collaborative Research Center 631 «Solid State Quantum Information Processing Systems».

WMI is particularly pleased that MQC, which was founded in 2014 as a 'virtual center', gets now continuous financial support from both Munich universities starting from 2019. MQC hosts all scientists and engineers in the greater Munich area working in the field of QST and therefore the number of people in MQC by far exceeds the number of Principal Investigators in MCQST or some Munich based BMBF or EU projects. Of course, the activities of MQC are closely coordinated with those of MCQST. MQC particularly aims at communicating recent advances and developments in the field of QST. Furthermore, MQC is a successful platform to enhance the outside visibility of the Munich research activities in the field of QST. To this end, MQC is joining forces with MCQST in organizing workshops and schools as well as in stimulating new coordinated research projects.

New Projects on the Horizon

Within the program «Quantentechnologien – von den Grundlagen zum Markt» the BMBF recently announced the new call «Anwendungsbezogene Forschung in der Quantensensorik, -metrologie sowie -bildgebung». As WMI has pioneered the field of quantum microwaves during the last decade, we are planning to contribute a project on quantum enhanced imaging in the microwave regime to this call. A particular application would be quantum radar. Several partners from industry and engineering faculties are highly interested in this topic. In this context, we are grateful to MCQST for seed-funding support, allowing us to extend our studies on Josephson parametric amplifiers, which are an important ingredient to this research direction.

quanten
technologien

Basic Research

Spin Transport in a Magnetic Insulator with Zero Effective Damping

T. Wimmer, M. Althammer, L. Liensberger, N. Vlietstra, S. Geprägs, M. Weiler, R. Gross, H. Huebl [1]

Since several years we are interested in pure spin current transport in magnetic insulators (MIs). In MIs, angular momentum is transported by quantized excitations of the spin lattice, referred to as magnons, and not via the spin of mobile charge carriers. However, since magnons are quasiparticles, they exhibit a finite lifetime. Various decay mechanisms in the MIs lead to a relaxation of the excitations of the spin lattice. In our experiments, we utilize the fact that we can locally increase or decrease the number of the thermally excited magnons in the MI by passing a charge current through an adjacent normal metal strip [1]. In the normal metal, the spin Hall effect (SHE) transforms the charge current into a pure spin current, which is then injected through the interface into the MI. There, magnons diffuse away from the injection region underneath the normal metal strip (injector). Utilizing the inverse effect, we can then detect the diffusive magnon current as a voltage drop in a second normal metal strip (detector) placed a few 100 nm away from the injector. Thus, we gain all-electrical access to the magnon mediated spin current transport in the MI. In the prototype ferrimagnetic insulator yttrium iron garnet (YIG), magnons feature a long room-temperature lifetime of 100 µs, corresponding to a magnon diffusion length of about 10 µm.

Regarding possible applications, a critical next step is to find schemes allowing for the control of the magnon flow in the MI. Inspired by experiments by Cornelissen *et al.* [2], we realized a more sophisticated all-electrical approach in YIG thin films. A key ingredient to our experimental success was the availability of high quality YIG films with thicknesses below 15 nm, fabricated by the state-of-the-art thin film equipment at WMI. The design of the device structure is illustrated in Fig. 1(a): Three Pt strips are deposited via lift-off and electron beam lithography on top of a 14 nm thick YIG layer grown via laser-MBE on a (100)-oriented $Gd_3Ga_5O_{12}$ substrate. In the experiment, we apply an AC charge current to the Pt injector strip and utilize a Lock-In detection technique to measure the first harmonic signal V_{ac} at the Pt detector strip. In addition, we apply a DC charge current to the Pt modulator strip. In the modulator, the charge current is transformed into a pure spin current and leads to the injection of magnons into the YIG layer, if the magnetization in the YIG and the spin direction are aligned parallel to each other, i.e. if the external magnetic field **H** is oriented along the $-\mathbf{y}$ ($\mathbf{y}$)-direction (corresponding to positive (negative) magnetic fields). Underneath the modulator, at

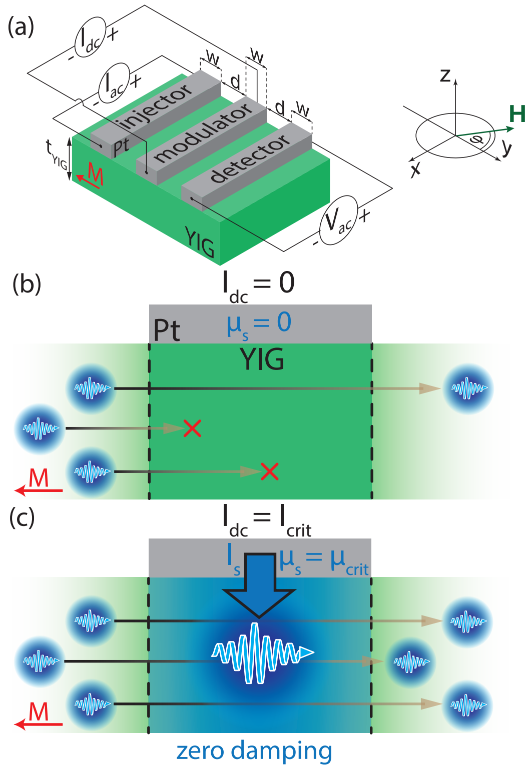

Figure 1: All-electrical magnon transistor experiments. (a) Illustration of the device setup and experimental external magnetic field geometry. Panels (b) and (c) show the magnon transport underneath the Pt modulator without and with a critical current applied to the modulator strip, respectively.

---

[1] We gratefully acknowledge financial support from the German Research Foundation via Germany's Excellence Strategy (EXC-2111-390814868) and projects AL 2110/2-1, WE 5386/4-1.

a critical charge current I_{crit} the magnon injection is large enough to compensate for the intrinsic damping rate of magnons in the YIG (see Fig. 1(b) and (c)). Thus, applying $I > I_{\text{crit}}$ to the modulator, magnons can diffuse without any damping underneath the modulator.

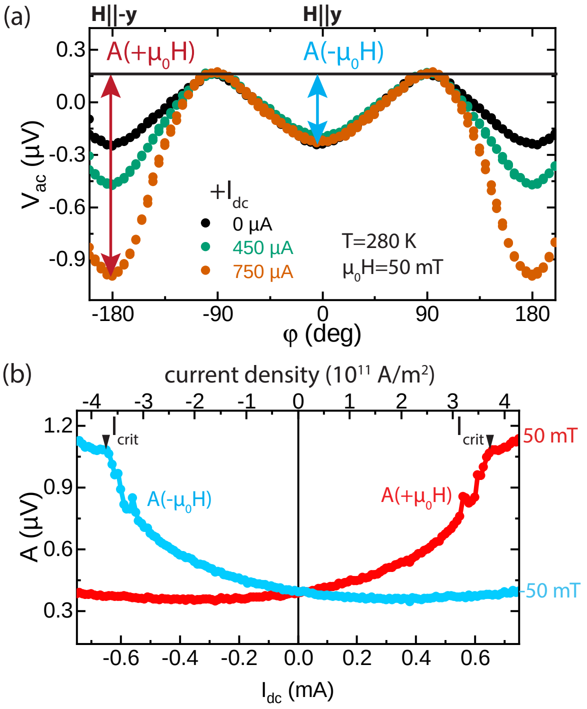

Figure 2: (a) Angular dependent magnon transport experiments as a function of the applied magnetic field orientation at 280 K and 50 mT. Upon application of I_{dc} to the modulator we observe a significant change in the angle-dependence. (b) Extracted amplitude A as a function of I_{dc} for positive and negative applied field. For large I_{dc} we observe a strong change of slope at I_{crit}.

We studied the magnon transport through the damping-compensated region underneath the modulator strip. In particular, we carried out angle-dependent measurements of V_{ac} as shown in Fig. 2(a) for positive charge currents I_{dc} applied to the modulator. Clearly, two distinct minima in V_{ac} are visible at $\mathbf{H} \parallel \mathbf{y}$ and $\mathbf{H} \parallel -\mathbf{y}$. These minima correspond to the magnetic field configuration, where a transport of magnons from the injector to the detector is possible. By changing I_{dc} we find that only one minima increases in depth, while the other remains nearly unaffected. This originates from two contributions that lead to changes in the magnon density. On the one hand, the magnon density underneath the modulator manipulated via the SHE (scaling linear with I_{dc}) only increases for $\mathbf{H} \parallel -\mathbf{y}$ (for positive current polarity), but decreases for $\mathbf{H} \parallel \mathbf{y}$. On the other hand, the finite Joule heating (scaling quadratically with I_{dc}) leads to a heating induced increase in magnon density independent of the magnetic field orientation. Following this argumentation, we find that for $\mathbf{H} \parallel -\mathbf{y}$, both SHE and Joule heating increase the magnon density and thus the measured detector signal. In contrast, for $\mathbf{H} \parallel \mathbf{y}$ both effects compensate each other and we thus observe no significant change in magnon transport.

For a better quantitative comparison, we extract the amplitudes $A(+\mu_0 H)$ (at $\mathbf{H} \parallel -\mathbf{y}$) and $A(-\mu_0 H)$ (at $\mathbf{H} \parallel \mathbf{y}$) as a function of I_{dc} (see Fig. 2(b)). For $|I_{\text{dc}}| \leq 400\,\mu\text{A}$, we find a linear and quadratic dependence of A on I_{dc}. However, for larger current values we observe for $\mu_0 H = 50\,\text{mT}$ and positive I_{dc} a strong increase in A, which levels of for $I_{\text{dc}} > I_{\text{crit}}$. In our recent publication [3] we showed that this critical current value can indeed be identified with the condition of magnon damping rate compensation. Moreover, we found good quantitative agreement with theoretical calculations [4] that predict the formation of a magnon Bose-Einstein condensate for large enough magnon densities under the modulator strip. This ground-breaking work enables us to gain experimental access to this regime via all-electrical means and explore new phenomena associated with the condensation of magnons.

References

[1] S. T. B. Goennenwein, R. Schlitz, M. Pernpeintner, K. Ganzhorn, M. Althammer, R. Gross, and H. Huebl, Appl. Phys. Lett. **107**, 172405 (2015).
[2] L. J. Cornelissen, J. Liu, B. J. van Wees, and R. A. Duine, Phys. Rev. Lett. **120**, 097702 (2018).
[3] T. Wimmer, M. Althammer, L. Liensberger, N. Vlietstra, S. Geprägs, M. Weiler, R. Gross, and H. Huebl, Phys. Rev. Lett. **123**, 257201 (2019).
[4] S. A. Bender, R. A. Duine, A. Brataas, and Y. Tserkovnyak, Phys. Rev. B **90**, 094409 (2014).

Exchange-enhanced Ultrastrong Magnon-Magnon Coupling in a Compensated Ferrimagnet

L. Liensberger, H. Maier-Flaig, S. Geprägs, A. Erb, R. Gross, H. Huebl, M. Weiler [1]
A. Kamra,[2,3] *S. T. B. Goennenwein,*[4] *W. Belzig*[5,6]

Antiferromagnets and ferrimagnets are promising candidates for future spintronic devices due to the co-existence of two magnetic sublattices, leading to multiple magnonic modes. The coherent control and engineering of their rich spin dynamics opens applications in magnonics [1] and antiferromagnetic spintronics [2]. The typical magnetic resonance dynamics in antiferromagnets in the THz-range makes them however experimentally challenging to investigate. Compensated ferrimagnets in contrast allow us to tune the sublattice magnetizations to bring their resonance frequencies down to the GHz-range. This makes them ideal candidates to investigate coupled spin dynamics in the quasi-antiferromagnetic limit. The coupling between magnon modes in two magnetic materials mediated by the weak interlayer exchange interaction has been recently demonstrated. Nevertheless, the much stronger intrinsic exchange interaction has not been utilized to explore magnon-magnon coupling phenomena.

Here, we experimentally investigate the magnetization dynamics in a compensated, effectively two-sublattice ferrimagnet in the collinear state [3]. Close to the compensation temperature, this system mimics a quasi-antiferromagnet due to the almost identical sublattice magnetizations $M_\mathrm{A} \gtrsim M_\mathrm{B}$. In a classical description of the uniform spin dynamics, the eigenmodes of the system are either precessing in the clockwise or in the counterclockwise direction, corresponding to spin-down or spin-up magnons. We are here particularly interested in studying the coupling between these two distinctive magnon modes to form a novel hybrid, linearly polarized spin excitation.

Such a mode hybridization requires two ingredients: First, mode coupling can only take place if a spin-up magnon can be coupled to its spin-down counterpart by a mechanism that violates the conservation of spin along the sublattice magnetization, and thus magnon spin direction [4]. Therefore, an anisotropy about the magnon spin axis is required to break the rotational invariance for the magnon modes to couple. Second, the weak magnetocrystalline anisotropy itself cannot yield large coupling effects. However, this weak coupling can in principle be strongly enhanced in quasi-antiferromagnets due to the two large, nearly equal and opposite spins on the two sublattices [5]. This so-called exchange enhancement provides a pathway to obtain much stronger coupling effects than we previously observed in magnetic heterostructures [6].

In our experiments, we study spin dynamics in a (111)-oriented single crystalline gadolinium iron garnet ($\mathrm{Gd_3Fe_5O_{12}}$, GdIG) by broadband ferromagnetic resonance spectroscopy with a vector network analyzer (VNA) as schematically depicted in Fig. 1(a). All experiments are performed at $T = 282\,\mathrm{K}$, slightly below the GdIG compensation point $T_\mathrm{comp} = 288\,\mathrm{K}$. We record the complex transmission parameter S_{21} as a function of the microwave frequency f for a fixed magnetic field $\mathbf{H}_0$ applied in the (111)-plane of the GdIG disk. We repeat these experiments for a range of magnetic field amplitudes H_0 and extract the resonance frequencies

---

[1] Financial support by the DFG via projects WE 5386/4-1 and WE 5386/5-1 and via Germany's Excellence Strategy (EXC-2111-390814868) is gratefully acknowledged.

[2] Center for Quantum Spintronics, Department of Physics, NTNU, Trondheim, Norway

[3] Financial support by the Research Council of Norway through its Centers of Excellence funding scheme, Project No. 262633 "QuSpin" is gratefully acknowledged.

[4] Institut für Festkörper- und Materialphysik, Technische Universität Dresden, Germany

[5] Department of Physics, University of Konstanz, Germany

[6] Financial support by the DFG through "SFB 767" is gratefully acknowledged.

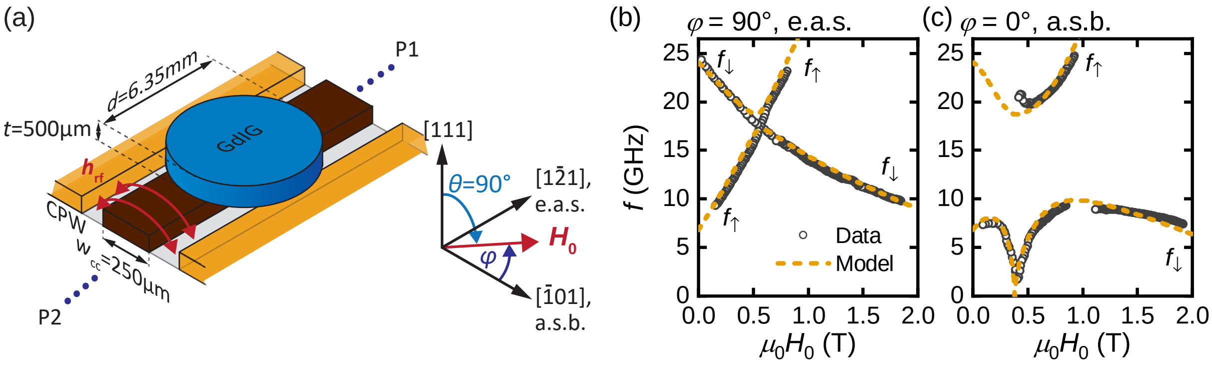

Figure 1: (a) Schematic broadband ferromagnetic resonance setup, with the GdIG disk on the coplanar waveguide (CPW). The angle φ defines the in-plane direction of the magnetic field $\boldsymbol{H}_0$. (b),(c) Mode frequencies f vs. applied magnetic field strength H_0 measured at $T = 282\,\mathrm{K}$ where $M_{\mathrm{Gd}} \gtrsim M_{\mathrm{Fe}}$. Open circles denote the measured resonance frequencies and dashed lines are model calculations.

f_{res} and the linewidths of the two observed magnon modes. The main results are presented in Fig. 1(b) and (c).

In our experiments, we observed a tuneable coupling between the two magnon modes dependent on the direction of the external magnetic field in the (111)-plane. If the static external magnetic field $\boldsymbol{H}_0$ is applied along an effectively axially symmetric (e.a.s.) direction of the magnetocrystalline anisotropy, we find weak coupling between the spin-up and spin-down magnons as evidenced by the crossing of the spin-up $f^\uparrow$ and spin-down $f^\downarrow$ dispersions in Fig. 1(b). By changing the direction of the magnetic field by 90° to a direction with broken axial symmetry (a.s.b.) of the magnetocrystalline anisotropy, we observe strong coupling between the two magnon modes (cf. Fig. 1(c)). The extracted coupling strength $g_c/2\pi = 6.38\,\mathrm{GHz}$ is much larger than the intrinsic linewidth of both magnon modes [3] and comparable to the intrinsic excitation frequency of $f_r = 17.2\,\mathrm{GHz}$. This results in a normalized coupling rate of $\eta = g_c/(2\pi f_r) = 0.37$. Consequently, we observe magnon-magnon hybridization in the ultrastrong coupling regime.

Our experimental results are in good agreement with model calculations (dashed lines in Fig. 1(b) and (c)) based on solving the coupled Landau-Lifshitz equations for the two magnetic sublattices, taking into account the cubic magnetocrystalline anisotropy of GdIG. Our findings demonstrate that weak magnetocrystalline anisotropies can lead to giant effects on spin dynamics if the conditions for exchange-enhancement are fulfilled. This opens exciting perspectives for studying ultrastrong coupling effects in nanoscale devices and exploring quantum-mechanical coupling phenomena beyond classical electrodynamics.

References

[1] A. V. Chumak, V. I. Vasyuchka, A. A. Serga, and B. Hillebrands, Nat. Phys. **11**, 453 (2015).

[2] P. Wadley, B. Howells, J. Elezny, C. Andrews, V. Hills, R. P. Campion, V. Novak, K. Olejnik, F. Maccherozzi, S. S. Dhesi, S. Y. Martin, T. Wagner, J. Wunderlich, F. Freimuth, Y. Mokrousov, J. Kune, J. S. Chauhan, M. J. Grzybowski, A. W. Rushforth, K. W. Edmonds, B. L. Gallagher, and T. Jungwirth, Science **351**, 587 (2016).

[3] L. Liensberger, A. Kamra, H. Maier-Flaig, S. Geprägs, A. Erb, S. T. B. Goennenwein, R. Gross, W. Belzig, H. Huebl, and M. Weiler, Phys. Rev. Lett. **123**, 117204 (2019).

[4] A. Kamra, U. Agrawal, and W. Belzig, Phys. Rev. B **96**, 020411(R) (2017).

[5] A. Kamra, E. Thingstad, G. Rastelli, R. A. Duine, A. Brataas, W. Belzig, and A. Sudbø, Phys. Rev. B **100**, 174407 (2019).

[6] S. Klingler, V. Amin, S. Geprägs, K. Ganzhorn, H. Maier-Flaig, M. Althammer, H. Huebl, R. Gross, R. D. McMichael, M. D. Stiles, S. T. Goennenwein, and M. Weiler, Phys. Rev. Lett. **120**, 127201 (2018).

Large spin Hall magnetoresistance in antiferromagnetic α-Fe_2O_3/Pt

J. Fischer[1]*, M. Althammer, H. Huebl, R. Gross, S. Geprägs, M. Opel* [2]

Despite lacking a net macroscopic magnetization, antiferromagnetic (AF) materials have moved into the focus of spintronics research. This class of magnetic materials brings along two important advantages compared to ferromagnets: (i) better scalability and higher robustness against magnetic field perturbations and (ii) orders of magnitudes faster dynamics and switching times. From an application perspective, however, it is evident that their vanishing net moment and stray fields call for new magnetization control and read-out strategies. Spin currents were shown to interact with individual magnetic sublattices via spin transfer torques. A particular manifestation is the dependence of the resistivity of a metallic thin film with large spin-orbit coupling on the direction of the magnetization in an adjacent material with long range magnetic order, denoted as spin Hall magnetoresistance (SMR). In our seminal work in ferrimagnetic $Y_3Fe_5O_{12}$/Pt bilayers, we demonstrated that the SMR manifests itself as a sinusoidal oscillation of the Pt resistivity, characterized by amplitude and phase [1]. For the SMR in *anti*ferromagnetic NiO/Pt, we reported a phase shift of 90°, since the AF ordered magnetic sublattices are oriented orthogonal to the applied magnetic field [2, 3]. The SMR amplitude, however, is still a matter of debate. Here, we substantially complement the SMR data by investigating AF α-Fe_2O_3/Pt bilayers.

The AF electrical insulator α-Fe_2O_3 (hematite) can be described in the hexagonal system and exhibits a Néel temperature of 953 K. We study α-Fe_2O_3/Pt bilayer heterostructures, fabricated at WMI on single crystalline, (0001)-oriented Al_2O_3 [4]. We restrict our investigation to room temperature, where the Fe^{3+} ions order ferromagnetically in the easy (0001) planes, which form an AF "$+--+$" sequence. For transport measurements, a Hall bar was patterned into the bilayer via optical lithography and Ar ion milling. For a dc current of $\pm 100\,\mu$A applied in the $[10\bar{1}0]$ direction, the longitudinal (ρ_{long}) and the transverse (ρ_{trans}) resistivities are measured. Similar to the situation in NiO [2, 3], α-Fe_2O_3 displays three AF domains rotated by 120° with respect to each other and a domain population dependent on the direction and magnitude of the external magnetic field. We perform angle-dependent magnetoresistance (ADMR) measurements by rotating an external magnetic field $\mathbf{H}$ in three orthogonal planes: in the (0001)-plane ("ip"), the $(10\bar{1}0)$- ("oopj"), and the $(1\bar{2}10)$-plane ("oopt") (Fig. 1).

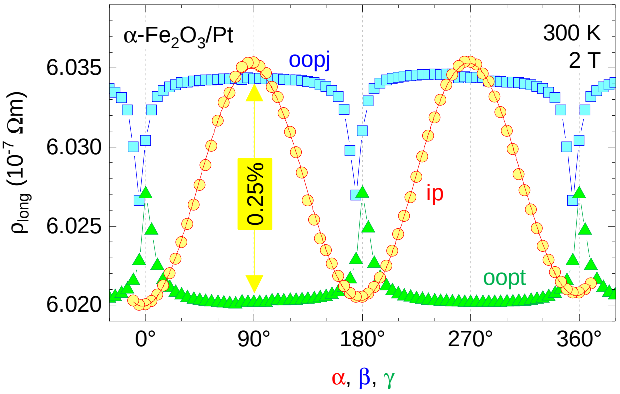

Figure 1: ADMR of a (0001)-oriented α-Fe_2O_3/Pt heterostructure. The longitudinal resistivity ρ_{long} (symbols) is recorded at 300 K while an external magnetic field of 2 T is rotated in three different planes: in the film plane (ip, angle α, red circles), perpendicular to the current direction $\mathbf{j}$ (oopj, β, blue squares), and perpendicular to the transverse direction $\mathbf{t}$ (oopt, γ, green triangles). The red line is a fit to the ip data according to Eq. (1).

For the oopj and oopt rotations, ρ_{long} changes significantly only close to $\mathbf{H}\perp(0001)$ for $\beta = \gamma = 0°, 180°, 360°$ (Fig. 1). According to the SMR model for a multidomain antifer-

---

[1] Present address: Unité Mixte de Physique, CNRS/Thales, Université Paris-Sud, Palaiseau, France

[2] We gratefully acknowledge financial support by the German Research Foundation via Germany's Excellence Strategy (EXC-2111-390814868).

romagnet [2, 3], we interpret this observation with the “decay” into a three-domain state, whenever **H** points orthogonal to the (0001) plane [4]. For ip rotations, $\rho_{\text{long}}(\alpha)$ displays the characteristic SMR oscillations (Fig. 1). The minima and maxima represent the signature of the AF (“negative”) SMR [2, 3] with a phase shift of 90° compared to the ferromagnetic (“positive”) SMR in ferrimagnetic $Y_3Fe_5O_{12}$/Pt [1]. However, the measured SMR amplitude is as high as 0.25%, larger than for any other reported bilayer compound so far.

We further perform ip ADMR measurements of ρ_{long} at different magnitudes of the magnetic field from 10 mT to 17 T. The data are well described by

$$\rho_{\text{long}} = \rho_0 + \frac{\rho_1}{2}(1 - \cos 2\alpha) \tag{1}$$

(red line in Fig. 1) with ρ_0 approximately equal to the normal resistivity of the Pt layer and ρ_1 representing the longitudinal SMR coefficient. This angular dependence is fully consistent with the model introduced earlier for NiO/Pt [2, 3] and clearly shows that our α-Fe_2O_3 is AF with the resistivity of Pt being sensitive to the Néel vector, which rotates coherently in the easy (0001) plane perpendicular to **H** [4].

For a detailed analysis of the field dependence of ρ_{long}, we fit our data according to Eq. (1) (red solid line in Fig. 1) and plot the SMR amplitude SMR_{long} as a function of the magnetic field magnitude (Fig. 2). We find a field evolution qualitatively different from the one in AF NiO/Pt [2, 3]. In α-Fe_2O_3/Pt, SMR_{long} saturates already around 3 T and then gradually decreases again from 5 T to 17 T. This gradual decrease can be traced back to an increasing canting of the AF sublattices. The fast saturation, on the other hand, points to a lower destressing energy compared to NiO.

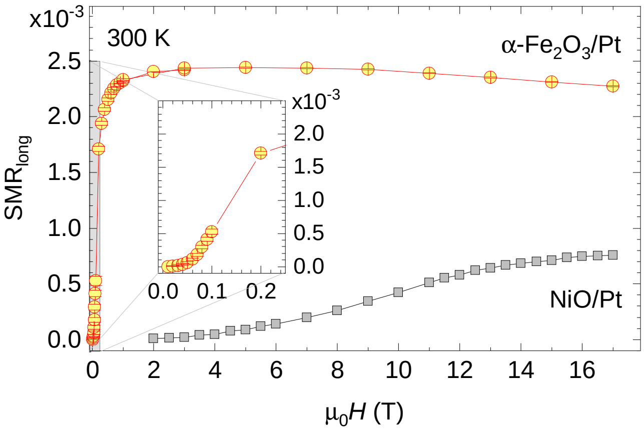

Figure 2: SMR amplitudes SMR_{long} (red circles) of a (0001)-oriented α-Fe_2O_3/Pt heterostructure, derived from ADMR measurements at 300 K in different external magnetic fields H. The earlier data of (111)-oriented NiO/Pt taken from Ref. [3] are shown for comparison (black squares).

In summary, we find a surprisingly large SMR amplitude of 0.25% in AF α-Fe_2O_3/Pt [4], much higher than in AF NiO/Pt [2, 3] and twice as large as in ferrimagnetic $Y_3Fe_5O_{12}$/Pt [1]. This finding supports the picture that both AF sublattices contribute to the SMR at the interface, regardless of the material’s net magnetization. The large SMR amplitude together with a moderate saturation field of ∼3 T establishes α-Fe_2O_3/Pt as a viable future SMR source and paves the way towards room temperature AF spintronic applications.

References

[1] H. Nakayama, M. Althammer, Y.-T. Chen, K. Uchida, Y. Kajiwara, D. Kikuchi, T. Ohtani, S. Geprägs, M. Opel, S. Takahashi, R. Gross, G. E. W. Bauer, S. T. B. Goennenwein, and E. Saitoh, Phys. Rev. Lett. **110**, 206601 (2013).

[2] J. Fischer, K. Ganzhorn, N. Vlietstra, M. Althammer, H. Huebl, M. Opel, R. Gross, S. Geprägs, O. Gomonay, R. Schlitz, and S. Goennenwein, WMI Ann. Rep. **2017**, 47–49 (2017).

[3] J. Fischer, O. Gomonay, R. Schlitz, K. Ganzhorn, N. Vlietstra, M. Althammer, H. Huebl, M. Opel, R. Gross, S. T. B. Goennenwein, and S. Geprägs, Phys. Rev. B **97**, 014417 (2018).

[4] J. Fischer, M. Althammer, N. Vlietstra, H. Huebl, S. T. Goennenwein, R. Gross, S. Geprägs, and M. Opel, Phys. Rev. Appl. submitted (2019).

High Spin-Wave Propagation Length Consistent with Low Damping in a Metallic Ferromagnet

L. Flacke, L. Liensberger, M. Althammer, H. Huebl, S. Geprägs, R. Gross, M. Weiler [1]
K. Schultheiss, A. Buzdakov, T. Hula, H. Schultheiss [2,3]
E. R. J. Edwards, H. T. Nembach, J. M. Shaw [4]

Spintronic devices offer alternative and complementary approaches to semiconductor transistor technology, since they make use of the electronic spin degree of freedom for information storage and processing. Novel functionalities are intensively sought after, especially in the field of magnon spintronics, where quantized spin waves are used as information carriers. Besides employing spin transfer and spin orbit torques, the implementation of magnonic devices relies on efficient spin wave (SW) propagation. Thus, a crucial material parameter for magnonic devices is a low magnetic damping rate, in combination with highly efficient spin torques typically found in metallic heterostructures.

Recently, Schoen *et al.* [1] reported ultra-low damping in $Co_{25}Fe_{75}$ (CoFe). This triggered the work reported on here [2]. We systematically investigate magnetic damping, spin pumping contributions, and SW propagation lengths (PL) in sputter-deposited heterostructures containing CoFe as a ferromagnetic (FM) layer.

To this end, we deposit several heterostructure samples of Ta(3 nm)/Cu(3 nm)/CoFe(t nm)/Cu(3 nm)/Ta(3 nm) with varying thickness t via magnetron sputtering. The dynamic magnetic properties and, hence, the damping are measured by broad-band ferromagnetic resonance spectroscopy using a vector network analyzer. The slope of the resonance linewidth vs. frequency plots allows us to determine the phenomenological Gilbert damping parameter α. In Fig. 1(a), the linewidth vs. frequency dependence of two exemplary samples with thickness t =1.8 nm and t =26 nm is presented. After subtraction of extrinsic contributions to α, due to radiative damping and eddy currents, we find that spin pumping [3] is the dominant contribution to α in our samples. This is corroborated by the linear dependence of α on the inverse thickness of the ferromagnet as shown in Fig. 1(b). That is, spin pumping associated with the emission and absorption of spin angular momentum into the adjacent metals well describes the damping of the magnetization dynamics in CoFe. From the intercept of the red line in Fig. 1(b), we find a new record low intrinsic damping value for metallic ferromagnets $\alpha_0 \leq 3.18 \times 10^{-4}$.

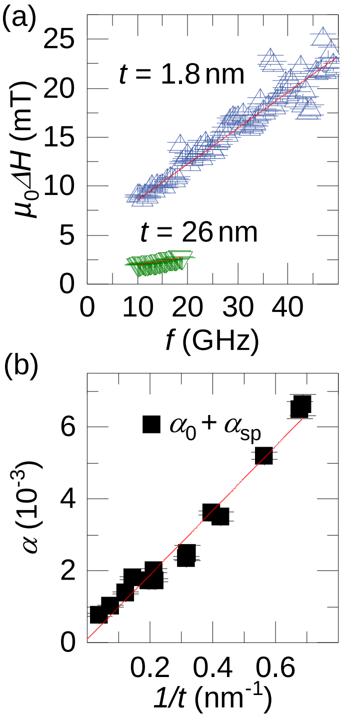

Figure 1: (a) Resonance linewidth of two Ta(3 nm)/Cu(3 nm)/CoFe(t nm)/Cu(3 nm)/Ta(3 nm) samples with t = 1.8 nm and t = 26 nm. The Gilbert damping parameter is extracted from the slope of the red fit. (b) $\alpha_0 + \alpha_{sp}$ (intrinsic and spin pumping contribution) vs. the reciprocal thickness of the FM thickness are plotted. The red line is a fit to the data. The intercept is given by α_0 and the slope depends on α_{sp}.

The low magnetic damping rate is expected to have a direct impact on the spin wave propagation length (SWPL), as the lifetime of magnons increases with decreasing damping. To

---

[1] Financial support of the German Research Foundation via projects WE5386/4-1, WE5386/5-1, and Germany's Excellence Strategy (EXC-2111-390814868) is gratefully acknowledged.

[2] Helmholtz-Zentrum Dresden-Rossendorf, 01328 Dresden, Germany

[3] Financial support of the German Research Foundation via project SCHU2922/1 is gratefully acknowledged.

[4] Quantum Electromagnetics Division, NIST, Boulder, Colorado 80305, USA

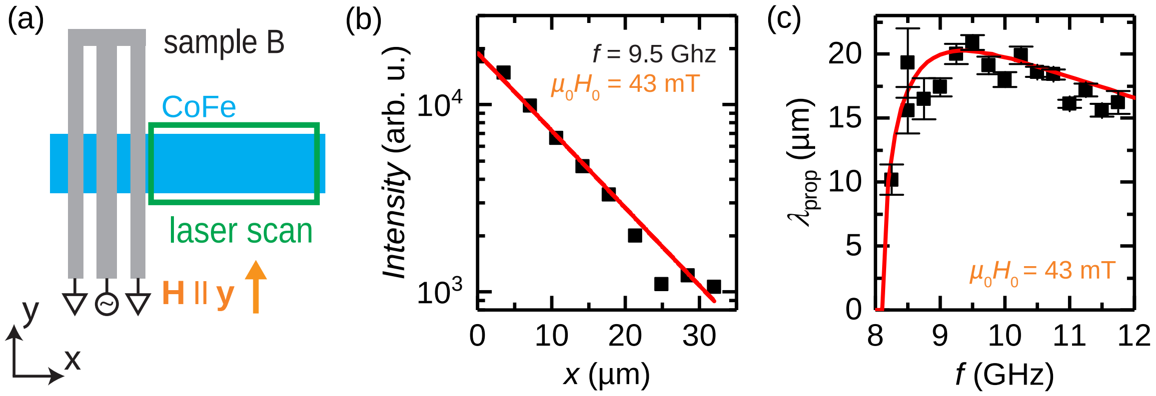

Figure 2: (a) A top view sketch of the sample structure. The gold antenna is used to excite spin dynamics in the strip magnetized along the y-direction. (b) The intensity decays exponentially with distance from the antenna. The decay length is extracted from the fit and plotted vs. frequency in (c). The red curve in (c) is a model prediction based on measured parameters and Kalinikos-Slavin's spin wave dispersion.

confirm this conjecture, we measure Brillouin light scattering (BLS) on microstructured samples in order to obtain the actual SWPL within the metal stacks. A 5 μm by 100 μm strip consisting of Pt(3 nm)/Cu(3 nm)/CoFe(26 nm)/Cu(3 nm)/Ta(3 nm) together with a coplanar waveguide gold antenna is fabricated by e-beam lithography. A simple sketch of this device is depicted in Fig. 2(a).

An external magnetic field is applied perpendicular to the strip in order to excite Damon-Eshbach modes, which exhibit high SW group velocities between $10\,\mathrm{km\,s^{-1}}$ and $17\,\mathrm{km\,s^{-1}}$ due to the high saturation magnetization of CoFe. The SW intensity is recorded with a laser spot, which is scanned across the CoFe strip. The resulting x-dependence of the SW intensity is plotted in Fig. 2 (b). From the fit of the exponential decay the characteristic SW PL is extracted. The frequency dependence of the PL is shown in Fig. 2 (c), revealing a maximum SWPL of more than 20 μm. This value is comparable to common SWPL in Yttrium Iron Garnet (YIG) thin films [4]. The red line in Fig. 2 (c) is the result of a model based on $\lambda_{\mathrm{prop}} = v_{\mathrm{g}}\tau$, with the group velocity v_{g} and the lifetime τ of the SW. We calculate v_{g} from Kalinikos and Slavin's SW dispersion for $\mathbf{k}_{\mathrm{x}} \perp \mathrm{M}$ [5] and obtain τ from the solution to the Landau-Lifshitz-Gilbert equation and the measured α. This model is in excellent agreement with our data and, hence, confirms the low damping of our structures.

In summary, we were able to optimize the magnetic damping of CoFe thin-film heterostructures to a new record low damping value and measured the highest SWPL in metallic thin films so far. The SWPL is comparable to those found in YIG thin films, while our all-metallic heterostructures unite the benefits of low damping, high saturation magnetization, high SW group velocities, electrical conductivity, and easy and fast fabrication methods. Thus, magnonic devices based on CoFe have considerable great application potential in magnonics.

References

[1] M. A. W. Schoen, D. Thonig, M. L. Schneider, T. J. Silva, H. T. Nembach, O. Eriksson, O. Karis, and J. S. Shaw, Nat. Phys. **12**, 839 (2016).
[2] L. Flacke, L. Liensberger, M. Althammer, H. Huebl, S. Geprägs, K. Schultheiss, A. Buzdakov, T. Hula, H. Schultheiss, E. R. J. Edwards, H. T. Nembach, J. M. Shaw, R. Gross, and M. Weiler, Appl. Phys. Lett. **115**, 122402 (2019).
[3] Y. Tserkovnyak, A. Brataas, and G. Bauer, Phys. Rev. Lett. **88**, 117601 (2002).
[4] M. Collet, O. Gladii, M. Evelt, V. Bessonov, L. Soumah, P. Bortolotti, S. O. Dekomritov, Y. Henry, V. Cros, M. Bailleul, V. E. Demidov, and A. Anane, Appl. Phys. Lett. **110**, 092408 (2017).
[5] B. A. Kalinikos, and A. N. Slavin, J. Phys. C. **19**, 7013 (1986).

Quantum Fisher Information of Remotely Prepared Squeezed Microwave States

S. Pogorzalek, K. G. Fedorov, Q. Chen, Y. Nojiri, M. Renger, M. Partanen, A. Marx, F. Deppe, R. Gross [1]

In quantum information science, efficient means of communicating information play a central role. In our previous work [1], we realized remote state preparation (RSP) of propagating squeezed microwave states. For this fundamental quantum communication protocol, the goal is to prepare a known quantum state at a distant location. However, one can also consider to use RSP for communication of classical information. In such a scenario, the classical parameters of the prepared squeezed state are regarded as transmitted classical information.

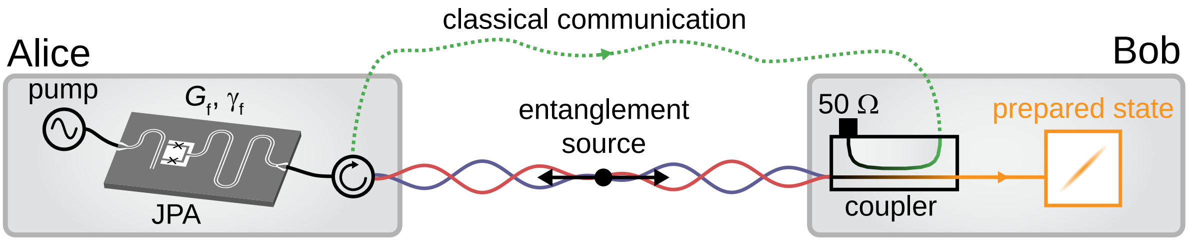

Figure 1: Schematic of experimentally implemented RSP using propagating microwaves. A two-mode squeezed state serves as an entangled resource. Alice decides on the prepared state by adjusting the feedforward gain G_f and feedforward angle γ_f of a JPA on her side. Bob obtains the target state by applying a unitary local operation, implemented with a directional coupler, on his part of the entangled state using the feedforward signal (classical communication).

In order to characterize how well we can encode information in a parameter θ of the prepared squeezed states, we use the quantum Fisher information (QFI). One way to define the QFI [2]

$$F_\theta = 4 \lim_{\epsilon\to 0} \frac{d_\mathrm{B}^2(\rho_\theta,\rho_{\theta+\epsilon})}{\epsilon^2} = 8 \lim_{\epsilon\to 0} \frac{1-\sqrt{f(\rho_\theta,\rho_{\theta+\epsilon})}}{\epsilon^2} \tag{1}$$

is via the Bures distance $d_\mathrm{B}^2(\rho_1,\rho_2) = 2\big(1-\sqrt{f(\rho_1,\rho_2)}\big)$ between two quantum states characterized by their density matrices $\rho_{1,2}$. Here, we use the Uhlmann fidelity $f(\rho_1,\rho_2) = \big(\mathrm{Tr}\sqrt{\sqrt{\rho_1}\rho_2\sqrt{\rho_1}}\big)^2$. The QFI quantifies how well we can distinguish between two quantum states ρ_θ and $\rho_{\theta+\epsilon}$. If the quantum state ρ_θ only weakly depends on θ, the QFI F_θ is small. On the other hand, if small changes in θ strongly alter ρ_θ, one obtains large values of F_θ. For general Gaussian states, one can find analytic expressions for F_θ in respect to various parameters of the Gaussian states. Here, we consider the squeezing phase φ of the prepared Gaussian squeezed state. For this parameter, the QFI is given by [3]

$$F_\varphi = \frac{1}{1+\mu^2}\frac{(1-\lambda^2)^2}{\lambda^2}, \tag{2}$$

where μ is the purity of the state and $\lambda = e^{-2r}$. We obtain the squeezing parameter r from the experimentally measured squeezed variance and antisqueezed variance, which we write as $\sigma_\mathrm{s}^2 = (1+2n_\mathrm{th})e^{-2r}/4$ and $\sigma_\mathrm{a}^2 = (1+2n_\mathrm{th})e^{2r}/4$, respectively. Here, n_th describes the thermal photon population of the prepared squeezed state.

We have used Eq. (2) to calculate F_φ for the prepared states during RSP. The result is shown in Fig. 2(a). We observe that the optimal operation point of RSP, where we achieve the highest

---

[1] We acknowledge support by Germany's Excellence Strategy (EXC-2111-390814868), the Elite Network of Bavaria through the program ExQM, and the EU Quantum Flagship via QMiCS (Grant No. 820505).

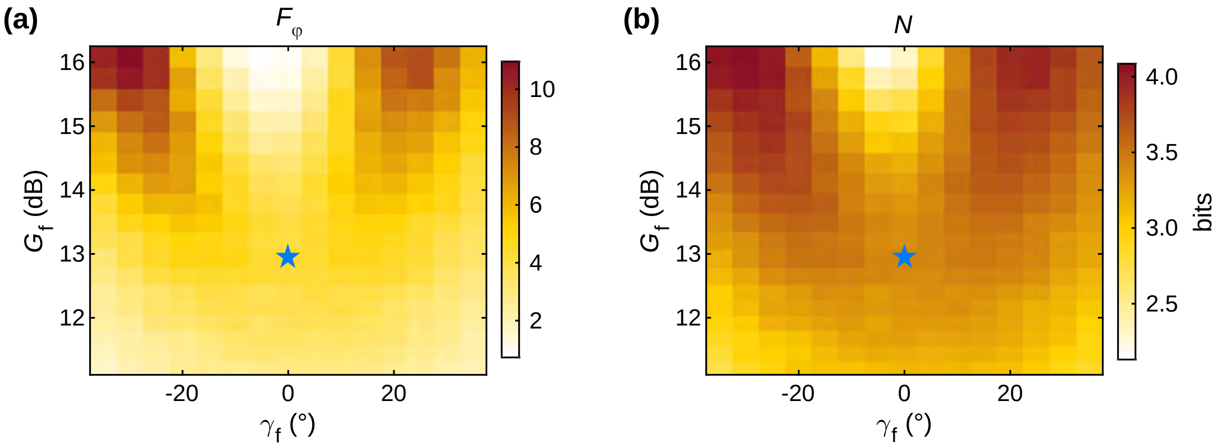

Figure 2: **(a)** Quantum Fisher information F_φ of the squeezing phase φ for the prepared states during RSP. **(b)** Upper bound of the effective number of bits N extractable from the squeezing phase φ. The prepared states are determined by the feedforward angle γ_f and the feedforward gain G_f. The optimal point of RSP is marked with the blue star.

purity of the prepared states, is not the best point for communication of classical information encoded in the squeezing phase φ. In particular, F_φ exhibits comparatively small values at the optimal point while much larger values can be reached away from this point. Intuitively, this observation can be understood by considering the squeezing level and antisqueezing level of the prepared squeezed states. For regions of high F_φ, the prepared states are squeezed below the vacuum limit and posses a comparatively high antisqueezing level (see Ref. [1] for details). Consequently, φ can be more precisely estimated in these regions compared to the optimal point, where the antisqueezing level is lower.

To quantify the amount of classical information sent via the prepared squeezed state, we estimate the effective number of bits N by assuming an ideal analog-to-digital converter which samples the reconstructed squeezing phase φ of the prepared state. When neglecting distortion effects of the signal, we can define $N = (\mathrm{SNR} - 1.76\,\mathrm{dB})/6.02\,\mathrm{dB}$ [4], where $\mathrm{SNR} = 10\log_{10}\left[\Delta\varphi^2/\sigma_\varphi^2\right]$ is the signal-to-noise ratio in decibel. Here, $\Delta\varphi = 2\pi$ is the full range of squeezing phases of a squeezed state and σ_φ is the standard deviation of φ. To obtain a lower bound for σ_φ, we use the quantum Cramér-Rao bound [5], which relates the quantum Fisher information to a lower bound of the estimation error of φ as $\sigma_\varphi^2 \leq 1/F_\varphi$. In Fig. 2(b), we show the resulting effective number of bits N for the prepared states. Similar as for F_φ, we observe the highest values of N of up to 4.1 bits away from the optimal point of RSP.

In summary, we have investigated the capability of RSP to transmit classical information encoded into the squeezing phase of the prepared state. Interestingly, the optimal point of quantum RSP, where we obtain the highest purity of prepared squeezed states, is not optimal for sending classical information. By using the Cramér-Rao bound, we find a maximal number of sent bits to be 4.1 bits per remotely prepared state.

References

[1] S. Pogorzalek, K. G. Fedorov, M. Xu, A. Parra-Rodriguez, M. Sanz, M. Fischer, E. Xie, K. Inomata, Y. Nakamura, E. Solano, A. Marx, F. Deppe, and R. Gross, Nat. Commun. **10**, 2604 (2019).
[2] D. Šafránek, A. R. Lee, and I. Fuentes, New J. Phys. **17**, 073016 (2015).
[3] O. Pinel, P. Jian, N. Treps, C. Fabre, and D. Braun, Phys. Rev. A **88**, 040102 (2013).
[4] W. Kester. *Data Conversion Handbook* (Elsevier, Oxford, 2005).
[5] S. L. Braunstein, and C. M. Caves, Phys. Rev. Lett. **72**, 3439 (1994).

Measuring the Imaginary Time Dynamics of Quantum Materials

D. Jost, T. Böhm, R. Hackl [1]
S. Lederer [2], *E. Berg*[3], *S. A. Kivelson*[4]

Theoretical approaches to condensed matter physics often work exclusively in the imaginary time domain. Such results cannot be compared directly to real-time experimental results. Analytic continuation allows one to determine response functions thereof on the real time axis, but introduces additional uncertainties. A way out of this dilemma is to reverse the problem by deriving the imaginary time correlation function $\tilde{\Lambda}(\tau)$ from experimental data. Generally, one can show, that the imaginary part of a response function $\chi''(\Omega, T)$ relates to $\tilde{\Lambda}(\tau)$ as

$$\tilde{\Lambda}(\tau) = \int \frac{d\Omega}{2\pi}\, \chi''(\Omega, T)\, \frac{\exp[\Omega(\tau - \beta/2)]}{\sinh[\Omega\beta/2]} \qquad (1)$$

with $\beta = 1/k_B T$. Inelastic light scattering experiments measure $\chi''(\Omega, T)$. Thereby, a transformation to imaginary times is straightforward and examples are shown in Fig. 1.

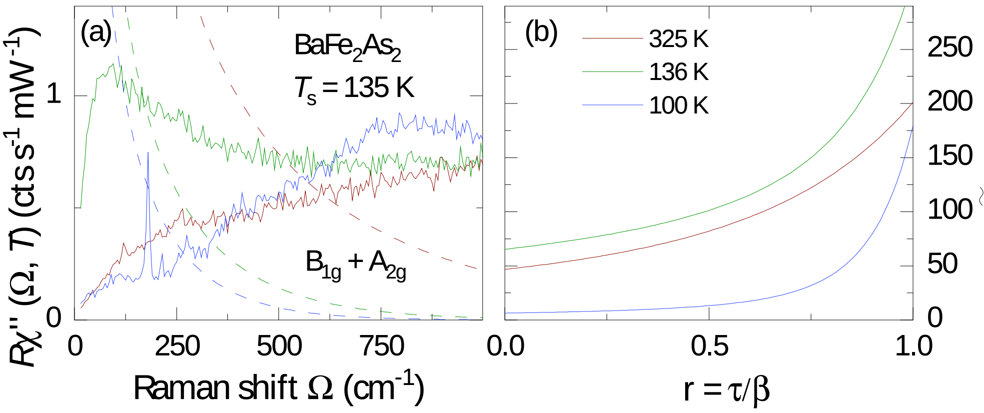

Figure 1: (a) Real frequency response $\chi''(\Omega, T)$ of BaFe$_2$As$_2$ undergoing a structural phase transition at $T_s = 135$ K which is dominated by particle-hole excitations at high temperatures (dark red). Close to the phase transition, fluctuations generate a low-frequency pile-up of spectral weight (green), collapsing below T_s. The dashed lines represent the weighting factor $[\sinh(\beta\Omega/2)]^{-1}$ for temperatures as indicated. (b) Imaginary-time ordered correlation function $\tilde{\Lambda}(r, T)$ for times normalised to β. From Ref. [1].

Quantum Monte Carlo (QMC) simulations, as an example, measure the behaviour of $\tilde{\Lambda}$ for long imaginary times of order $\tau \sim \beta/2$. Here, one finds that $\beta\tilde{\Lambda}(\beta/2)$ is bounded by the static susceptibility via

$$\beta\tilde{\Lambda}(\beta/2) \leq \int \frac{d\Omega}{\pi} \frac{\chi''(\Omega, T)}{\Omega} = \chi'(0, T). \qquad (2)$$

Thus, $\beta\tilde{\Lambda}(\beta/2, T)$ contains the same universal information as the static susceptibility under a wide range of assumptions. For instance, at a continuous phase transition at non-zero temperature, $\beta\tilde{\Lambda}(\beta/2)$ diverges in a similar fashion as χ', as depicted in Fig. 2. However, there is an uncertainty in the inferred values of $\chi'(0, T)$ resulting from the cut off in the Kramers-Kronig integral. In this case the result depends logarithmically on the cut-off. In contrast, the weight-

---

[1] Financial support: Friedrich-Ebert-Stiftung (D.J.), the German Research Foundation via SPP 1458 (D.J., T.B., and R.H., project no. HA 2071/7-2), the Collaborative Research Center TRR80 (D.J. and R.H.), and the Bavaria California Technology Center BaCaTeC (S.A.K., D.J., and R.H., project no. 21[2016-2]).

[2] Cornell University, Ithaca, NY 14850, USA. S.L. was supported by a Bethe/KIC fellowship at Cornell.

[3] The Weizmann Institute of Science, Rehovot 76100, Israel. E.B. was supported by the ERC under grant HQMAT (817799).

[4] Stanford University, CA 94305, USA. S.A.K. was supported in part by NSF grant DMR-1608055.

ing factor $[\sinh(\beta\Omega/2)]^{-1}$ in Eq. (2) decays exponentially, making the integral of $\beta\tilde{\Lambda}(\beta/2)$ unique so long as the spectra are measured up to energies of a few times the temperature.

Framing the analysis in terms of $\tilde{\Lambda}(\beta/2, T)$ has three advantages: (i) It can be computed directly and unambiguously from the measured χ'', (ii) $\beta\tilde{\Lambda}(\beta/2, T)$ can be directly compared with theoretical predictions performed on the imaginary time axis, and (iii) the computation of $\tilde{\Lambda}(\tau, T)$ makes it possible to derive the "resistivity proxy" $\rho = \partial_\tau^2\tilde{\Lambda}/(2\pi\tilde{\Lambda}^2)|_{\tau=\beta/2}$ calculated in simulations [3, 4] which remains entirely inaccessible to the Kramers-Kronig transformation.

The advantages of the methods presented here extend to almost any experimental probe which measures response functions at frequencies on the order of temperature. Such probes include optical conductivity, where $\tilde{\Lambda}(\beta/2, T)$ yields a measure of the low frequency Drude weight. Using inelastic neutron scattering, the evolution of a spin gap can be assessed by a drop of $\tilde{\Lambda}(\beta/2, T)$. In angle resolved photo-emission spectroscopy, $\tilde{\Lambda}(\beta/2, T)$ can be a proxy of the quasiparticle residue. The direct determination of imaginary time response functions from experiment is a potentially powerful tool both for the quantification of low frequency spectral properties, and for bridging experiment and theory. The method is particularly useful for the analysis of scale-free spectral features evolving approximately proportional to temperature such as critical fluctuations or marginal behaviour being present in many correlated systems.

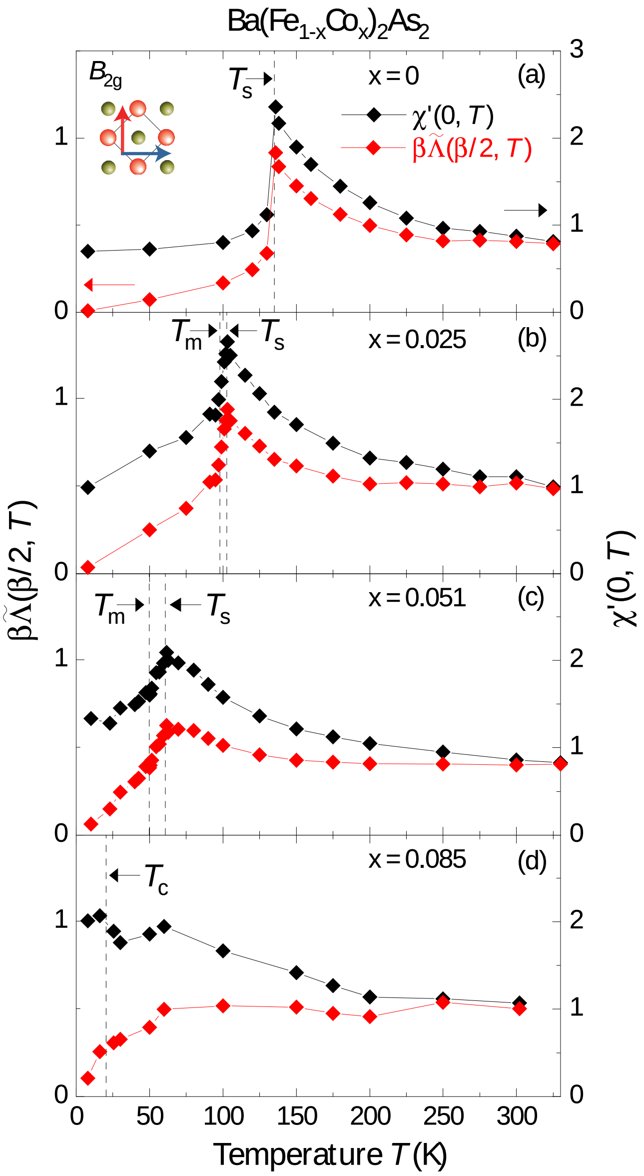

Figure 2: $\beta\tilde{\Lambda}(\beta/2)$ (red, left axis) and $\chi'(0, T)$ (black, right axis) of Raman data in the B_{2g} symmetry channel computed from the measured $\chi''(\Omega, T)$. Both quantities capture the singular temperature dependence of the Raman response near the structural transition. The two quantities differ most substantially near zero temperature, where $\tilde{\Lambda}(\beta/2, T \to 0)$ vanishes, since it captures the dynamics at frequencies of order T. From Ref. [2].

References

[1] D. Jost. *Cooper pairing and fluctuations in Fe-based compounds*. Ph.D. thesis, Technische Universität München (2019).

[2] S. Lederer, D. Jost, T. Böhm, R. Hackl, E. Berg, and S. Kivelson, arXiv e-prints (2019). `arXiv:1907.10182`.

[3] S. Lederer, Y. Schattner, E. Berg, and S. A. Kivelson, P. Natl. Acad. Sci. USA **114**, 4905–4910 (2017).

[4] E. W. Huang, R. Sheppard, B. Moritz, and T. P. Devereaux, Science **366**, 987–990 (2019).

Magnetic Origin of the Fermi Surface Reconstruction in the Electron-doped Cuprate Superconductor Nd$_{1.85}$Ce$_{0.15}$CuO$_4$

M. V. Kartsovnik, W. Biberacher, A. Erb, R. Gross [1]
T. Helm, E. Kampert, J. Wosnitza [2]
R. Ramazashvili, [3]*P. D. Grigoriev,* [4]

One of the central issues in the problem of high-T_c superconductivity in cuprates is the nature of the underlying strange metallic state. On the hole-doped side of the phase diagram, an intricate interplay between superconductivity and quasistatic charge order has been pointed out recently [1, 2]. On the electron-doped side, signatures of translational symmetry breaking have been found also for superconducting compounds. This is particularly seen in quantum oscillations of magnetoresistance (Shubnikov-de Haas (SdH) effect), which indicate a superstructure-induced reconstruction of the Fermi surface at doping levels covering the entire superconducting doping range [3]. However, the origin of the reconstruction remains unclear. While the $(\frac{\pi}{a}, \frac{\pi}{a})$ periodicity of the superstructure is compatible with the antiferromagnetic (AF) order observed in strongly underdoped, non-superconducting compounds, the coexistence of antiferromagnetism and superconductivity has been debated [4]. Alternative scenarios of the symmetry breaking have been proposed, including, in particular, charge order, which would imply a similarity with hole-doped cuprates [1].

We use the recently established Zeeman spin-orbit coupling (ZSOC) phenomenon in order to verify the role of antiferromagnetism in the Fermi surface reconstruction in the archetypal electron-doped cuprate Nd$_{2-x}$Ce$_x$CuO$_4$ (NCCO) at optimal doping, $x = 0.15$ [5]. A convenient probe for that is the angle dependence of SdH oscillations [6]. To this end, we have studied the SdH oscillations in NCCO in pulsed magnetic fields, in a broad range of the field orientations. The field was applied at different tilt angles θ with respect to the [001] axis, the normal to the CuO$_2$ layers, in the plane perpendicular to [100], as shown in the inset in Fig. 1.

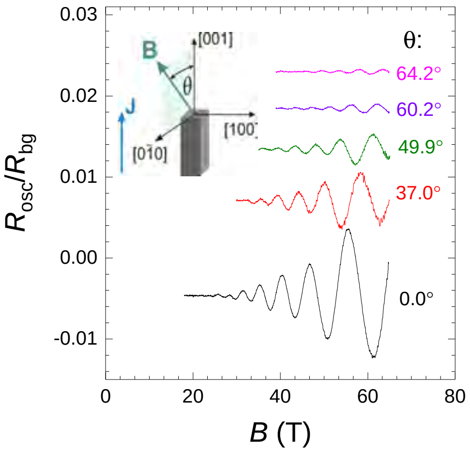

Figure 1: SdH oscillations in optimally doped NCCO at different field orientations. The oscillatory signal is normalized to the nonoscillating B-dependent background resistance. Inset: experimental configuration.

Fig. 1 shows examples of field sweeps of the interlayer resistance in optimally doped NCCO at different θ, at $T = 2.5$ K. The oscillations with the frequency $F \approx 290\,\mathrm{T}/\cos\theta$ originate from the small Fermi pocket presumably centered at the nodal point $(\frac{\pi}{2a}, \frac{\pi}{2a})$ of the Brillouin zone [3], see inset in Fig. 2. The $1/\cos\theta$ dependence points to a highly two-dimensional (2D) character of the electronic system. The angle dependence of the oscillation amplitude is plotted in the main panel of Fig. 2. The lines in Fig. 2 are fits to the experimental data using the standard Lifshitz-Kosevich (LK) formula [7] with different fixed values of the g-factor. The latter enters the LK formula via the spin reduction factor, which generally

---

[1] This work was supported by HLD at HZDR, a member of the European Magnetic Field Laboratory (EMFL).

[2] Hochfeld-Magnetlabor Dresden (HLD-EMFL) and Würzburg-Dresden Cluster of Excellence ct.qmat, Helmholtz-Zentrum Dresden-Rossendorf, Dresden, Germany

[3] Laboratoire de Physique Théorique, Université de Toulouse, CNRS, Toulouse, France.

[4] L. D. Landau Institute for Theoretical Physics, Chernogolovka, Russia. The work was supported in part by the Foundation for the Advancement of Theoretical Physics and Mathematics "BASIS".

oscillates with changing θ:

$$R_s(\theta) = \cos\left[\frac{\pi}{2} g \frac{m(\theta = 0)}{m_0 \cos\theta}\right], \tag{1}$$

where $m(\theta) = m(\theta = 0)/\cos\theta$ is the effective cyclotron mass on the associated orbit, and m_0 the free electron mass. Clearly, the experimental data are incompatible with a g-factor of the order of 2 expected from a conduction electron spin in a metal. On the other hand, an excellent fit to the data is achieved with $g = 0$, (solid red line in Fig. 2).

This highly unusual result can be consistently explained by the persistence of the $(\frac{\pi}{a}, \frac{\pi}{a})$ AF order in our superconducting sample, taking into account the novel ZSOC mechanism [5]. First of all, note that our field range of interest, $> 30\,\mathrm{T}$, by far exceeds the characteristic spin-flop field in NCCO, $B_{\mathrm{SF}} \approx 4\,\mathrm{T}$. Therefore, for all orientations except for a narrow interval $0^\circ < \theta < 8^\circ$, the staggered magnetization vector is perpendicular to the field. In this *transverse* geometry, the ZSOC renders $g_\perp = 0$ on the magnetic Brillouin zone boundary (dashed line in the inset in Fig. 2). Away, from this boundary, $g_\perp(\mathbf{k})$ is an odd function of the distance from the $g_\perp = 0$ line [8], see red line in the inset. Because of the $\mathbf{k}$-dependence, the g-factor in Eq. (1) has to be replaced by a value, $\overline{g_\perp}$, averaged over the Fermi surface orbit. Furthermore, due to the double-commensurability of the AF wave vector with the underlying crystal lattice, every point $\mathbf{k}$ on the reconstructed Fermi surface has a symmetric counterpart $(-\mathbf{k} + \mathbf{Q})$ such that $g_\perp(\mathbf{k}) = -g_\perp(-\mathbf{k} + \mathbf{Q})$. As a result, the average value $\overline{g_\perp}$ *exactly vanishes* and the spin reduction factor for the oscillations $R_s = 1$ for all θ, implying spin degeneracy of the Landau-quantized cyclotron orbits.

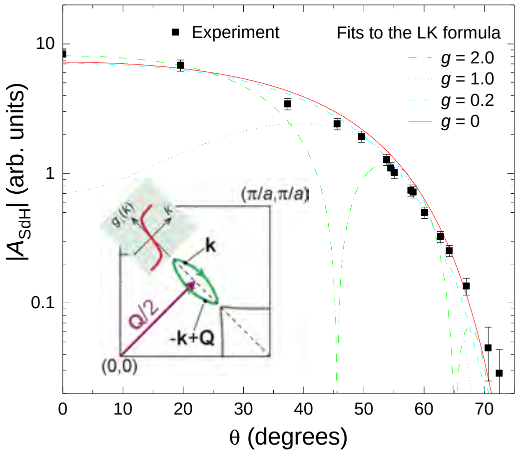

Figure 2: Angle dependence of the SdH amplitude in optimally doped NCCO. The lines are LK fits with different g-factor values. Inset: The 1st quadrant of the Brillouin zone with the Fermi surface reconstructed by a potential with the wave vector $\mathbf{Q} = (\frac{\pi}{a}, \frac{\pi}{a})$. If this potential involves Néel order, $g_\perp(\mathbf{k})$ is an odd function of the distance from the magnetic Brillouin zone boundary, at which $g_\perp = 0$, as shown by the red line in the inset.

Thus, we conclude that the monotonic angular dependence of the SdH amplitude over the broad angle range, presented in Fig. 2, is a direct consequence of ZSOC in an AF metal. This provides a conclusive evidence of a magnetic origin of the Fermi surface reconstruction in optimally doped NCCO and thereby further extends the electron-hole asymmetry in the generic phase diagram of high-T_c cuprate superconductors.

References

[1] R. Comin, and A. Damascelli, Annu. Rev. Condens. Matter Phys. **7**, 369 (2016).

[2] Z. Dai, Y.-H. Zhang, T. Senthil, and P. A. Lee, Phys. Rev. B **97**, 174511 (2018).

[3] T. Helm, M. V. Kartsovnik, C. Proust, B. Vignolle, C. Putzke, E. Kampert, I. Sheikin, E.-S. Choi, J. S. Brooks, N. Bittner, W. Biberacher, A. Erb, J. Wosnitza, and R. Gross, Phys. Rev. B **92**, 094501 (2015).

[4] N. P. Armitage, P. Fournier, and R. L. Greene, Rev. Mod. Phys. **82**, 2421 (2010).

[5] R. Ramazashvili, P. D. Grigoriev, T. Helm, F. Kollmannsberger, M. Kunz, W. Biberacher, E. Kampert, H. Fujiwara, A. Erb, J. Wosnitza, R. Gross, and M. V. Kartsovnik. Zeeman spin-orbit coupling and magnetic quantum oscillations in antiferromagnetic conductors. `arXiv:1908.01236` (2019).

[6] M. Kunz, W. Biberacher, K. Neumaier, N. D. Kushch, and M. V. Kartsovnik, WMI Ann. Rep. **2019**, 43 (2019).

[7] D. Shoenberg. *Magnetic Oscillations in Metals* (Cambridge University Press, Cambridge, 1984).

[8] R. Ramazashvili, Phys. Rev. B **79**, 184432 (2009).

Zeeman Spin-Orbit Coupling and Magnetic Quantum Oscillations in an Antiferromagnetic Organic Metal

F. Kollmannsberger, M. Kunz, W. Biberacher, M. V. Kartsovnik [1]
R. Ramazashvili[2], *P. D. Grigoriev*[3], *H. Fujiwara*[4]

Spin-orbit coupling (SOC) in solids intertwines electron orbital motion with its spin, generating a variety of fundamental effects. Usually, SOC originates from the Pauli term $\mathcal{H}_{\mathcal{P}} = \hbar(4m_0^2)^{-1}\boldsymbol{\sigma}\cdot\mathbf{p}\times\boldsymbol{\nabla}V(\mathbf{r})$ in the electron Hamiltonian [1]. Remarkably, a Néel-type antiferromagnetic (AF) order may give rise to SOC of an entirely different nature, via the Zeeman effect [2]:

$$\mathcal{H}_{\mathcal{Z}}^{so} = -\frac{\mu_B}{2}\left[g_{\parallel}(\mathbf{B}_{\parallel}\cdot\boldsymbol{\sigma}) + g_{\perp}(\mathbf{k})(\mathbf{B}_{\perp}\cdot\boldsymbol{\sigma})\right] , \tag{1}$$

where $\mu_{\mathrm{B}} = e\hbar(2m_0)^{-1}$ is the Bohr magneton, $\mathbf{B}$ the magnetic field, $\boldsymbol{\sigma}$ the electron spin, and $g_{\parallel}$ and $g_{\perp}$ are the g-tensor components with respect to the Néel axis. Due to inherent symmetry of the Néel state the component $g_{\perp}$ must vanish at certain locations in the Brillouin zone, acquiring substantial momentum dependence around these locations. The novel Zeeman SOC was predicted to produce unusual effects such as spin degeneracy of Landau levels in a purely transverse field $\mathbf{B}_{\perp}$ [3] and spin-flip transitions induced by AC electric field [4]. However, none of these effects have been experimentally verified as yet. Here, we employ the layered organic AF superconductor κ-(BETS)$_2$FeBr$_4$ (hereafter κ-BETS) as a model system for testing the theoretical predictions, using the Shubnikov-de Haas (SdH) effect, a sensitive tool for quantifying Zeeman splitting of Landau levels [5].

In κ-BETS, conducting organic layers parallel to the crystallographic *ac* plane alternate with insulating layers containing paramagnetic Fe^{3+} ions. The Fermi surface [blue dashed lines in Fig. 1(a)] consists of a weakly warped cylinder centered at $\mathbf{k} = (\pi/a, 0)$ and a pair of open sheets separated from the cylinder by a small gap Δ_0 at the Brillouin zone boundary. At $T_{\mathrm{N}} \approx 2.5\,\mathrm{K}$ and at fields below $B_c \simeq 5\,\mathrm{T}$, the localized Fe^{3+} spins develop an AF order with the Néel axis $\mathbf{N}\|\mathbf{a}$ and the unit cell doubling along the c axis [6]. The exchange interaction between the Fe^{3+} spins and conduction electrons causes a double-folding of the Brillouin zone along k_c, hence a reconstruction of the Fermi surface in the AF state, as shown in Fig. 1(a). In particular, a small Fermi pocket is formed in the corner of the magnetic Brillouin zone, which is manifested in slow SdH oscillations emerging in the AF state, see Fig. 1 (b). Shown in this Figure is the resistance of κ-BETS measured as a function of magnetic field applied at different tilt angles θ between the field and the normal to the layers [7]. The field is rotated in the *bc* plane, that is, perpendicular to $\mathbf{N}$, see the inset in Fig. 1 (b). Thanks to high crystal quality, even at the relatively low fields, corresponding to the AF region, the SdH oscillations can be traced in a wide angular range, $|\theta| \leq 70°$.

The angular dependence of the oscillation amplitude A_{SdH} is shown in Fig. 1(c). The amplitude was determined by the fast Fourier transform (FFT) of the oscillating magnetoresistance component in the field window between 3.0 and 4.2 T to stay below $B_c(\theta)$ for all field orientations. The lines in Fig. 1(c) are fits using the Lifshitz-Kosevich (LK) formula for the SdH amplitude [5]:

$$A_{\mathrm{SdH}} = A_0\frac{m^2}{\sqrt{B}}R_{\mathrm{MB}}\frac{\exp(-KmT_D/B)}{\sinh(KmT/B)}R_s(\theta)\,, \tag{2}$$

---

[1] The work was supported in part by the German Research Foundation, grant No. KA 1652/4-1.

[2] Laboratoire de Physique Théorique, Université de Toulouse, CNRS, UPS, France.

[3] L. D. Landau Institute for Theoretical Physics, Chernogolovka, Russia. The work was supported in part by the Foundation for the Advancement of Theoretical Physics and Mathematics “BASIS”.

[4] Department of Chemistry, Graduate School of Science, Osaka Prefecture University, Osaka, Japan.

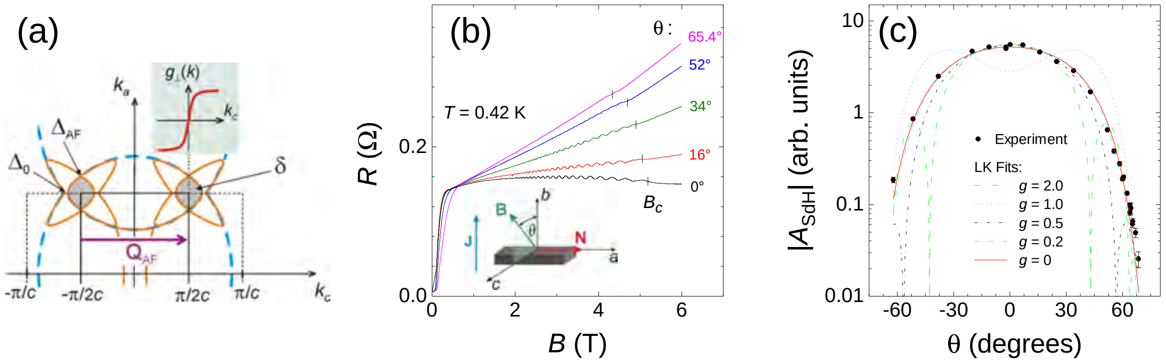

Figure 1: (a) 2D Fermi surface of κ-BETS in the upper half of the Brillouin zone: in the paramagnetic state (dashed blue lines) and in the AF state (orange lines) with the wave vector $\mathbf{Q}_{\mathrm{AF}} = (\pi/c, 0)$. The shaded area in the corner of the magnetic Brillouin zone is the δ pocket responsible for the SdH oscillations in the AF state. The inset shows the function $g_\perp(\mathbf{k})$ around $\mathbf{k} = (k_a, \frac{\pi}{2c})$. (b) B-dependent interlayer reistance at different field orientations. Vertical dashes indicate the critical field B_c suppressing the AF state. Inset: schematic of the experiment. (c) Angular dependence of the SdH amplitude in the AF state. The lines are fits to Eq. (2) with different values of the g-factor.

where A_0 is a field-independent prefactor, $B = 3.5\,\mathrm{T}$ (the midpoint of the FFT window), $m = 1.1m_0/\cos\theta$ the effective cyclotron mass [8], $K = 2\pi^2 k_B/\hbar e$, $T = 0.42\,\mathrm{K}$, T_D the Dingle temperature, R_{MB} the MB factor, and R_s the spin-splitting factor. The latter is determined by the ratio between Zeeman splitting $g\mu_{\mathrm{B}}B$ and the Landau level spacing $\hbar\omega_c(\theta) = \hbar eB/m(\theta)$ [5]:

$$R_s(\theta) = \cos\left[\pi\frac{g\mu_{\mathrm{B}}B}{\hbar\omega_c(\theta)}\right] = \cos\left[\frac{\pi}{2}g\frac{m}{m_0\cos\theta}\right]. \tag{3}$$

Generally $R_s(\theta)$ has an oscillating angular dependence. For $g = 2.0$ found in the high-field, paramagnetic state [9], Eq. (3) yields two *spin-zeros*, at $|\theta| \approx 43^\circ$ and 64°, see dashed green line in Fig. 1(c). Contrary to this, we observe *no* spin-zeros in the entire angular range. In fact, the comparison between the data and theoretical fits in Fig. 1(c) rules out a finite constant g [7]. On the other hand the data can readily be explained by taking into account the Zeeman SOC effect. Indeed, in our geometry, $\mathbf{B} \perp \mathbf{N}$, the first term in the right-hand side of Eq. (1) is zero and the g-factor in Eq. (3) should be replaced by the component $g_\perp(\mathbf{k})$, averaged over the cyclotron orbit δ in Fig. 1(a). It can be shown based on symmetry arguments [7] that $\overline{g_\perp(\mathbf{k})} = 0$ for the Fermi pocket δ due to the AF origin of the Fermi surface reconstruction. Thus, our results reveal spin degeneracy of Landau levels and thereby present the first experimental evidence of the novel Zeeman SOC mechanism in an antiferromagnetic metal.

References

[1] C. Kittel. *Quantum Theory of Solids* (John Wiley & Sons Inc., New York – London, 1963).
[2] R. Ramazashvili, Phys. Rev. Lett. **101**, 137202 (2008).
[3] V. V. Kabanov, and A. S. Alexandrov, Phys. Rev. B **77**, 132403 (2008).
[4] R. Ramazashvili, Phys. Rev. B **80**, 054405 (2009).
[5] D. Shoenberg. *Magnetic Oscillations in Metals* (Cambridge University Press, Cambridge, 1984).
[6] H. Fujiwara, E. Fujiwara, Y. Nakazawa, B. Z. Narymbetov, K. Kato, H. Kobayashi, A. Kobayashi, M. Tokumoto, and P. Cassoux, J. Am. Chem. Soc. **123**, 306 (2001).
[7] R. Ramazashvili, P. D. Grigoriev, T. Helm, F. Kollmannsberger, M. Kunz, W. Biberacher, E. Kampert, H. Fujiwara, A. Erb, J. Wosnitza, R. Gross, and M. V. Kartsovnik. Zeeman spin-orbit coupling and magnetic quantum oscillations in antiferromagnetic conductors. `arXiv:1908.01236` (2019).
[8] T. Konoike, S. Uji, T. Terashima, M. Nishimura, S. Yasuzuka, K. Enomoto, H. Fujiwara, E. Fujiwara, B. Zhang, and H. Kobayashi, Phys. Rev. B **72**, 094517 (2005).
[9] M. Kartsovnik, M. Kunz, L. Schaidhammer, F. Kollmannsberger, W. Biberacher, N. Kushch, A. Miyazaki, and H. Fujiwara, J. Supercond. Nov. Magn. **29**, 3075–3080 (2016).

Transport and relaxation in normal Fermi systems

D. Einzel

Introduction. In this paper we consider the transport properties of a many body system consisting of N fermions in a volume V with density $n = N/V$. The energy spectrum is assumed to have the form $\epsilon_{\mathbf{k}} = \xi_{\mathbf{k}} + \mu(T)$, with $\mu(T)$ the temperature–dependent chemical potential. Classical vs. degenerate behavior of such a system is associated with the size of the de Broglie wavelength $\lambda_T = [2\pi m k_{\mathrm{B}} T]^{-\frac{1}{2}}$ (classical limit: $n\lambda_T^3 \ll 1$, degenerate limit: $n\lambda_T^3 \gg 1$). The degeneracy transition occurs at a temperature T^*, where $n\lambda_{T^*}^3 = \mathcal{O}(1)$. The aim of this contribution is an analytic study of the transport properties of a Fermi many body system at *arbitrary* temperatures. The formulation of a transport theory, which is compatible with the conservation laws for the density ($\delta n_0 = \delta n$) and energy density ($\delta n_1 = \delta u$) fluctuations must be based on the choice of the correct *collisional invariants* $a_{\mathbf{k}}$. While in the degenerate limit, $a_{\mathbf{k}} = 1$ (density conservation) and $a_{\mathbf{k}} = \xi_{\mathbf{k}}$ (energy conservation), it turns out that at arbitrary temperatures the temperature–dependence of the chemical potential $\mu(T)$ can no longer be neglected and one has to replace $\xi_{\mathbf{k}} \to \bar{\xi}_{\mathbf{k}} = \epsilon_{\mathbf{k}} - \bar{\mu}$ with $\bar{\mu} = \mu - \underline{T(\partial\mu/\partial T)}$ with the underlined term vanishing in the degenerate limit. Defining $\alpha = \mu/k_{\mathrm{B}}T$, one may introduce the *fugacity* $z = \mathrm{e}^{\alpha}$ and the equilibrium Fermi–Dirac distribution function assumes the form $f^0_{\mathbf{k}} = z[\exp(\epsilon_{\mathbf{k}}/k_{\mathrm{B}}T) + z]^{-1}$, with derivative $\varphi_{\mathbf{k}} = \partial f^0_{\mathbf{k}}/\partial\mu$. Defining momentum sums generally via $\langle A_{\mathbf{p}}\rangle = V^{-1}\sum_{\mathbf{p}\sigma} A_{\mathbf{p}}$, we may introduce averages $f_\nu =< \epsilon^\nu_{\mathbf{p}} f^0_{\mathbf{p}} >$ and $\varphi_\nu =< \epsilon^\nu_{\mathbf{p}}\varphi_{\mathbf{p}} >$. The particle density may then be expressed as $n = f_0$, which serves as a condition for the determination of the chemical potential $\mu(T)$. In the same way, the equilibrium energy density may be expressed as $u = f_1$. Finally, the equilibrium entropy density $s(T)$ can be written in the compact form $s(T) = 2[\varphi_2 - \mu\varphi_1]/3T$ [1]. It is worth noting that one may get rid of the awkward temperature derivative $\partial\mu/\partial T$ in $\bar{\mu}$ by using the relation $\langle\bar{\xi}_{\mathbf{p}}\varphi_{\mathbf{p}}\rangle = 0$ (rather than $\langle\xi_{\mathbf{p}}\varphi_{\mathbf{p}}\rangle = 0$ in the degenerate limit!), or equivalently $\bar{\mu} \equiv \varphi_1/\varphi_0$.

Transport and relaxation

In what follows, we assume that the Fermi system is subject to external perturbations, characterized by the electromagnetic scalar ($\Phi(\mathbf{r},t)$) and vector ($\mathbf{A}(\mathbf{r},t)$) potential in the form $\delta\epsilon_{\mathbf{k}} = e\Phi - e\mathbf{v}_{\mathbf{k}}\cdot\mathbf{A}/c$ with the group velocity $\mathbf{v}_{\mathbf{k}} = \partial\epsilon_{\mathbf{k}}/\hbar\mathbf{k}$. From Φ and $\mathbf{A}$ one may construct the gauge–invariant form of the electric field $\mathbf{E} = -\nabla\phi - \partial\mathbf{A}/c\partial t$. The linear response of the Fermi system is then described by the deviation $\delta f_{\mathbf{k}}(\mathbf{r},t) = f_{\mathbf{k}}(\mathbf{r},t) - f^0_{\mathbf{k}}$. It is convenient to work with an alterative distribution function $\delta n_{\mathbf{k}} = \delta f_{\mathbf{k}} - \varphi_{\mathbf{k}} e\mathbf{v}_{\mathbf{k}}\cdot\mathbf{A}/c$, for which the linearized *Landau–Boltzmann equation* is of the standard form [2]

$$\left(\frac{\partial}{\partial t} + \mathbf{v}_{\mathbf{k}}\cdot\nabla\right)\delta n_{\mathbf{k}} = e\varphi_{\mathbf{k}}\mathbf{v}_{\mathbf{k}}\cdot\mathbf{E} + \delta I_{\mathbf{k}} \;\;;\;\; \delta I_{\mathbf{k}} = -\frac{1}{\tau}\left(\delta n_{\mathbf{k}} - \varphi_{\mathbf{k}}\sum_{\nu=0,1}\bar{\xi}^{\nu}_{\mathbf{k}}\frac{\delta n_\nu}{\chi_{\nu\nu}}\right) \tag{1}$$

From $\delta n_{\mathbf{k}}$ one obtains the relevant macroscopic observables of the fermi system, namely the generalized fluctuations $\delta n_\mu = \langle\bar{\xi}^{\mu}_{\mathbf{k}}\delta n_{\mathbf{k}}\rangle$ of density ($\delta n_0 \equiv \delta n$) and of energy ($\delta n_1 \equiv \delta u$). Note that in *local equilibrium* one may write $\delta n_0^{\mathrm{loc}} \equiv \delta n = (\partial n/\partial\mu)\,\delta\mu = \chi_n\delta\mu$ as well as $\delta n_1^{\mathrm{loc}} \equiv \delta u = (\partial u/\partial T)\,\delta T = c_V\delta T$. This leads to the definition of a generalized response function $\chi_{\nu\nu} =< \bar{\xi}^{2\nu}_{\mathbf{p}}\varphi_{\mathbf{p}} >, \nu = 0,1$ with the identifications $\chi_{00} = \partial n/\partial\mu = \varphi_0 = \chi_n$ and $\chi_{11} = Tc_V = \varphi_2 - \bar{\mu}\varphi_1$ [1]. Here, the quantities χ_n and c_V denote the density response function and the specific heat capacity, respectively. Note that the spin susceptibility χ_s [3] of a fermi system can be expressed through χ_n via $\chi_s = \mu_{\mathrm{B}}^2\chi_n$, where μ_{B} denotes the Bohr magneton. In (1) $\delta I_{\mathbf{k}}$ represents the *collision integral*, for which we have used a *conserving relaxation* *time approximation* (CRTA). Here τ represents a phenomenological transport (or current relaxation) time. As a consequence of the CRTA structure of the collision integral, one obtains a set of conservation laws, which can be expressed in the form of continuity equations for the generalized densities δn_μ, by which expressions for the thermodynamically conjugated generalized current densities $\mathbf{j}_\mu$ are generated:

$$\frac{\partial}{\partial t}\delta n_\mu + \nabla\cdot\mathbf{j}_\mu = 0 \quad ; \quad \mathbf{j}_\mu = \left\langle \bar{\xi}^{\mu}_{\mathbf{p}}\mathbf{v}_{\mathbf{p}}\delta n_{\mathbf{p}}\right\rangle \;;\; \mu = 0,1 \tag{2}$$

Note the $\mathbf{j}_\mu$ represents the particle current ($\mu = 0$) and the energy current ($\mu = 1$) density, respectively. As a next step, one may derive from the Landau–Boltzmann equation (1) for $\delta n_{\mathbf{k}}$ an acceleration/relaxation equation for the current densities $\mathbf{j}_\mu$ of the form ($\mathbf{\Pi}_\mu$: generalized stress tensor)

$$\left(\frac{\partial}{\partial t} + \frac{1}{\tau}\right)\mathbf{j}_\mu + \nabla\cdot\mathbf{\Pi}_\mu = e\mathbf{K}_\mu\cdot\mathbf{E} \;;\; \mathbf{\Pi}_\mu = \left\langle \bar{\xi}^{\mu}_{\mathbf{p}}\mathbf{v}_{\mathbf{p}} : \mathbf{v}_{\mathbf{p}}\delta n_{\mathbf{p}}\right\rangle \;;\; \mu = 0,1 \tag{3}$$

Here we have defined local current response tensors through $\mathbf{K}_\mu = K_\mu\mathbf{1}$, $K_\mu = 2\left\langle \varphi_{\mathbf{p}}\epsilon_{\mathbf{p}}\bar{\xi}^{\mu}_{\mathbf{p}}\right\rangle/3m$. In order to proceed with the calculations, we approximate the distribution function $\delta n_{\mathbf{p}}$ in the expression for $\mathbf{\Pi}_\mu$ by its local equilibrium form $\delta n_{\mathbf{p}} \approx \delta n^{\mathrm{loc}}_{\mathbf{p}} = \varphi_{\mathbf{p}}\sum_{\nu=0,1}\bar{\xi}^{\nu}_{\mathbf{p}}\delta n_\nu/\chi_{\nu\nu}$. This procedure corresponds to the standard leading order *gradient expansion* of the Landau–Boltzmann equation (1). If we assume furthermore a harmonic time dependence $[\partial/\partial t \to -i\omega, \tilde{\tau} = \tau/(1-i\omega\tau)]$, we may distinguish the following two important cases: (i) no temperature fluctuations ($\delta T = 0$: Drude's law) and (ii) no density fluctuations ($\delta n = 0$: thermoelectric current coupling)

$$\text{(i)}\;\; \mathbf{j}_0 = \mathbf{j} = K_0\tilde{\tau}\left(e\mathbf{E} - \nabla\frac{\delta n}{\chi_n}\right) \;;\; \text{(ii)}\;\; \mathbf{j}_\mu = \tilde{\tau}\left[eK_\mu\mathbf{E} - K_{\mu+1}\nabla\frac{\delta T}{T}\right] \;;\; \mu = 0,1 \tag{4}$$

Degeneracy transition

The averages f_ν and φ_ν may conveniently be evaluated with the aid of generalized *polylogarithm* functions [4] [$\alpha = \mu(T)/k_{\mathrm{B}}T = \ln z$]:

$$\mathrm{Li}^{(-)}_{x}(z) = \frac{z}{\Gamma(x)}\int_0^\infty \frac{dt\,t^{x-1}}{\mathrm{e}^t + z} \overset{z\to 0}{=} \underbrace{\sum_{k=1}^{\infty}(-1)^{k+1}\frac{z^k}{k^x}}_{\text{fugacity expansion}} \overset{z\to\infty}{=} \underbrace{2\sum_{\nu=0}^{\infty}\frac{\eta(2\nu)\alpha^{x-2\nu}}{\Gamma(x+1-2\nu)}}_{\text{Sommerfeld expansion}} \tag{5}$$

Here η denotes the Dirichlet η–function [5]. The chemical potential $\mu(T)$ is fixed by the condition $n\lambda_T^3 = 2\mathrm{Li}^{(-)}_{3/2}(z)$, the degeneracy temperature $T^*(\neq T_{\mathrm{F}})$ can then be obtained from $n\lambda_{T^*}^3 = 2\mathrm{Li}^{(-)}_{3/2}(1) = 2\eta(3/2)$, and reads $k_{\mathrm{B}}T^* = 2\pi(\hbar^2/m)[n/2\eta(3/2)]^{2/3}$. As a consequence, there is a mapping between the two scales z (fugacity) and T/T^* (reduced temperature) via $T/T^* = [\mathrm{Li}^{(-)}_{3/2}(1)/\mathrm{Li}^{(-)}_{3/2}(z)]^{2/3}$. The following general results for the temperature or z–dependence of f_ν and φ_ν emerge from the analysis: $f_\nu = n(k_{\mathrm{B}}T)^\nu t_\nu(z)\Gamma(\nu+3/2)/\Gamma(3/2)$ and $\varphi_\nu = n(k_{\mathrm{B}}T)^{\nu-1}t_{\nu-1}(z)\Gamma(\nu+3/2)/\Gamma(3/2)$. Here we have defined so–called transition functions $t_\nu(z) = \mathrm{Li}^{(-)}_{\nu+3/2}(z)/\mathrm{Li}^{(-)}_{3/2}(z)$, which describe the transition of f_ν and φ_ν from the classical ($z \to 0$) to the degenerate ($z \to \infty$) limit. Note that the quantity $\bar{\mu}$ assumes the values $\bar{\mu} = \mu(0) = \epsilon_{\mathrm{F}}$ in the degenerate limit ($z \to \infty$) and $\bar{\mu} = 3k_{\mathrm{B}}T/2$ in the classical limit ($z \to 0$). The lowest order current response functions K_ν can be written as follows: $K_0 = 2\varphi_1/3m = n/m$, $K_1 = 2[\varphi_2 - \bar{\mu}\varphi_1]/3m = 2Tc_V/3m$, $K_2 = 2[\varphi_3 - 2\bar{\mu}\varphi_2 + \bar{\mu}^2\varphi_1]/3m$.

Results

The following results, valid at *all* temperatures, can be deduced from our calculations:

1. Local density response function $\chi_n = nt_{-1}(z)/k_\mathrm{B}T$
2. Specific heat capacity $c_V = 3nk_\mathrm{B}[5t_1(z) - 3/t_{-1}(z)]/4$
3. Drude conductivity $\sigma = e^2K_0\tilde{\tau} = e^2n\tilde{\tau}/m$
4. Drude resistivity $\rho = \sigma^{-1}$
5. Seebeck–coefficient $S = 2c_V/3n = k_\mathrm{B}[5t_1(z) - 3/t_{-1}(z)]/2$
6. Peltier coefficient $\Pi = TS = 2Tc_V/3n = k_\mathrm{B}T[5t_1(z) - 3/t_{-1}(z)]/2$
7. diffusive thermal conductivity $\kappa T = K_2 - K_1^2/K_0 = n\tilde{\tau}(k_\mathrm{B}T/2)^2[35t_2(z) - 25t_1^2(z)]$
8. shear viscosity $\eta = 4\varphi_2\tilde{\tau}/15 = nk_\mathrm{B}T\tilde{\tau}t_1(z)$ (this result requires a separate treatment [6]).

In Fig. 1 we have plotted the density response function $\chi_n(T)$ as well as the entropy density $s(T)$ and the specific heat capacity $c_V(T)$ as a function of reduced temperature T/T^*. In the left panel, the dashed line represents the Curie behavior, expected near the classical limit. In the right panel, the dashed line represents the classical result $c_V = 3nk_\mathrm{B}/2$ for the specific heat capacity. Well above T^*, the entropy density is seen to display the temperature dependence expected from the analysis by Sackur and Tetrode in the classical gas limit [7, 8].

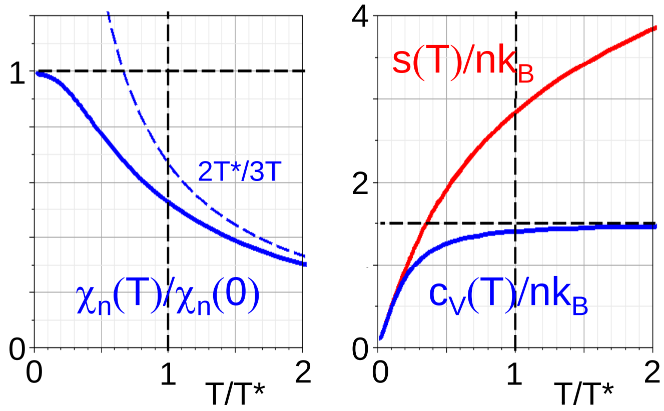

Figure 1: The density response function $\chi_n = \chi_{00} = \varphi_0$ (left panel) and the specific heat capacity $c_V = \chi_{11}/T = (\varphi_2 - \bar{\mu}\varphi_1)/T$ and entropy density $s(T) = 2(\varphi_2 - \mu\varphi_1)/3T$ (right panel) vs. reduced temperature T/T^*.

Discussion

It should be kept in mind that the melting point of typical metals lies well below the degeneracy temperature T^*. An application of our results is nevertheless possible to liquid ^{3}He, for which $T^* = \mathcal{O}(1\mathrm{K})$.

The Sommerfeld expansion, applicable in the degenerate regime $T \ll T^*$ [9], emerges from our formulation *analytically* as the asymptotic form of the polylogarithm functions $\mathrm{Li}_x^{(-)}(z)$ in the limit $z \to \infty$ (see Eq. (5)) .

The phenomenological current relaxation time τ is well known in the fermi liquid regime of normal ^{3}He $T \ll T^*$ to read $\hbar/\tau = \langle W \rangle\,(\pi k_\mathrm{B}T)^2/24\mu(0)$, with $\langle W \rangle$ some angular average of the effective two–particle scattering cross section [10]. In the classical gas limit, on the other hand, one is left with $\tau \approx$ const. Clearly, for intermediate temperatures, particularly near the degeneracy transition, the value of τ is unknown, but can possibly be determined from the experimental observation, for example from the thermal conductivity or the shear viscosity of the fermi system.

In the degenerate limit *fermi liquid corrections*, represented by a set of dimensionless [spin–symmetric (s) and spin–antisymmetric (a)] interaction parameters $F_\ell^{\mathrm{s,a}}$, lead to renormalizations of the mass $[m^* = m(1 + F_1^\mathrm{s}/3)]$, the charge $[\chi_n^* = \chi_n/(1 + F_0^\mathrm{s})]$ and the spin

$[\chi_s^* = \chi_s/(1+F_0^s)]$ susceptibility [11]. It is not clear, to which extent these corrections can be thought to perpetuate into the regime of higher temperatures and across the degeneracy temperature T^*.

References

[1] D. Einzel, WMI Ann. Rep. **2017**, 39–42 (2012).
[2] R. Gross, A. Marx, D. Einzel, and S. Geprägs. *Festkörperphysik, Aufgaben und Lösungen* (De Gruyter, Berlin, 2018).
[3] J. Fairbank, B. Deaver Jr., C. Everitt, and P. Michelsen (eds.) *Near Zero* (W.H. Freeman and Co., New York, 1988).
[4] A. Jonquière, Bulletin de la S. M. F. **17**, 142–152 (1889).
[5] M. Abramowitz, and I. A. Stegun (eds.) *Handbook of Mathematical Functions* (Taylor and Francis, London, 1990).
[6] D. Einzel. On the Viscosity in Normal Fermi Systems. To be published, 2020 (2020).
[7] O. Sackur, Ann. Phys. **36**, 958–980 (1911).
[8] H. Tetrode, Ann. Phys. **38**, 434–442 (1912).
[9] A. Sommerfeld, Z. Phys. **47**, 1–32 (1928).
[10] D. Einzel, and J. Parpia, J. Low Temp. Phys. **109**, 1–105 (1997).
[11] D. Vollhardt, and P. Wölfle. *The Superfluid Phases of Helium 3* (Taylor and Francis, London, 1990).

Application–Oriented Research

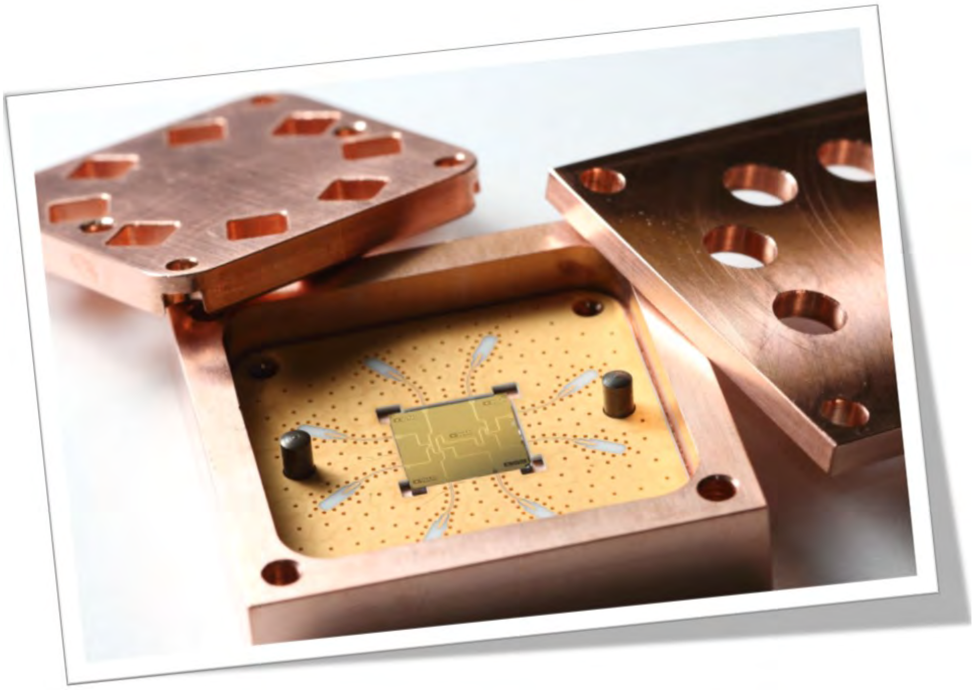

Measurement of the Second-Order Correlation Functions Under Different Signal-To-Noise Ratios

Q. Chen, F. Deppe, Y. Nojiri, S. Pogorzalek, M. Renger, M. Partanen, K. G. Fedorov, A. Marx, R. Gross[1]

Measuring the photon statistics is of great importance regarding the understanding of the quantum nature of light. In particular, the normalized zero-time correlation measurements provide a direct way to characterize the degree of coherence for an electromagnetic field, as well as a criterion to distinguish “classical" from “quantum" light. In superconducting circuits, the correlation functions can be obtained from moment measurements [1, 2], histogram measurements [3–5], or from direct Wigner function measurements [6–8]. Here, we employ the moment measurement method and measure the normalized zero-time correlation functions of a coherent state under different signal-to-noise ratios (SNR).

The first two orders of the normalized zero-time correlation functions are defined as

$$g^{(1)} = \langle a^\dagger a\rangle / |\langle a^\dagger\rangle|^2, \qquad g^{(2)} = \langle a^\dagger a^\dagger a a\rangle / |\langle a^\dagger a\rangle|^2. \tag{1}$$

Here, a and $a^\dagger$ denote the annihilation and creation operators for the signal field A. Because the strength of A is usually very weak in superconducting quantum circuits, one has to amplify the signal field before delivering it to the acquisition card. By convention, we assume the input and the output fields of a phase-insensitive linear amplifier are related by the formula $s = \sqrt{G}a + \sqrt{G-1}h^\dagger$ [9]. Here, G is the power gain of the amplifier and $h^\dagger$ is the conjugate field of the amplification noise. If we assume $G \gg 1$ and that the signal field is uncorrelated with the noise field, we obtain the following relation between the measured moments of the field S and the moments of the signal field A

$$\langle s^{\dagger m} s^n\rangle = G^{mn/2} \sum_{m'=0}^{m} \sum_{n'=0}^{n} C_m^{m'} C_n^{n'} \langle (a^\dagger)^{m'} a^{n'}\rangle \langle h^{m-m'} (h^\dagger)^{n-n'}\rangle. \tag{2}$$

To further extract information on A, we employ the reference-state method which allows one to determine the noise moments from a pre-known state [10]. For example, if A is in the vacuum state, $\langle a^{\dagger m'} a^{n'}\rangle \neq 0$ if and only if $m' = n' = 0$. The measured moments satisfy

$$\langle s_{\mathrm{ref}}^{\dagger}{}^{m} s_{\mathrm{ref}}^{n}\rangle = G^{mn/2} \langle h^m (h^\dagger)^n\rangle, \tag{3}$$

where the subscript *ref* indicates the measurement results with the reference state. Replacing the moments of the noise field in Eq. (2) by Eq. (3), we can extract the moments of the signal field by algebraic inversion. Thus, the first two orders of the correlation functions can be obtained by measuring the moments up to the 4th order, i.e., $m + n \leq 4$.

To measure the correlation functions in microwave experiments, we use a microwave generator (R&S-SMF 100A) to generate coherent states with frequency $\omega_{\mathrm{RF}}/2\pi = 6.9\,\mathrm{GHz}$ and a controllable signal power P_{MW}. At room temperature, the generator output field is modelled as a combination of a coherent state and a thermal state. This combined field is then delivered to a receiver, where it is demodulated and down-converted to the intermediate frequency $\omega_{\mathrm{IF}}/2\pi = 12.5\,\mathrm{MHz}$, amplified, and finally measured by the acquisition card (Gage PCIE Gen3 EON Express). When turning off the generator, the measured signal is merely the room temperature noise. The measurement bandwidth is chosen as $B = 400\,\mathrm{kHz}$, which corresponds to the noise power $P_{\mathrm{N}} \approx -105\,\mathrm{dBm}$ referenced back to the generator output. Thus, by changing P_{MW} from -140 to $-60\,\mathrm{dBm}$ we obtain different $\mathrm{SNR} = P_{\mathrm{MW}} - P_{\mathrm{N}}$ approximately from -35 to $45\,\mathrm{dB}$.

---

[1] We acknowledge support by Germany’s Excellence Strategy (EXC-2111-390814868), the Elite Network of Bavaria through the program ExQM, and the EU Quantum Flagship project QMiCS (Grant No. 820505).

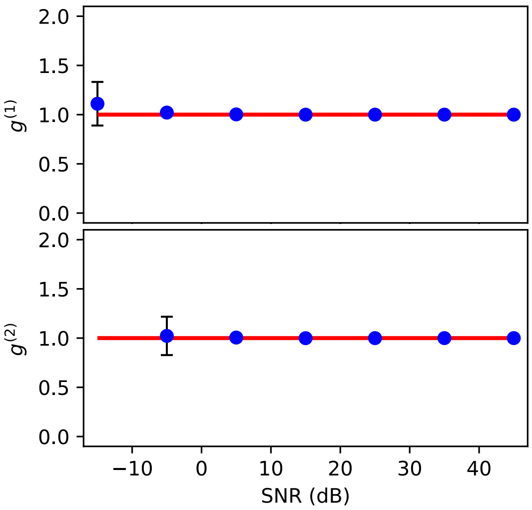

Figure 1: Measurements of the first and second order zero-time correlation functions for a coherent state under different SNRs. The data for $SNR < -15$ are not shown since the expectation values are outside the scope.

In our experiment, we set the data acquisition rate to 250 MHz, which corresponds to 2×10^8 data points in one trigger. For each 20 data points, we obtain one measurement result for the field quadratures, which are used to calculate the normally ordered moments up to the fourth order [1]. These results are divided into 10 ensembles, which are then averaged over their $\sim 10^6$ elements to give one expectation value for each moment operator. From the 10 ensembles, we compute the averaged correlation functions and the corresponding error bars. Figure 1 shows the measured correlation functions under different SNRs. The amplification gain $G = 2.88 \times 10^5$ photons/V is calibrated by comparing the measured photon number with the output power of the generator at $P_{\mathrm{MW}} = -60$ dBm. On the one hand, the measured $g^{(1)}$ and $g^{(2)}$ are very close to one for SNR ≥ -5 dB. This is what we expect for coherent states. This demonstrates that our method provides reliable correlation measurements under relatively large noise. On the other hand, when SNR $= -15$ dB we observe that $g^{(1)} \approx 1$ while $g^{(2)} \gg 1$ (not shown), but its error bar still includes the unity value. This observation meets the theoretical expectation that the statistical error of the measured moments increases with increasing order [10, 11].

To sum up, we employ the moment measurement method and measure the first two orders of the correlation functions for a coherent field under different SNRs. By using the reference-state method, we observe that the measurement results are consistent with the theoretical expectations for SNR ≥ -5 dB. This demonstrates the ability to measure photon correlations under relatively large noise levels. Our measurement results also indicate that, in order to further decrease the variance of the measured moments, one could either average over more data ensembles or employ the histogram measurement technique, which measures only the field quadratures. These improvements will be studied in future experiments.

References

[1] E. P. Menzel, F. Deppe, M. Mariantoni, M. A. A. Caballero, A. Baust, T. Niemczyk, E. Hoffmann, A. Marx, E. Solano, and R. Gross, Phys. Rev. Lett. **105**, 100401 (2010).
[2] E. P. Menzel, R. D. Candia, F. Deppe, P. Eder, L. Zhong, M. Ihmig, M. Haeberlein, A. Baust, E. Hoffmann, D. Ballester, K. Inomata, T. Yamamoto, Y. Nakamura, E. Solano, A. Marx, and R. Gross, Phys. Rev. Lett. **109**, 250502 (2012).
[3] C. Eichler, D. Bozyigit, C. Lang, L. Steffen, J. Fink, and A. Wallraff, Phys. Rev. Lett. **106**, 220503 (2011).
[4] C. Eichler, D. Bozyigit, C. Lang, M. Baur, L. Steffen, J. M. Fink, S. Filipp, and A. Wallraff, Phys. Rev. Lett. **107**, 113601 (2011).
[5] C. Eichler, D. Bozyigit, and A. Wallraff, Phys. Rev. A **86**, 032106 (2012).
[6] L. G. Lutterbach, and L. Davidovich, Phys. Rev. Lett. **78**, 2547–2550 (1997).
[7] P. Bertet, A. Auffeves, P. Maioli, S. Osnaghi, T. Meunier, M. Brune, J. M. Raimond, and S. Haroche, Phys. Rev. Lett. **89**, 200402 (2002).
[8] F. Mallet, M. A. Castellanos-Beltran, H. S. Ku, S. Glancy, E. Knill, K. D. Irwin, G. C. Hilton, L. R. Vale, and K. W. Lehnert, Phys. Rev. Lett. **106**, 220502 (2011).
[9] C. M. Caves, Phys. Rev. D **26**, 1817–1839 (1982).
[10] R. D. Candia, E. P. Menzel, L. Zhong, F. Deppe, A. Marx, R. Gross, and E. Solano, New J. Phys. **16**, 015001 (2014).
[11] M. P. d. Silva, D. Bozyigit, A. Wallraff, and A. Blais, Phys. Rev. A **82**, 043804 (2010).

Quantum Memory with Optimal Control

Y. Nojiri, S. Trattnig, E. Xie, M. Renger, Q. Chen, S. Pogozarek, M. Partanen, K.G. Fedorov, F. Deppe, A. Marx, R. Gross[1]

After companies such as Google, IBM and Rigetti succeeded to build quantum computers close to commercial use, quantum computers based on superconducting circuits have received much attention in the field of quantum information, quantum simulation, and quantum engineering. In this context, one important aspect is the sufficiently long storage of (quantum) information. A device that is used to store information for immediate use in a quantum computer is called "quantum memory", motivated by the memory used in classical computing. In order to be able to store quantum information for a sufficiently long period of time, a qubit has to be isolated from its environment. However, if we want to realize fast readout of the qubit state, the qubit has to be coupled in a controlled way to its environment. Therefore, the simultaneous realization of long storage and fast readout in a single device is difficult.

For superconducting quantum circuits, it has turned out that 3D waveguide cavities coupled to transmon qubits are suitable for storing quantum information in the form of microwave photons. Furthermore, by using a compact quantum memory the long-lived storage mode of a 3D cavity and the fast readout of the transmon qubit state can be realized simultaneously [1]. The so far achieved fidelity of the storage process of roughly 82% is limited by a trade-off between qubit relaxation and state leakage due to the limited transmon qubit anharmonicity. The latter can be overcome by pulse shaping using optimal control strategies [2]. Henceforth, we implement a search algorithm to find optimized pulses promising higher gate fidelities, the so-called covariance matrix adaption evolution strategy (CMA-ES) optimization algorithm. The great advantage of the CMA-ES for the optimal control is the black-box optimization meaning there is no need to model the system.

In a first step, we optimize single drive pulses using the qubit readout signal (phase shift of the readout tone) as a figure of merit by varying the carrier frequency carrier power, carrier phase, and pulse length by making use of the optimization algorithm. Since the memory protocol makes use of qubit control and blue sideband transition, we search for best parameters for the qubit pulse and

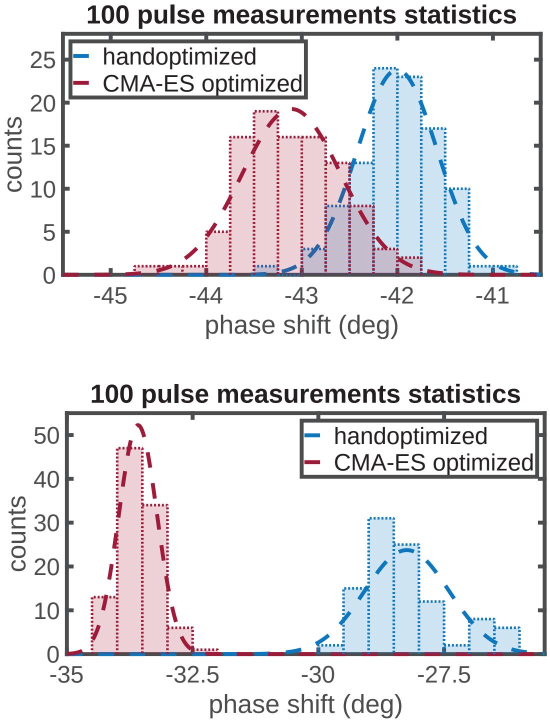

Figure 1: Comparison between the hand optimized and CMA-ES optimized pulse for qubit pulse (top) and for blue sideband pulse (bottom). The histograms (bars) are taken over 100 measurements each. Their shape can be fitted with a Gaussian (broken lines). The separation between the histograms indicaters an improved readout phase over hand-optimized pulses in both cases.

---

[1] We acknowledge support by Germany's Excellence Strategy (EXC-2111-390814868), the Elite Network of Bavaria through the program ExQM, and the EU Quantum Flagship project QMiCS (Grant No. 820505).

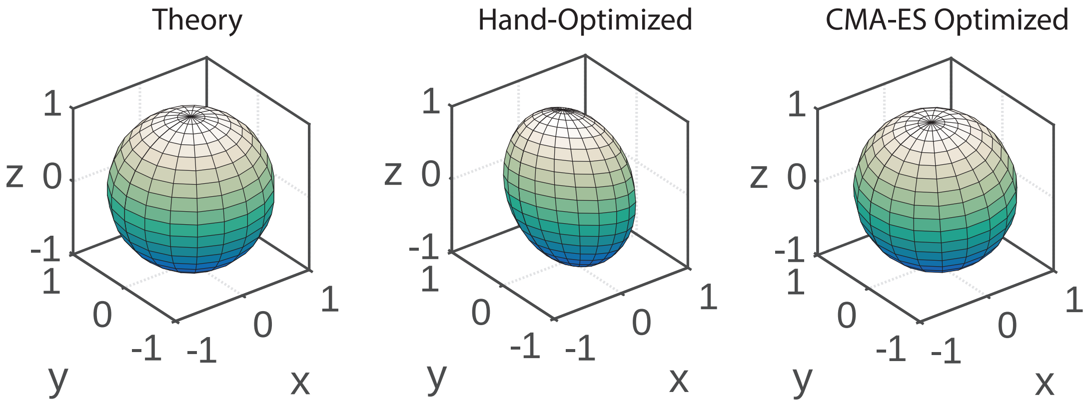

Figure 2: The Bloch sphere representation of the qubit after a π-pulse according to the quantum process tomography. The theoretically expected Bloch sphere (left) compared to that for the hand optimized pulse (center) and of the CMA-ES optimized pulse (right).

blue sideband pulse. As depicted in Fig. 1, in both pulses the CMA-ES optimized case gives a better fidelity compared to the hand optimized case.

We further compare the CMA-ES optimized results with the hand optimized results with the quantum process tomography on qubit pi-pulse. As shown in Fig. 2, we see the Bloch sphere is deformed in the hand optimized case, while it preserves its spherical form in the CMA-ES indicating good fidelity. This shows the decoherence effect on the qubit state is quite large with the hand optimized pulse leading to a deformation of the Bloch sphere. The reason is because the ideal qubit state has a unit vector length. In contrast, the CMA-ES optimized pulse achieves better quantum process such that the decoherence effect on the qubit is minimized.

In conclusion, we find the CMA-ES optimized pulse indeed increases the gate fidelity. We now are in the position to perform the memory protocol with those optimized pulses. It is expected that the use of optimized pulse shapes together with improved transmon qubits can significantly improve the fidelity of the storage process in quantum memories based on 3D waveguide cavities coupled to transmon qubits.

References

[1] E. Xie, F. Deppe, M. Renger, D. Repp, P. Eder, M. Fischer, J. Goetz, S. Pogorzalek, K. G. Fedorov, A. Marx, and R. Gross, Appl. Phys. Lett. **112**, 202601 (2018).
[2] S. Machnes, E. Assémat, D. Tannor, and F. K. Wilhelm, Phys. Rev. Lett. **120**, 150401 (2018).

Magnetoelasticity of $Co_{25}Fe_{75}$ Thin Films

D. Schwienbacher, M. Pernpeintner, L. Liensberger, M. Weiler, R. Gross, H. Huebl[1]
E.R.J. Edwards, H.T. Nembach, J.M. Shaw [2]

Cobalt iron (CoFe) alloys are presently intensely studied due to their ultra-low damping rate for magnetization dynamics [1] being on-par with rates reported for yttrium iron garnet thin films [2]. The outstanding magnetic properties of CoFe combined with the fact that it is electrically conducting makes it highly attractive for various spintronic applications. In this context, quantification of magnetoelastic properties of thin film CoFe is essential, as they allow for tailoring magnetic anisotropy. In previous magnetoelastic studies [3, 4] only bulk alloys of CoFe have been studied.

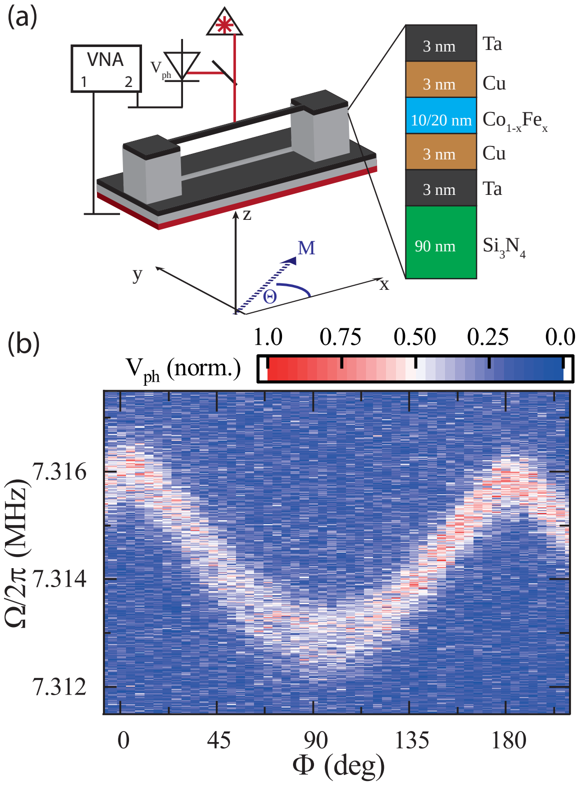

Figure 1: (a) Schematic of a doubly clamped Si_3N_4 nano-string covered with the deposited CoFe layer stack (black) and the interferometric setup. The whole sample is mounted on a piezo-actuator (red) providing a time dependent oscillating force for the excitation of an out-of-plane mechanical motion. By analyzing the mechanical amplitude response in form of the photo-diode voltage V_{ph}, we obtain the mechanical response spectrum. Panel (b) shows V_{ph} as a function of magnetic field direction Θ.

Here, we investigate the magnetostrictive properties of $Co_{25}Fe_{75}$ and $Co_{10}Fe_{90}$ thin films with a thickness of 10 and 20 nm. The CoFe films were grown onto pre-suspended nanostrings via sputter deposition using the same recipe as the ultra-low damping material of Ref. [1]. By analyzing the mechanical resonance frequency as a function of the magnetization direction, we determine the magnetoelastic constant to $\lambda_{\parallel} = (-20.72 \pm 0.33) \times 10^{-6}$ for the $Co_{25}Fe_{75}$ compound and $\lambda_{\parallel} = (-9.8 \pm 0.12) \times 10^{-6}$ for the $Co_{10}Fe_{90}$ compound [3].

To measure the magnetoelastic constant of the ultra-low magnetization damping material Co_xFe_{1-x} we deposit the layer stacks reported in Ref. 1 onto a doubly clamped, suspended silicon nitride string (cf. Fig. 1(a)). The resonance frequency of this multilayer string scales approximately as $\Omega/2\pi = 1/L\sqrt{\sigma_{\mathrm{eff}}/\rho_{\mathrm{eff}}}$, where L is the length of the string, σ_{eff} is the effective stress along the string, and ρ_{eff} is the effective mass density of the whole layer stack. σ_{eff} is directly related to the static stress σ_0 in the system. Moreover, when we measure the resonance frequency as a function of the magnetization direction Θ (cf. Fig. 1(b)), we expect a modulation of the resonance frequency because the magnetoelastic interaction changes the stress in the sample which depends on the magnetization direction as $\sigma_{\mathrm{eff}} = \sigma_0 + \sigma_1 \cos^2 \Theta$. The additional stress σ_1 allows us to determine the magnetostrictive constant [5]: $\lambda_{\parallel} = \sigma_1 t/(t_{\mathrm{CoFe}} E_{\mathrm{CoFe}})$. Note that due to the specific geometry of the string, we can access only the parallel part ($\lambda_{\parallel} \parallel x$) of the magnetostrictive constant, because only stress variations in the x-direction affect the string's resonance frequency. This magnetostrictive constant relates to the magnetoelastic constant b

---

[1] Funded by the German Research Foundation via Germany's Excellence Strategy (EXC-2111 – 390814868) and project WE5386/4-1.

[2] National Institute of Standards and Technology, Boulder, CO 80305, USA.

via [7]: $b = B/M_\mathrm{s} = -3\lambda_\parallel G/(M_\mathrm{s})$, with shear modulus G of the CoFe alloy and its saturation magnetization M_s.

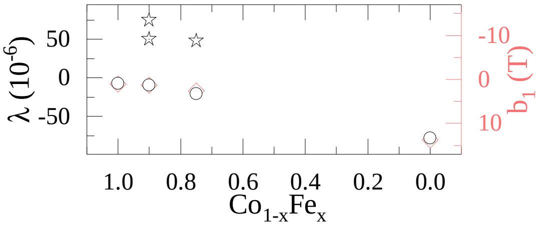

Figure 2: Magnetostrictive and magnetoelastic constants for the two investigated $\mathrm{Co}_{1-x}\mathrm{Fe}_x$ thin films and pure metals (Co [5],Fe [6]) for reference. Circles show the magnetostrictive contant ($\lambda_\parallel$) on the left scale, while diamonds (red) depict the corresponding magnetoelastic constant (b) on the right scale. The star shaped data points correspond to literature values from Refs. 3, 4.

To set these results in context, we plot the extracted values of $\lambda_\parallel$ and b for the two investigated thin film CoFe alloys ($\mathrm{Co}_{25}\mathrm{Fe}_{75}$ and $\mathrm{Co}_{10}\mathrm{Fe}_{90}$) as well as the values for thin-film Co [5] and bulk Fe [6] in Fig. 2. The ultra-low damping material investigated here seems to follow the simple trend of interpolating the magnetostrictive constant between the bulk values of the constituent elements. For comparison, Fig. 2 also shows the data of 500 nm thick $\mathrm{Co}_x\mathrm{Fe}_{1-x}$ films [8] and bulk crystal discs [4]. These earlier measurements report significantly different values, even with opposite sign. We note, however, that the seed layer material used here causes interface effects between the seed and the CoFe layer and represents a crucial component for the realization of ultra-low damping materials [9]. Thus, we rationalize that the magnetoelastic properties are significantly altered by these interface effects. Low damping $\mathrm{Co}_{25}\mathrm{Fe}_{75}$ was realized so far on SiO_x [9] and Si [10] using the same seed layers as in this work. To ensure that the low-damping behavior of the Co-Fe is still present when changing the substrate from Si [1] to SiN used in our work, we performed ferromagnetic resonance (FMR) experiments on unpatterned CoFe-stacks on SiN samples and find a Gilbert damping of $\alpha = (2.1 \pm 0.1) \times 10^{-3}$ which is in agreement with the values from Schoen *et al.* [1].

In summary, we extract a magnetostrictive constant of $\lambda_\parallel = (-20.72 \pm 0.33) \times 10^{-6}$ which corresponds to a magnetoelastic constant of $b = 2.62(5)$ T for the ultra low damping $\mathrm{Co}_{25}\mathrm{Fe}_{75}$ compound, as well as $\lambda_\parallel = (-9.8 \pm 0.12) \times 10^{-6}$ and $b = 1.30(2)$ T for the $\mathrm{Co}_{10}\mathrm{Fe}_{90}$ compound. This shows that the magnetoelastic properties of the two investigated alloys have the same order of magnitude as the constituent elements but differ significantly between the low-damping and normal damping case. The ultra-low damping compound $\mathrm{Co}_{25}\mathrm{Fe}_{75}$ shows a sizeable magnetoelastic constant and thus is a promising candidate for sensing and magnetization dynamic applications.

References

[1] M. A. W. Schoen, D. Thonig, M. L. Schneider, T. J. Silva, H. T. Nembach, O. Eriksson, O. Karis, and J. M. Shaw, Nat. Phys. **12**, 839–842 (2016).
[2] M. Collet, O. Gladii, M. Evelt, V. Bessonov, L. Soumah, P. Bortolotti, S. Demokritov, Y. Henry, V. Cros, M. Bailleul *et al.*, Appl. Phys. Lett. **110**, 092408 (2017).
[3] D. Schwienbacher, M. Pernpeintner, L. Liensberger, E. R. Edwards, H. T. Nembach, J. M. Shaw, M. Weiler, R. Gross, and H. Huebl, J. Appl. Phys. **126**, 103902 (2019).
[4] R. C. Hall, J. Appl. Phys. **30** (1959).
[5] M. Pernpeintner, R. B. Holländer, M. J. Seitner, E. M. Weig, R. Gross, S. T. B. Goennenwein, and H. Huebl, J. Appl. Phys. **119**, 093901 (2016).
[6] F. Cardarelli. Ferrous Metals and Their Alloys. In **Materials Handbook: A Concise Desktop Reference**, 101–248 (Springer International Publishing, 2018).
[7] S. Chikazumi. *Physics of Ferromagnetism (International Series of Monographs on Physics)* (Clarendon Press, 1997).
[8] D. Hunter, W. Osborn, K. Wang, N. Kazantseva, J. Hattrick-Simpers, R. Suchoski, R. Takahashi, M. L. Young, A. Mehta, L. A. Bendersky, S. E. Lofland, M. Wuttig, and I. Takeuchi, Nat. Commun. **2**, 518 (2011).
[9] E. R. Edwards, H. T. Nembach, and J. M. Shaw, Phys. Rev. Appl. **11** (2019).
[10] M. A. W. Schoen, J. Lucassen, H. T. Nembach, T. J. Silva, B. Koopmans, C. H. Back, and J. M. Shaw, Phys. Rev. B **95**, 134410 (2017).

Quantitative Modeling of Superconducting Planar Resonators for Electron Spin Resonance[1]

S. Weichselbaumer, P. Natzkin, C. W. Zollitsch, M. Weiler, R. Gross, H. Huebl[2]

Microwave resonators are a key part of any electron spin resonance (ESR) experiment. They enhance the microwave magnetic field at the sample location and offer an enhanced sensitivity for the inductive detection of magnetization dynamics. Conventional ESR resonators based on three-dimensional (3D) microwave cavities provide a homogeneous microwave magnetic field but typically suffer from small filling factors and, in turn, a low sensitivity for small sample volumes. Planar microresonators are one pathway to reduce the mode volume, leading to an increased filling factor and therefore an enhanced sensitivity compared to 3D cavities. In addition, planar resonators operated at low temperatures allow one to use superconducting materials, offering small losses and extraordinarily high quality factors.

So far, a quantitative modeling complemented by experimental benchmarking of planar resonator designs is missing. In this work, we employ finite element simulations and continuous-wave ESR experiments to investigate three different resonator geometries. We characterize their microwave magnetic field distribution and the collective coupling rate between the microwave resonator and a spin ensemble of phosphorus donors in ^{nat}Si.

In Fig. 1, we present two of the three studied resonator geometries along with the simulated microwave magnetic field distribution. Fig. 1(a) shows a capacitively-shunted resonator (CR), coupled to a transmission line used for measuring the complex transmission S_{21}. The CR is a lumped-element microwave resonator, where a meander-shaped inductor is shunted by an interdigitated finger capacitor. In Fig. 1(b), we show the corresponding microwave magnetic field distribution $|B_1^{yz}|$ driving the spin resonance transition. The meander shape of the CR results in a counter-flow of the high-frequency currents in neighboring meander strips, resulting in a localization of the electromagnetic field close to the surface. This leads to a significant inhomogeneity of the B_1 field in the proximity of the structure and a fast decay of the magnetic field along the out-of-plane axis. The SR (Fig. 1(c)) has a coil-like arrangement of the wire. Here, the capacitance is provided by the inter-line capacitance of the wires. The arrangement of the wires leads to a parallel current flow in adjacent lines and thus to a much more homogeneous magnetic field, as shown in Fig. 1(d). Additionally, the decay length of the magnetic field along the z axis is about one order of magnitude larger than for the CR.

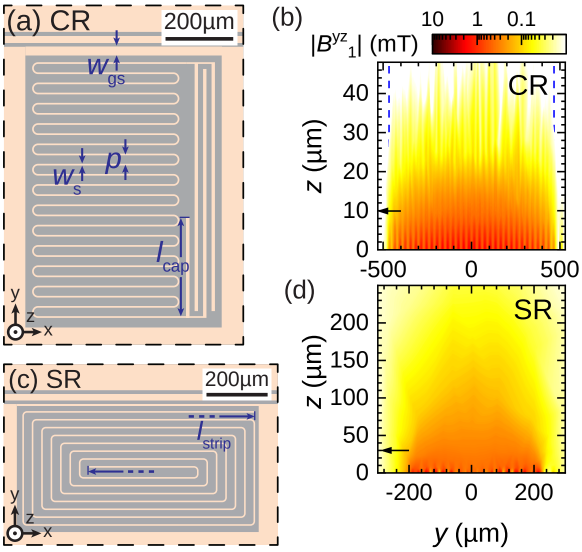

Figure 1: Schematic illustration of the resonator designs studied in this work. (a) Capacitively shunted meander-shaped resonator (CR), consisting of a finger capacitor and a meandering inductor. (b) Simulated magnetic field distribution $|B_1^{yz}|$ for the CR. (c) Spiral-shaped resonator (SR), with a two-dimensional coil-like arrangement of the wire. (d) Simulated magnetic field distribution $|B_1^{yz}|$ for the SR in the yz-plane. Anti-parallel current flow in adjacent wires results in a highly inhomogeneous field for the CR, while parallel current flow leads to a more homogeneous field for the SR.

---

[1] This report is a summary of results recently published in Physical Review Applied [1].

[2] We acknowledge financial support from the German Research Foundation via SPP 1601 (HU 1896/2-1).

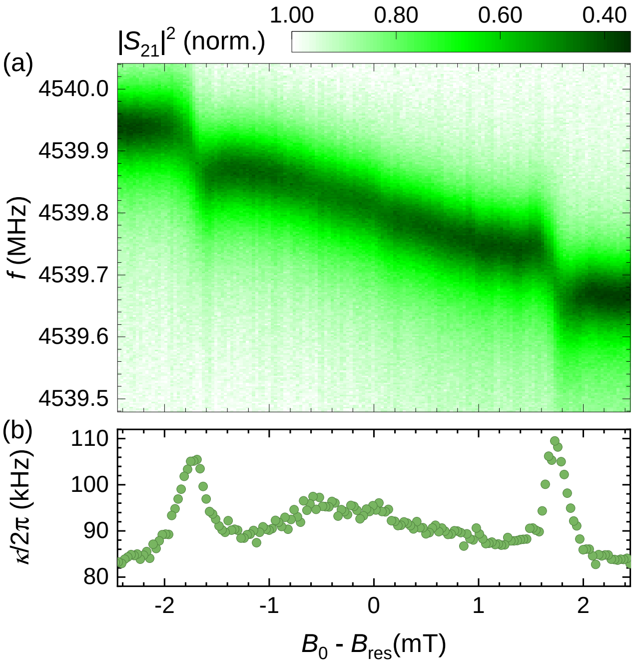

Figure 2: (a) Transmission magnitude $|S_{21}|^2$ as a function of frequency and applied magnetic field. The two distinct features indicate the phosphorus hyperfine transitions. (b) Extracted linewidth $\kappa/2\pi$ (HWHM) as a function of the magnetic field. The two peaks correspond to the hyperfine transitions. The features at intermediate fields are compatible with Pb_0/Pb_1 dangling bond defects and P_2 dimers.

We perform continuous-wave ESR measurements by placing a phosphorus-doped ^{nat}Si crystal with a doping concentration of $[P] = 2 \times 10^{17}\,\mathrm{cm}^{-3}$ on top of the resonator. We apply a static magnetic field parallel to the superconducting film surface and measure S_{21} using a vector network analyzer. In Fig. 2 (a), we show $|S_{21}|^2$ as a function of the excitation frequency and applied magnetic field (relative to the central resonance field). When the excitation frequency is in resonance with the microwave resonator, we observe a reduced transmission of $|S_{21}|^2 \approx 0.35$. The observed shift of the resonator frequency with the applied magnetic field is attributed to the field-dependence of the kinetic inductance of the superconductor. Further, we observe two distinct features at $\pm 1.7\,\mathrm{mT}$, which are identified as the two hyperfine transitions of the phosphorus donors in silicon.

For a more detailed analysis we determine the resonator linewidth κ as a function of the applied magnetic field. For this, we extract κ from the transmission spectra for each magnetic field step (see Fig. 2 (b)). This corresponds to a conventional continuous-wave ESR measurement, where the quality factor (absorption signal) of the resonator is measured. Besides the two prominent peaks, which are again associated with the two hyperfine transitions, we find in the magnetic field range between the two peaks an additional broad feature compatible with (i) dangling bond defects at the Si/SiO_2 interface, known as Pb_0/Pb_1 defects ($\approx -0.5\,\mathrm{mT}$), and (ii) exchange-coupled donor pairs forming P_2 dimers ($\approx 0\,\mathrm{mT}$).

For a quantitative comparison between the experimental data and the microwave magnetic field distribution we utilize the spin-resonator coupling rate. To this end, we quantitatively extract the spin-resonator coupling from the data presented in Fig 2 (b). A comparison of this experimentally determined coupling strength with the coupling computed from the finite element simulations gives excellent agreement.

In summary, we have analyzed three designs for superconducting planar lumped element resonators. We performed finite element method based simulations to calculate the characteristic magnetic field distribution of each resonator. Each of the resonator geometries has its own advantages, like reduced mode volume or large excitation field homogeneity. Our research demonstrates the power of finite element method based simulations to predict the spin-resonator coupling rate and gives insight into the different application cases of the resonator designs.

References

[1] S. Weichselbaumer, P. Natzkin, C. W. Zollitsch, M. Weiler, R. Gross, and H. Huebl, Phys. Rev. Appl. **12**, 024021 (2019).

Inductively Coupled Nano-electromechanics

P. Schmidt, M. Amawi, T. Luschmann, S. Pogorzalek, D. Schwienbacher, S. Weichselbaumer F. Deppe, A. Marx, R. Gross, H. Huebl[1]

Light-matter interaction in optomechanical systems provides the basis for ultra-sensitive detection schemes, ranging from gravitational wave detection to mass sensing of adsorbed atoms [1]. The underlying interaction Hamiltonian can also be implemented with superconducting circuits, defining the research field called nano-electromechanics. Until today, superconducting nano-electromechanics successfully demonstrated many interresting phenomena such as ground state cooling of mechanical systems, electromechanically induced transparency or squeezing of phonon states. However, present realizations suffer from the intrinsically weak photon-phonon coupling and do not unleash the full potential of the intrinsically nonlinear Hamiltonian. If stronger coupling can be realized, topics such as mechanical quantum state preparation or phonon-induced photon blockade can be immediately addressed.

So far, nano-electromechanical devices rely on coupling schemes based on a mechanically compliant capacitance. With such systems vacuum photon-phonon coupling rates g_0 of up to 300 Hz [2] have been demonstrated. As an alternative approach, already early proposals discussed the implementation of strong electromechanical coupling using a mechanically compliant inductance. The latter can be realized by a superconducting quantum interference device (SQUID) embedded into a microwave resonator [3]. Here, the electromechanical interaction is obtained via the flux dependent inductance of the SQUID. In more detail, the mechanical displacement of a freely suspended part of the SQUID loop modifies the flux threading the SQUID and hence changes the resonance frequency of the microwave resonator. We follow this approach and discuss an experimental realization of such a device.

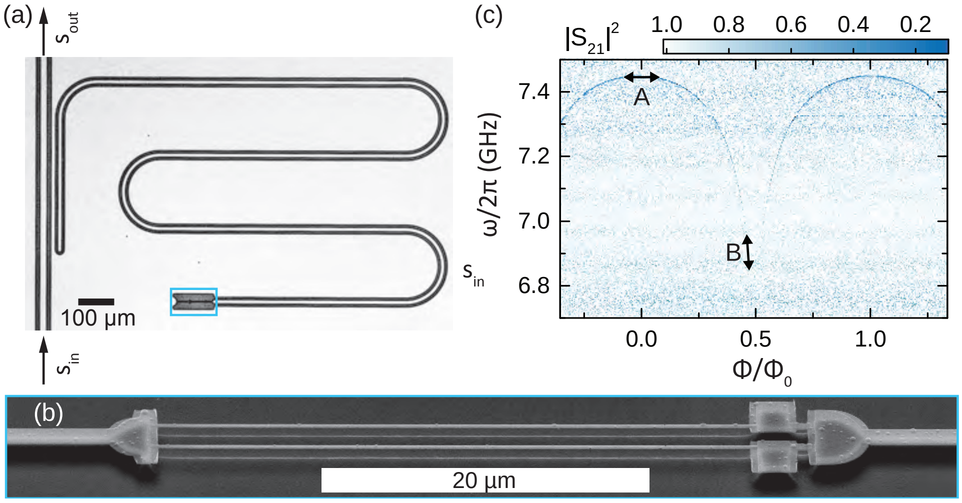

Figure 1: Sample layout and resonator flux-tuning. Panel (a) and (b) show a optical microscope and a SEM image of the sample, consisting of the superconducting microwave resonator and the partly suspended dc SQUID. The SEM image shows the mechanically compliant nano-strings. For a magnetic field B_{ext} applied perpendicular to the sample surface, the displacement of the nano-strings modifies the loop area of the SQUID, which corresponds to a change of the flux Φ threading the SQUID loop and, in turn, of the SQUID inductance. This realizes the electromechanial interaction Hamiltonian. Panel (c) shows the microwave transmission magnitude of the device as function of the applied flux Φ/Φ_0. The absorption of the resonator is visible as dark signature, demonstrating the flux-tunability of the device.

---

[1] This project is funded by the EU Horizon 2020 research and innovation program under grant agreement No. 736943 and by the German Research Foundation via Germany's Excellence Strategy (EXC-2111 – 390814868).

For this device type, the vacuum coupling strength is given by

$$g_0 = \frac{\partial \omega_c}{\partial \Phi} B_{\mathrm{ext}} \alpha \ell x_{\mathrm{zpf}}, \tag{1}$$

with the applied magnetic field B_{ext}, the modeshape factor α (here $\alpha \approx 1$), the length of the string ℓ, and the zero-point amplitude x_{zpf}. In addition, the important factor $\partial\omega_c/\partial\Phi$ describes the flux-to-frequency transfer function, relating flux changes to changes of the resonance frequency. As this transfer function depends on the applied flux or magnetic field, the electromechanical coupling becomes tunable and more importantly has the potential to reach the vacuum photon-phonon strong coupling limit [4].

We have designed, fabricated and characterized an inductively coupled nano-electromechanical system by embedding a partly suspended dc SQUID with a loop containing two mechanical nano-string resonators into a superconducting coplanar waveguide microwave resonator (see Fig. 1(a) and (b)). To investigate the electromechanical interaction, we performed microwave spectroscopy on the device cooled down to mK temperatures in a commercial dilution refrigerator.

As shown in Fig. 1(c), we can tune the resonance frequency of the microwave resonator by changing the SQUID inductance with an applied magnetic field. As expected we find a periodic variation of the resonance frequency as function of the applied magnetic field B_{ext}, respectively the normalized flux Φ/Φ_0. By the flux dependence of the resonance frequency we obtain a strongly tunable flux-to-frequency transfer $\partial\omega_c/\partial\Phi \approx 0$ function and hence electromechanical interaction. At point "A", $\partial\omega_c/\partial\Phi \approx 0$ and hence we have a vanishing electromechanical interaction. In contrast, a quantitative analysis of the data at point "B" yields $\partial(\omega_c/2\pi)/\partial\Phi = 6.7\,\mathrm{GHz}/\Phi_0$. At this operation pint we expect a large coupling strength.

Next, we operate the microwave resonator at point "B" and study the displacement noise of one of the nano-strings kept in thermal equilibrium at different temperatures. For this measurement we used a weak microwave probe tone at GHz frequencies and fW powers. Employing sideband spectroscopy, i.e. analyzing the Stokes-field of the scattered microwave photons, we observe a mechanical resonance frequency of $\Omega_m/2\pi = 6.343\,11\,\mathrm{MHz}$. Using a calibration tone technique similar to Ref. [5], we determine an electromechanical coupling rate of $g_0/2\pi = 1.62\,\mathrm{kHz}$ for $T = 186\,\mathrm{mK}$. Knowing g_0, we can calculated the power spectral density of the thermal displacement noise presented in Fig. 2. We find that the peak area, corresponding to the amount of thermal phonons populating the nano-string, increases with temperature as expected. Moreover, we can compare the experimentally determined $g_0/2\pi = 1.62\,\mathrm{kHz}$ with the prediction of Eq. (1). Using the parameters $\alpha = 1$, $B_{\mathrm{ext}} = 470\,\mu\mathrm{T}$, and $x_{\mathrm{zpf}} = 47\,\mathrm{fm}$ we theoretically expect an electromechanical coupling rate of 1.48 kHz, which is in good agreement with our experimental findings.

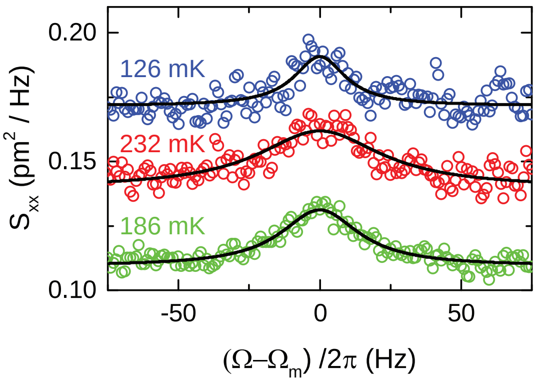

Figure 2: The Mechanical displacement spectrum of the device, showing the thermal sideband spectra of the nano-string, recorded at different temperatures. We find an increasing peak area and in particular linewidth when increasing the temperature.

In conclusion, our study of an inductively coupled nano-electromechanical system demonstrates a significant improvement of the electromechanical coupling strength of the inductive coupling scheme compared to the more traditional capacitive schemes. As the inductive coupling scheme has the potential to reach the strong single-photon single-phonon coupling limit [4], our findings offer a promising route to unlock the full potential of the nonlinear optomechanical interaction Hamiltonian. This allows one to realize fascinating quantum experiments such as the synthesis of phononic and photonic quantum states.

References

[1] M. Aspelmeyer, T. J. Kippenberg, and F. Marquardt, Rev. Mod. Phys. **86**, 1391 (2014).

[2] A. P. Reed, K. H. Mayer, J. D. Teufel, L. D. Burkhart, W. Pfaff, M. Reagor, L. Sletten, X. Ma, R. J. Schoelkopf, E. Knill, and K. W. Lehnert, Nat. Phys. **13**, 1163–1167 (2017).

[3] M. P. Blencowe, and E. Buks, Phys. Rev. B **76**, 014511 (2007).

[4] O. Shevchuk, G. A. Steele, and Y. M. Blanter, Phys. Rev. B **96**, 014508 (2017).

[5] M. L. Gorodetsky, A. Schliesser, G. Anetsberger, S. Deleglise, and T. J. Kippenberg, Optics Express **18**, 23236 (2010).

Materials, Thin Film and Nanotechnology, Experimental Techniques

Fast FPGA-based Measurements of Quantum Microwaves

K. G. Fedorov, R. Neagu, M. Renger, S. Pogorzalek, Y. Nojiri, Q. Chen, M. Partanen, A. Marx, F. Deppe, R. Gross[1]

Quantum state tomography is one of the central experimental tasks in quantum information processing and communication. Tomography of propagating quantum microwaves, generated by superconducting circuits, can be experimentally performed by using conventional ADC cards, such as the Acqiris card, and a subsequent PC-based data processing [1, 2]. This approach has proven to be very flexible and straightforward but has the disadvantage of being relatively slow due to the required data transfer between the ADC card and the PC. Taking into account that tomography of complex multi-partite quantum states may take months in real time, speeding up these measurements is of utter importance for various experiments in quantum information processing. Here, we demonstrate the application of a new generation of field programmable gate arrays (FPGA) for fast signal detection and real-time data processing. At the same time, these new FPGAs can be directly programmed using the conventional LabVIEW programming language which makes the image development much faster and easier in comparison with previous generations of FPGAs that required deep expertise in the rather user-unfriendly VHDL language.

In order to implement the quantum state tomography of propagating microwave states, we exploit the reference state reconstruction method. The latter relies on a calculation of statistical moments of field quadratures. By calculating all combinations of these quadrature moments one can, potentially, reconstruct the full density matrix of the studied quantum state. Real-time calculation of these quadrature moments computationally is a very demanding task. However, it can be very efficiently parallelized on a FPGA, such as the National Instruments board PXIe-7972R based on the chip Kintex-7 from Xilinx. A specific FPGA image has been developed by using the LabVIEW programming language. It includes digital demodulation, finite impulse response filtering, and quadrature moment calculation up to the fourth order as required for our quantum state tomography routines.

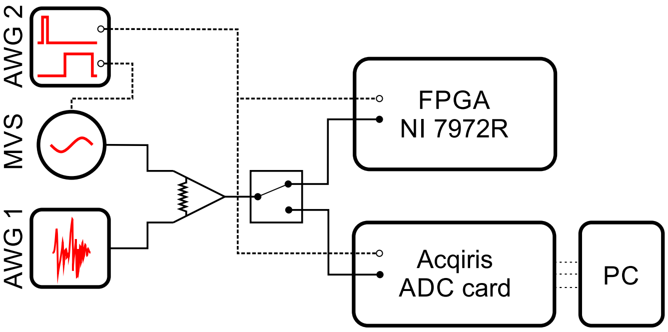

Figure 1: Scheme for experimental benchmarking of the FGPA-based versus the Acqiris-based microwave tomography approaches. We combine a pulsed continuous coherent tone at the frequency $f = 11\,\mathrm{MHz}$ and power $P = -53\,\mathrm{dBm}$ from the microwave vector source (MVS) with a continuous broadband noise with a peak-to-peak amplitude of $500\,\mathrm{mV}$ generated by the arbitrary waveform generator (AWG). The second AWG provides trigger and modulation pulses as required for the reference state reconstruction. The noisy signal is measured by either the FPGA or the Acqiris card. The second order correlation function $g^{(2)}$ is reconstructed from these measurements and used as a performance benchmark.

In order to quantify the performance of the FPGA-based tomography, it is reasonable to compare it directly to the already well-tested Acqiris card as shown in Fig. 1. We use the second order correlation function $g^{(2)}$ as a benchmark. It is defined as $g^{(2)} = \langle \hat{a}^\dagger \hat{a}^\dagger \hat{a} \hat{a} \rangle / \langle \hat{a}^\dagger \hat{a} \rangle^2$, where $\hat{a}^\dagger$ and $\hat{a}$ are the creation and annihilation operators of the signal mode. The $g^{(2)}$-function relies on the fourth-order signal moments of a propagating signal, and thus, serves as a perfect performance hallmark for our tasks. As a test microwave state, we use a coherent signal, with a known $g^{(2)} = 1$, in a noisy background and measure its standard deviation

---

[1] The authors acknowledge support by the Germany's Excellence Strategy (EXC-2111-390814868), the Elite Network of Bavaria through the program ExQM, and the EU Quantum Flagship project QMiCS (GrantNo.820505).

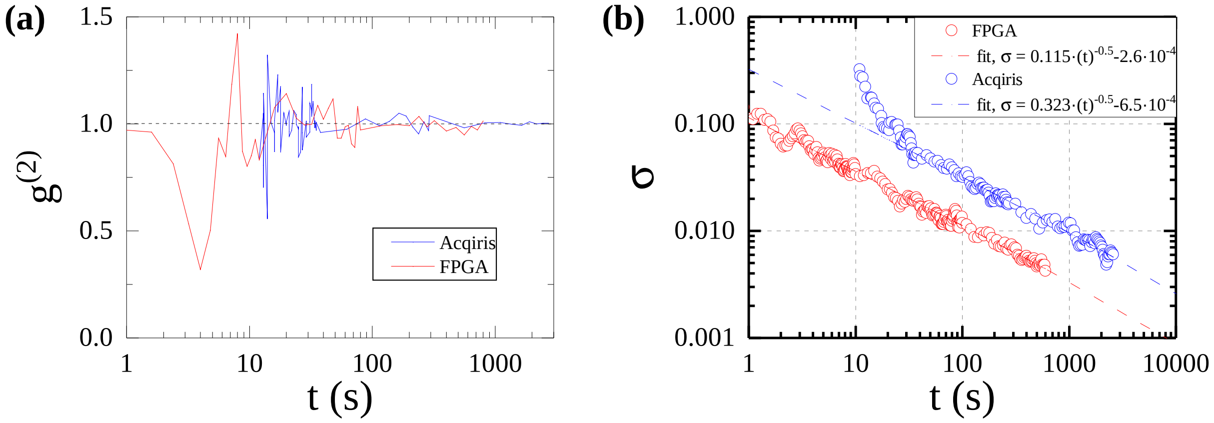

Figure 2: Measurements of the second order correlation function $g^{(2)}$ of a coherent tone in a noisy background. Plot **(a)** shows typical $g^{(2)}$ fluctuations as a function of averaging time t. Plot **(b)** demonstrates a comparison of $g^{(2)}$ standard deviations σ for the FPGA-based data acquisition & processing and for the Acqiris card data acquisition with the subsequent PC-based data processing. Here, the FPGA-based tomography clearly shows a consistent speed-up of $\simeq 7.5$ times over the Acqiris-based approach.

$\sigma = \sqrt{\langle (g^{(2)})^2 \rangle - \langle g^{(2)} \rangle^2}$. Results of these measurements are shown in Fig. 2. In Fig. 2(a), we observe a successful convergence of our measurements towards the coherent limit $g^{(2)} \to 1$ for sufficiently large averaging times $t > 100\,\mathrm{s}$. In Fig. 2(b), we show a comparison between the FPGA-based and the Acqiris-based approaches in terms of σ which quantifies the measurement precision for a certain averaging time. We observe a speed-up of $\simeq 7.5$ times of the FPGA-based set-up versus the Acqiris-based one. This is very close to a maximal theoretically expected speed-up of $\simeq 8$ times defined by the set of experimental parameters such as the measurement trigger rate, sampling rate, duty cycle, etc.

Finally, the FPGAs are indispensable not only because they offer a significant averaging speed-up. Many quantum protocols, such as quantum teleportation, rely on a feed-forward operation which consists of a local measurement, classical communication, and local operation [3]. For a successful quantum teleportation, all these tasks must be performed on a timescale less than the relative dephasing time of entangled signals. This time is usually on the order of several hundred of nanoseconds for propagating two-mode squeezed microwaves [4] and conventional ADC-based data processing setups are too slow for such feed-forward applications. However, by using an FPGA with digital-to-analog output capabilities and developing further the respective image, it is potentially possible to generate a feed-forward signal within the aforementioned dephasing time, and thus, open a way towards various applied quantum communication protocols with propagating microwaves.

References

[1] K. G. Fedorov, L. Zhong, S. Pogorzalek, P. Eder, M. Fischer, J. Goetz, E. Xie, F. Wulschner, K. Inomata, T. Yamamoto, Y. Nakamura, R. Di Candia, U. Las Heras, M. Sanz, E. Solano, E. P. Menzel, F. Deppe, A. Marx, and R. Gross, Phys. Rev. Lett. **117**, 020502 (2016).

[2] S. Pogorzalek, K. G. Fedorov, M. Xu, A. Parra-Rodriguez, M. Sanz, M. Fischer, E. Xie, K. Inomata, Y. Nakamura, E. Solano, A. Marx, F. Deppe, and R. Gross, Nat. Commmun. **10** (2019).

[3] R. Di Candia, K. G. Fedorov, L. Zhong, S. Felicetti, E. P. Menzel, M. Sanz, F. Deppe, A. Marx, R. Gross, and E. Solano, EPJ Quantum Technol. **2**, 25 (2015).

[4] K. G. Fedorov, S. Pogorzalek, U. Las Heras, M. Sanz, P. Yard, P. Eder, M. Fischer, J. Goetz, E. Xie, K. Inomata, Y. Nakamura, R. Di Candia, E. Solano, A. Marx, F. Deppe, and R. Gross, Sci. Rep. **8**, 6416 (2018).

Chained Josephson Parametric Amplifiers

M. Renger, K. G. Fedorov, S. Pogorzalek, Y. Nojiri, Q. Chen, M. Partanen, A. Marx, F. Deppe, R. Gross[1]

Squeezed states are an essential resource for many protocols in quantum information processing with continuous variables. In particular, remote state preparation [1] or quantum teleportation [2] in the microwave regime exploit entangled two-mode squeezed states as such quantum resources. These states can be generated using flux-driven Josephson parametric amplifiers (JPAs) in combination with linear microwave beam splitters.

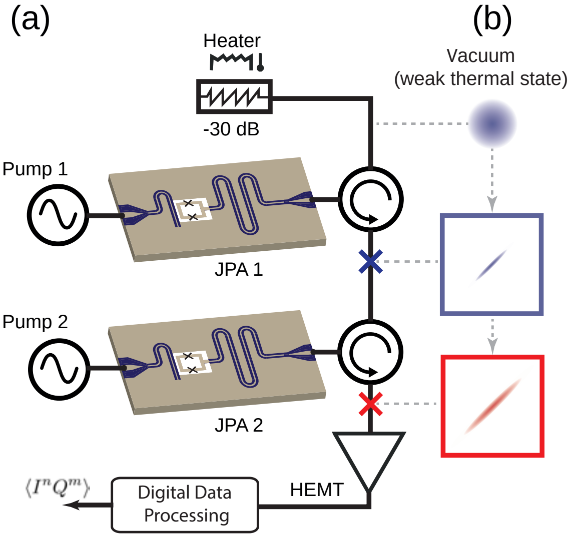

Figure 1: (a) Experimental realization of an amplification chain consisting of two JPAs and a cryogenic high electron mobility transistor (HEMT) amplifier. A heatable attenuator serves as a source of a weak thermal state. The blue (red) cross marks the reconstruction point for JPA 1 (JPA 2). (b) Schematic illustration of the protocol to increase the purity by amplifying the same quadrature with both JPAs.

The success of these protocols depends on the purity $\mu = 1/(4\sqrt{\det\sigma})$ of the two-mode squeezed states, where σ denotes a respective covariance matrix. However, μ decreases with increasing squeeze factors r which results from the gain dependence of the noise $\mathcal{A}(r)$ added by the JPA. Although, it is in principle possible to achieve noiseless amplification with degenerate parametric amplifiers, noise in a coherent pump signal, such as thermal noise or Poissonian fluctuations of the pump photon number, imply that $\mathcal{A}(r)$ is a monotonically increasing function of the degenerate gain $G = e^{2r}$ [3]. Thus, one may try to increase the purity of the squeezed state by using two serially connected (chained) degenerate JPAs which amplify the same quadrature, as shown in Fig. 1 (b). With the squeezed variance $v_\mathrm{s} = e^{-2r}(1+2\mathcal{A})/4$ and the respective anti-squeezed variance $v_\mathrm{a} = e^{2r}(1+2\mathcal{A})/4$, we find $\mu = 1/(4\sqrt{v_\mathrm{s} v_\mathrm{a}}) = 1/(1+2\mathcal{A})$ for the case where we only use one JPA for amplification. In the following, we analyze the case where we chain two JPAs as illustrated in Fig. 1 (a). Under the assumption that both JPAs are identical and linear, and JPA 1 (JPA 2) amplifies with the squeeze factor r_1 (r_2), with $r_1 + r_2 = r$, we can generalize the chained degenerate amplification and express the squeezed (anti-squeezed) variances $\tilde{v}_\mathrm{s}$ ($\tilde{v}_\mathrm{a}$) as

$$\tilde{v}_\mathrm{s} = \frac{e^{-2r_2}}{4}\left[e^{-2r_1}(1+2\mathcal{A}(r_1)) + 2\mathcal{A}(r_2)\right], \qquad \tilde{v}_\mathrm{a} = \frac{e^{2r_2}}{4}\left[e^{2r_1}(1+2\mathcal{A}(r_1)) + 2\mathcal{A}(r_2)\right]. \tag{1}$$

Thus, chaining two JPAs improves the resulting purity of the squeezed state if

$$\mathcal{A}(r_1) + \mathcal{A}(r_1)^2 + \mathcal{A}(r_2)\cosh(2r_1) + \mathcal{A}(r_2)^2 \leq \mathcal{A}(r) + \mathcal{A}(r)^2. \tag{2}$$

We experimentally investigate whether Eq. (2) is fulfilled using the setup in Fig. 1 (a) with the JPA operated at the frequency $\omega_0/2\pi = 5.435\,\mathrm{GHz}$. The input signal is a weak thermal state at $T = 35\,\mathrm{mK}$ with the variance close to the vacuum limit of $1/4$. For the individual JPA measurements, one JPA is pumped at $2\omega_0$ and the other JPA frequency is shifted away from ω_0 in order to avoid unwanted interference. Assuming a linear dependence of $\mathcal{A}(r)$ on the

---

[1] We acknowledge support by Germany's Excellence Strategy (EXC-2111-390814868), the Elite Network of Bavaria through the program ExQM, and the EU via the Quantum Flagship project QMiCS (GrantNo.820505).

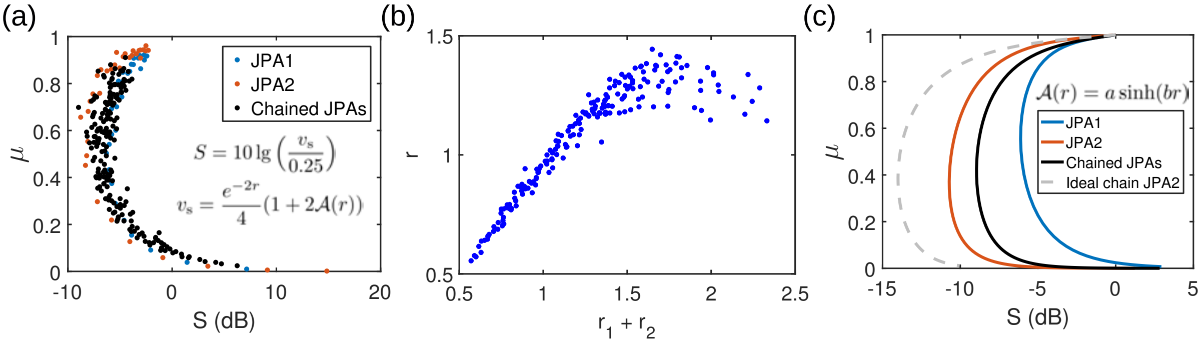

Figure 2: (a) Comparison of purity versus varying squeezing level S for the individual JPA 1 (JPA 2) and for the chained JPAs. (b) Experimental comparison of the effective squeeze factor r to the expected $r = r_1 + r_2$ behavior. Deviations from a linear correspondence for larger squeeze factors are caused by an unwanted pump crosstalk between indiviual JPAs. (c) Theoretical prediction of the squeezing level under the assumption that the number of added noise photons obeys a power law dependence on G. The measured noise photon number for the individual JPA measurements is fitted with $\mathcal{A}(r) = a\sinh(br)$ and μ is calculated from the resulting variances. For the chained JPAs, Eq. (1) is used. The gray dashed line shows the predicted squeezing level $\mu(S)$ for the case where JPA 1 is exactly equivalent to JPA 2 with no crosstalk.

degenerate gain and $\mathcal{A}(0) = 0$, we can model $\mathcal{A}(r) = \mathcal{A}_0 \sinh(2r)$, where the constant $\mathcal{A}_0$ is determined by the noise power in the pump line. We measure $\mathcal{A}_0 \simeq 0.053$ and estimate from Eq. (1) that chaining does not provide an advantage for $0.1 \leq r \leq 2.8$ which coincides with the range of our measured squeezing factors. For $\mathcal{A}_0 \geq 0.2$, we should always obtain an advantage in purity with the chained setup according to Eq. (2). We demonstrate the experimentally extracted purities versus the squeezing level $S = 10\lg\left(e^{-2r}(1+2\mathcal{A}(r))\right)$ for the individual JPAs and the chained JPAs in Fig. 2 a). Assuming that the noise added by each JPA obeys a power law dependence on the gain G, we fit the measured noise photon numbers for JPA 1 and JPA 2 using $\mathcal{A}(r) = a\sinh(br)$ which allows us to find $\mu(S)$ for the individual JPA measurements. In Fig. 2 (b), we plot the effective squeeze factor r as a function of $r_1 + r_2$. We observe that $r_1 + r_2 > r$ for large squeezing which is a result of a crosstalk between the JPAs. To model crosstalk, we define the parameter $\lambda \equiv (r_1 + r_2)/r$. In the absence of crosstalk, we have $\lambda = 1$, whereas λ becomes larger with increasing influence of crosstalk. To achieve a certain squeeze factor r with chained JPAs, on average, both JPAs must amplify with a squeeze factor $\lambda r/2$. Thus, each JPA adds noise $\mathcal{A}(\lambda r/2) > \mathcal{A}(r/2)$ in the chained case, implying that chaining can decrease the purity for a given r if λ is reasonably large. In Fig. 2 c), we plot the calculated $\mu(S)$ for the indidual JPAs as well as for the chained case using Eq. (1) and $\lambda \simeq 4/3$, the latter we extract from Fig. 2 (b) for high squeeze factors r. We observe a qualitative agreement between the experimental data in Fig. 2 (a) and theory in Fig 2 (c). Squeezing or purity advantage is not yet observed in the current experiment due to a big difference between JPA 1 and JPA 2 noise parameters. Additionally, chaining would lead to an increased purity in the case of higher noise power in the pump signal. The dashed line in Fig. 2 (c) shows the expected $\mu(S)$ for the case where JPA 1 is equal to JPA 2 and $\lambda = 1$. Thus, we predict a significant improvement in purity and squeezing by chaining two equal JPAs with negligible pump crosstalk.

References

[1] S. Pogorzalek, K. G. Fedorov, M. Xu, A. Parra-Rodriguez, M. Sanz, M. Fischer, E. Xie, K. Inomata, Y. Nakamura, E. Solano, A. Marx, F. Deppe, and R. Gross, Nat. Commun. **10**, 2604 (2019).

[2] R. Di Candia, K. G. Fedorov, L. Zhong, S. Felicetti, E. P. Menzel, M. Sanz, F. Deppe, A. Marx, R. Gross, and E. Solano, EPJ Quantum Technol. **2**, 25 (2015).

[3] P. Kylemark, M. Karlsson, and P. A. Andrekson, IEEE Photon. Technol. Lett. **18**, 1255 (2006).

Superconducting Cables for Microwave Quantum Communication over Kilometer Distances

M. Partanen, M. Pfeiffer, S. Pogorzalek, M. Renger, Q. Chen, Y. Nojiri, A. Marx, K. G. Fedorov, F. Deppe, R. Gross[1]

Quantum technologies based on superconducting microwave circuits provide fascinating opportunities for revolutionizing our everyday life. For example, these circuits enable secure communication [1, 2] which is of utmost importance in our modern society. Furthermore, quantum circuits may provide an advantage over classical ones in sensing applications such as radar [3, 4]. However, quantum signals are extremely sensitive to unwanted energy dissipation and noise that prevent an efficient transfer of quantum information. Therefore, the interconnections within a quantum circuit require precise engineering to mitigate the dissipation and decoherence mechanisms. Here, we report on measurements and characterization of the losses in superconducting coaxial cables and, especially, at a physical connector between such cables. Our experimental results show that the connector developed by KEYCOM enables quantum communication over distances of the order of a kilometer.

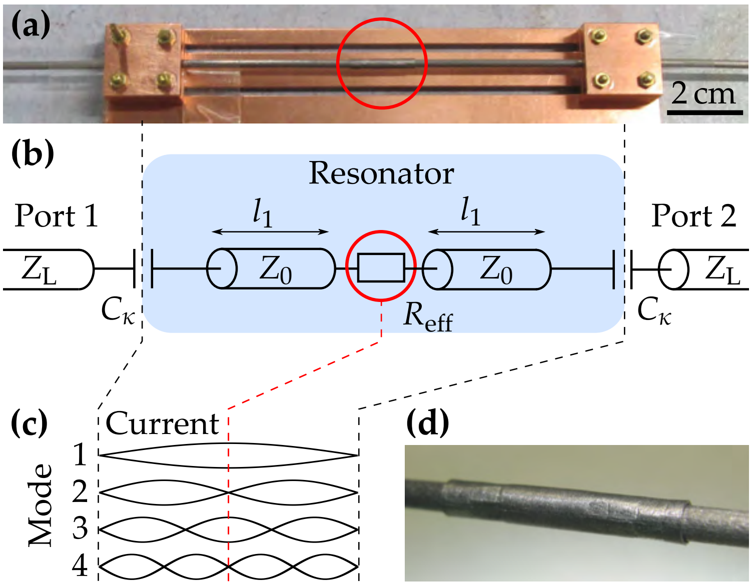

Figure 1: Experimental setup and the corresponding circuit diagram together with current mode profiles. (a) Photograph showing the studied cable resonator with the connector (marked by the red circle). The coupling capacitances consist of copper blocks shielding a gap between the resonator and external cables. (b) Circuit diagram of the sample. The connector is represented by an effective resistance R_{eff}. The connector divides the resonator into two parts with an equal length l_1, and a characteristic impedance Z_0. The coupling capacitances, C_κ, are nominally identical. (c) The current profiles of the four lowest resonance modes. The odd modes have a current antinode and the even modes have a node at the position of the connector. (d) Photograph of the connector point. The visible part of the connector has a length of 17 mm.

The losses in transmission lines can be accurately measured in a resonator configuration [5]. Figure 1 shows the structure of our resonator setup together with the corresponding circuit diagram. We study superconducting coaxial cables with and without a connector joining two separate cable parts. The cable has a diameter of 2.19 mm, and the center conductor and the shield are fabricated out of NbTi. In the resonator configuration, the signal bounces back and forth between the endpoints of the resonator, i.e., capacitors C_κ. The losses of the resonator can be characterized with a quality factor which indicates how many times, on average, the signal travels across the resonator before it is dissipated. The total losses are described by the loaded quality factor $Q_L = (Q_{\text{int}}^{-1} + Q_{\text{ext}}^{-1})^{-1}$, where Q_{int} presents the internal and Q_{ext} the external losses. Due to the signal bouncing, the resonator effectively corresponds to a cable with a length equal to the resonator length multiplied by Q_L. This method allows for a precise experimental estimation of ultra-low transmission

---

[1] We thank KEYCOM for developing the connectors for superconducting cables. We acknowledge support via Germany's Excellence Strategy (EXC-2111-390814868), the Elite Network of Bavaria through the program ExQM, and the EU Quantum Flagship project QMiCS (Grant No. 820505).

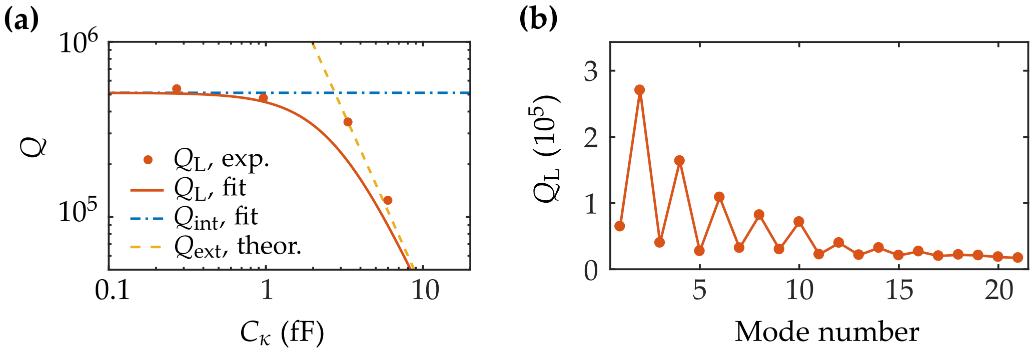

Figure 2: Experimental results. (a) Loaded quality factor Q_L as a function of the coupling capacitance C_κ for the fundamental mode ($f_0 = 1.4\,\mathrm{GHz}$) of the resonator without a connector at $T = 4.2\,\mathrm{K}$. The horizontal dash-dotted line indicates the extracted internal quality factor and the yellow dashed line the calculated external quality factor. (b) Loaded quality factor as a function of the mode number for the resonator with the connection point. Here, the fundamental mode is $f_0 = 0.9\,\mathrm{GHz}$, the coupling capacitance is $C_\kappa \approx 1\,\mathrm{fF}$, and the temperature is 4.2 K.

losses in superconducting cables.

We measure the transmission and reflection coefficients of the resonator using a vector network analyzer (Rohde & Schwarz, ZVA 24). The resonator is measured at temperatures of approximately 1.6 K and 4.2 K in a ^{4}He cryostat. We can extract the internal and external losses by varying the coupling capacitance, as shown in Fig. 2(a) for a resonator without the connection point. The quality factors on the order of half a million indicate very low losses in the cable. Furthermore, we analyze the connector at different frequencies by measuring the quality factors of several modes, as shown in Fig. 2(b). Since the connector is positioned in the middle of the resonator, it couples strongly to the odd modes owing to the current antinode [see Fig. 1(c)]. We describe the connector as an effective resistance with frequency dependent magnitude. Its value can be extracted from the measured quality factors of the odd modes. Finally, we estimate the losses per kilometer in the cable with connectors every two meters. Importantly, the signal can propagate approximately 1.5 km before half of the incident power is dissipated at the frequencies around 6 GHz, which are relevant for modern quantum communication protocols with superconducting circuits.

In conclusion, our results indicate that quantum communication over superconducting transmission lines is feasible over distances in the range of a kilometer. Thus, our work contributes to the development of a quantum local area network utilizing superconducting circuits. Moreover, intracity networks connecting quantum hubs are feasible in the future by utilizing amplifiers and further improving the low-loss superconducting cables. Notably, the cables and connection points studied here can be operated at temperatures reachable with liquid ^{4}He which is a substantial technological advantage over millikelvin temperatures requiring more complicated ^{3}He/^{4}He dilution refrigerators.

References

[1] K. G. Fedorov, S. Pogorzalek, U. Las Heras, M. Sanz, P. Yard, P. Eder, M. Fischer, J. Goetz, E. Xie, K. Inomata, Y. Nakamura, R. Di Candia, E. Solano, A. Marx, F. Deppe, and R. Gross, Sci. Rep. **8**, 6416 (2018).
[2] S. Pogorzalek, K. G. Fedorov, M. Xu, A. Parra-Rodriguez, M. Sanz, M. Fischer, E. Xie, K. Inomata, Y. Nakamura, E. Solano, A. Marx, F. Deppe, and R. Gross, Nat. Commun. **10**, 2604 (2019).
[3] U. Las Heras, R. Di Candia, K. G. Fedorov, F. Deppe, M. Sanz, and E. Solano, Sci. Rep. **7**, 9333 (2017).
[4] M. Sanz, K. G. Fedorov, F. Deppe, and E. Solano. Challenges in Open-air Microwave Quantum Communication and Sensing. In **2018 IEEE Conference on Antenna Measurements Applications (CAMA)**, 1–4 (2018).
[5] P. Kurpiers, T. Walter, P. Magnard, Y. Salathe, and A. Wallraff, EPJ Quantum Technol. **4**, 8 (2017).

Experimental Facilities

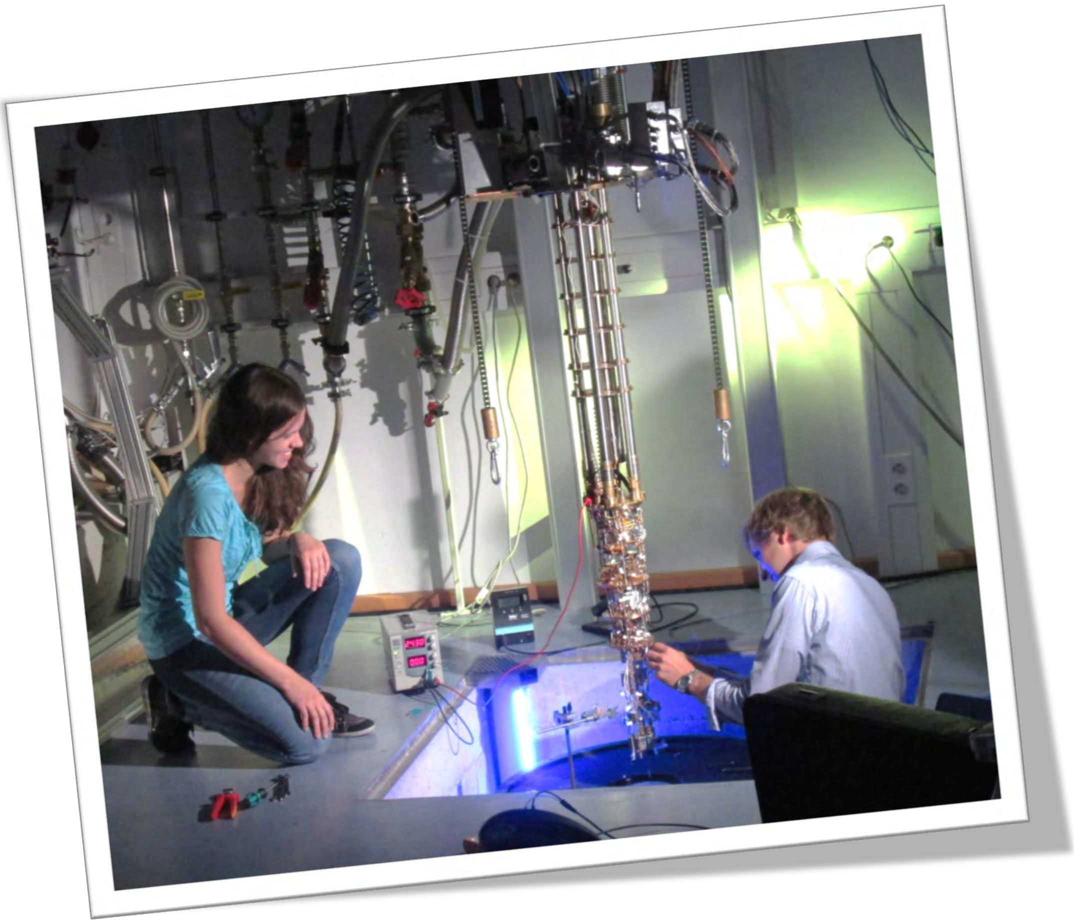

Overview of Key Experimental Facilities and Infrastructure

In the following basic information on the key experimental facilities and components of the technical infrastructure installed at the Walther-Meißner-Institute (WMI) is given.

UHV Laser-MBE

The WMI operates an UHV Laser-Molecular Beam Epitaxy (L-MBE) system for the growth of complex oxide heterostructures. The system has been designed to meet the special requirements of oxide epitaxy. The UHV cluster tool consists of the following main components:

- central transfer chamber;
- load-lock chamber with a heater system for substrate annealing;
- laser deposition chamber with a KrF excimer laser, *in-situ* reflection high energy electron diffraction (RHEED) system, laser substrate heating system, and atomic oxygen/nitrogen source; the RHEED system has been modified to allow for the operation at high oxygen partial pressure up to 0.5 mbar;
- surface characterization chamber with UHV scanning atomic force microscope (Omicron);
- metallization chamber with a four heart electron gun system and a liquid nitrogen cooled sample stage. The sample holder can be tilted for shadow evaporation.

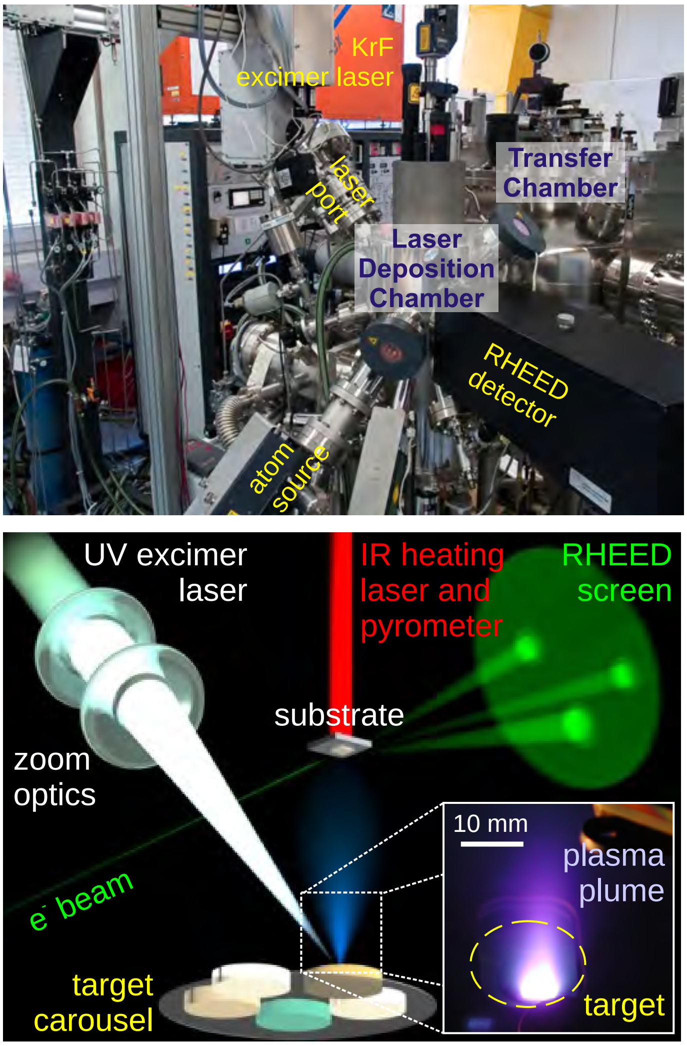

Figure 1: Top: UHV laser-molecular beam epitaxy system. Bottom: principle of the deposition process.

The system is used for the growth of complex oxide heterostructures consisting of superconducting, ferromagnetic, ferroelectric, and semiconducting materials such as high-temperature superconductors, doped manganites, (double) perovskites, magnetite, zinc oxide, rare earth iron garnets, pyrochlore iridates, etc.

The original laser molecular beam epitaxy system (laser-MBE) designed already in 1995/96 has been continuously upgraded and modified until today. In particular, the substrate heating system and the temperature control unit were changed from a resistive radiation heater to an infrared laser heating system (see Fig. 3, left) including a pyrometer for determining the sample temperature. In addition, a source for atomic oxygen and nitrogen has been installed. The main advantage of the new heating system is that only the substrate is heated while the surrounding parts are hardly affected (Fig. 3, right). In this way one can achieve a substantially better vacuum at temperatures well above 1000 °C. The achievable substrate temperature is limited by the melting point and the size of the substrate material (approx. 1410 °C for a 5 mm × 5 mm silicon substrate). The laser heating system has already been successfully used for removing the amorphous silicon oxide layer from the surface of silicon substrates at 1150 °C.

Figure 2: Pulsed Laser Deposition (PLD): When the pulse of the UV laser (KrF excimer laser, 248 nm) hits the target, the target material is ablated and the so-called laser "plume" containing highly excited atoms and molecules is formed.

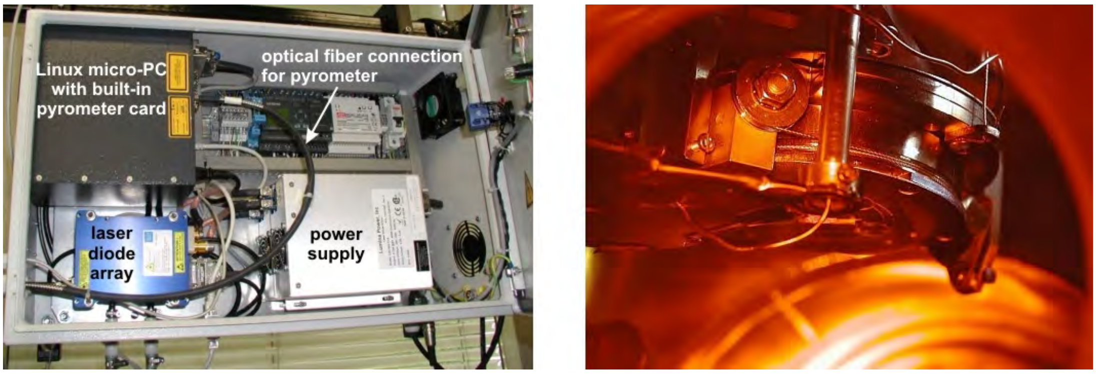

Figure 3: Components of the laser heating system: The substrate is heated using an IR diode laser head that is located in a separate box far away from the deposition chamber (left). The laser light is brought to the substrate (right) via an optical fiber.

We have further developed and installed a home-made telescope zoom optics for the pulsed UV laser light, consisting of in total five lenses on sliding lens holders allowing for a movement over a total distance of 1200 mm. The lens holders are attached to independent stepper motors, each connected to a controller providing an accurate positioning precision. The controllers are driven via a PC, thus allowing for a full automation of the lens system itself. With this telescope zoom optics we are able to change the area of the UV laser spot on the target, resulting in an accessible range of laser fluences from $\rho_\mathrm{L} = 0.5\,\mathrm{J/cm^2}$ to $5\,\mathrm{J/cm^2}$. To maintain a stable laser fluence at the target, we have installed a so-called *intelligent* window (PVD Products) at the laser entrance port combining two unique features. First, it keeps the inner side of the entrance window free of coatings by blocking the ablated plasma plume via a rotatable disc consisting of UV grade fused silica. Second, an insertable mirror positioned in the light path after the disc allows to guide the incoming UV laser pulse through a side window, where its energy is determined by a pyroelectric detector. These measures help to improve the deposition processes by accurately monitoring ρ_L as one of the most critical process parameters.

UHV Sputter Deposition System – SUPERBOWLS

The UHV sputter deposition system was set up in 2017 and allows for the fully-automated fabrication of complex multilayers consisting of superconducting and magnetic materials. To avoid cross-contamination of the superconducting and magnetic materials the system consists of two separate deposition chambers (see Fig. 4). One deposition chamber is dedicated for superconducting materials (Non-Ferromagnet Chamber: NFC) and the other for the growth of magnetic materials (All Ferromagnet Chamber: AFC). The loadlock chamber is positioned between the two deposition chambers. It serves for inserting substrates and masks into the deposition chambers and enables the in-situ transfer of samples between the two deposition chambers. The system is designed for a face-down substrate orientation with the sputter source residing at the bottom of the deposition chambers. Both deposition chambers achieve a base pressure well below 8×10^{-10} mbar, paving the way for the deposition of high purity materials.

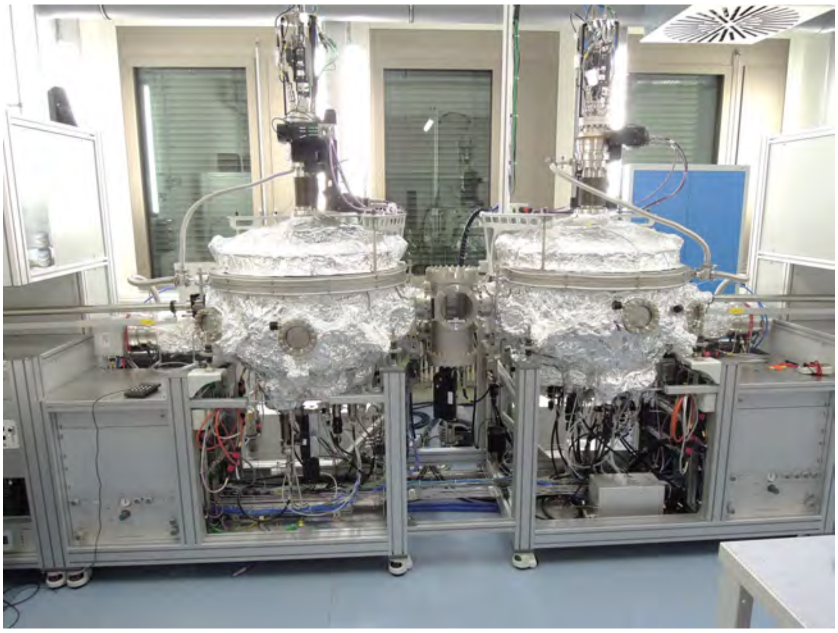

Figure 4: UHV sputter deposition system named «**SUPERBOWLS**». Left chamber is the NFC dedicated to the deposition of superconducting materials, right chamber is the AFC equipped with magnetic materials. Between the two deposition chambers resides the loadlock (LL).

The loadlock chamber is equipped with a substrate and mask storage cassette for up to six substrates. Halogen lamp heaters are installed in the loadlock for thermal precleaning of the substrates. The NFC is currently equipped with two 3 inch magnetrons and one 2 inch magnetron. In the AFC, eight 2 inch tiltable magnetrons are installed. In this chamber the sources can be either oriented into two confocal deposition clusters from 4 sources or 4 sources for face-to-face deposition, providing a large flexibility in the deposition conditions and enabling the fabrication of quaternary alloys from single element targets. All deposition sources are equipped with pneumatically actuated shutters, tilts, and linear translations. This allows for both face-to-face and confocal deposition from all three sources.

Both chambers are equipped with versatile substrate manipulators. They can accommodat substrates with a diameter of up to 2 inch and feature a resistive heater for substrate temperatures up to 800 °C, a motorized substrate shutter for wedge and step-profile deposition, a motorized linear translation for changing the source to substrate position, a main rotation to move the substrate in the chamber to the different deposition positions, a motorized substrate rotation at up to 40 rpm for homogenous deposition, and a quartz crystal microbalance (QCM) for growth rate monitoring. In addition, a Kaufmann source for reactive ion etching is installed in the system for in-situ surface cleaning procedures or even etching processes. Several 1 kW DC power and 600 W RF power supplies are used for the operation of the magnetrons. Mass flow controllers allow to change the composition of the process gas for reactive sputtering processes. More details can be found in the Annual Report 2017.

UHV Sputter Deposition System – ULTRADISC

In 2018, a new UHV sputter deposition system (1600 l/s turbo molecular pump, base pressure: $< 1 \times 10^{-9}$ mbar, automatic up- or down-stream pressure regulation: 8×10^{-4} mbar to 1×10^{-1} mbar) for the fabrication of superconducting thin films on large substrate areas has been installed.[1] The system consists of a main deposition chamber and a load lock, which is equipped with a motorized storage cassette for up to six substrates, a stab-in heater and a linear transfer arm for moving samples into and out of the main deposition chamber.

Figure 5: UHV sputter deposition system named «**ULTRADISC**». The main chamber contains the deposition sources in the bottom flange and the substrate manipulator on the top flange.

The main deposition chamber has been designed for flexible and homogeneous deposition on substrates with a diameter of up to 100 mm. The substrate holder is electrically isolated to allow for a plasma directly underneath the substrate via applying a DC or RF bias to the substrate holder. A radiative carbide heater is used to homogeneously heat the substrate up to 950 °C. The substrate manipulator has 3 degrees of freedom to move the substrate in the deposition chamber. The main substrate rotation allows to move the substrate over the different deposition clusters. In addition, the distance between substrate and sources can be tuned by 100 mm via a motorized z-shift of the manipulator. For homogeneous deposition, the substrate itself can rotate with up to 30 rpm. An automated substrate shutter allows to protect the substrate from unintentional deposition. Moreover, a motorized wedge shutter enables the fabrication of controlled thickness variations over the area of the substrate.

Flexibility in materials choice is ensured by a total of 11 magnetron sources installed in the chamber. A total of 7 sources can be used for face-to-face deposition on the substrate for high growth rate deposition (several 10 nm/min). In addition, 8 sources can be manually tilted into three separate confocal deposition clusters, which enables simultaneous deposition from up to 3 sources. Automated control of the deposition times is achieved by the motorized shutters attached to each magnetron. The high-purity gas supply is realized via 4 independent mass flow controllers, allowing for flexible gas compositions for reactive sputter deposition of oxide and nitride materials. For more flexibility in reactive sputtering processes and for substrate cleaning purposes the confocal cluster is equipped with a RF discharge ion source (up to 1.0 kV). Two different grids suitable for nitrogen and oxygen or argon are currently available for the system. Two separate mass flow controllers are used to supply the high purity gases to the ion source. The system is fully automated by the supplied computer and software. More details can be found in the Annual Report 2018.

---

[1] The system is running under the acronym «ULTRADISC »: **U**nlimited **L**egendary **T**ool for **R**eliable **A**chievements in the **D**eposition of **I**ntegrated **S**uperconducting **C**omponents.

UHV Electron Beam Evaporation System

The UHV metal MBE system allows for the growth of high quality metallic thin films by electron beam evaporation and molecular beam epitaxy. The system is optimized for the fabrication of superconducting persistent current qubits by aluminum shadow evaporation. It is equipped with an improved substrate holder allowing for multi-angle shadow evaporation. The main components of the system are:

- UHV system with a process chamber with a base pressure below $\sim 1 \times 10^{-8}$ mbar pumped by a 1000 l/s turbo molecular pump with magnetic suspension of the rotor adequate for corrosive gases.
- Load-lock chamber equipped with a magnetic transfer system (push-pull positioner) for sample transfer without breaking the vacuum in the process chamber.
- Downstream pressure control by an adaptive pressure controlled gate valve.
- Electron beam evaporator with six 8 cm^3 crucibles embedded in a linearly movable water cooled rail providing six different materials.
- Film thickness measurement and closed loop evaporation rate control by a quartz crystal microbalance in combination with the evaporation controller.
- Effusion cell for molecular beam epitaxy processes.
- Ion sputtering gun for in-situ sample cleaning
- Manipulator with UHV stepping motors for automated and precise sample tilt and options for rotating and cooling the sample.

A precise and reproducible tilt of the sample is realized by a sample manipulator with process specific degrees of freedom. The downstream pressure control allows for a fast adjustment and precise control of the oxygen partial pressure. This is crucial for a well-defined oxidation process of the Josephson junctions barriers. The entire process can be performed fully automated via a touch screen and is controlled by a LabView program. Up to six effusion cells can be optionally added to the system allowing for further materials. The manipulator allows for further degrees of freedom that can be used to align the sample to the effusion cells, the ion sputtering gun and to measuring equipment such as ellipsometry or RHEED.

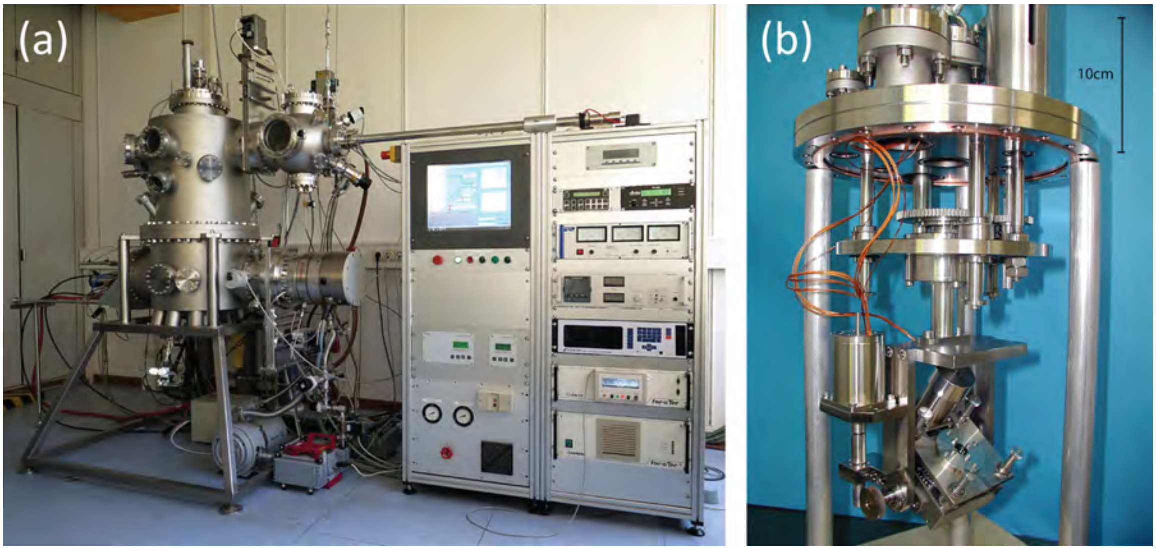

Figure 6: (a) Photograph of the UHV electron beam evaporation system. (b) Manipulator with UHV stepping motors for automated and precise sample tilt and options for rotation.

Single Crystal Growth and Synthesis of Bulk Materials

Transition metal oxides are of great interest due to their various interesting physical properties (e.g. high temperature superconductivity, colossal magnetoresistance, ferroelectricity, nonlinear optical properties etc.) and their high potential for applications. Therefore, the WMI operates a laboratory for the synthesis of bulk materials and single crystals of transition metal oxides. Besides various chamber- and tube furnaces a four-mirror image furnace is used for the crystal growth of various oxide systems. With this furnace crystals of many different compounds of the high temperature superconductors and various other transition metal oxides have been grown as single crystals using the traveling solvent floating zone technique. The furnace consists basically of 4 elliptical mirrors with a common focus on the sample rod and with halogen lamps in their other focus. By irradiation of the focused light the sample rod is locally heated and eventually molten. The molten zone can be moved up and down along the entire sample rod under simultaneous rotation. Due to the anisotropic growth velocity a preferential growth of those grains with the fastest growth velocity along the pulling direction is obtained and the formerly polycrystalline rod is transformed into a single crystal. Single crystal growth can be performed with this furnace at maximum temperatures up to 2200 °C in the pressure range from 10^{-5} mbar up to 10 bar and in oxidizing, reducing as well as inert atmosphere.

Figure 7: The four-mirror image furnace installed at the crystal laboratory of the WMI. Crystals can be grown by the floating zone and traveling solvent floating zone techniques at temperatures up to 2200 °C and pressures up to 10 bar.

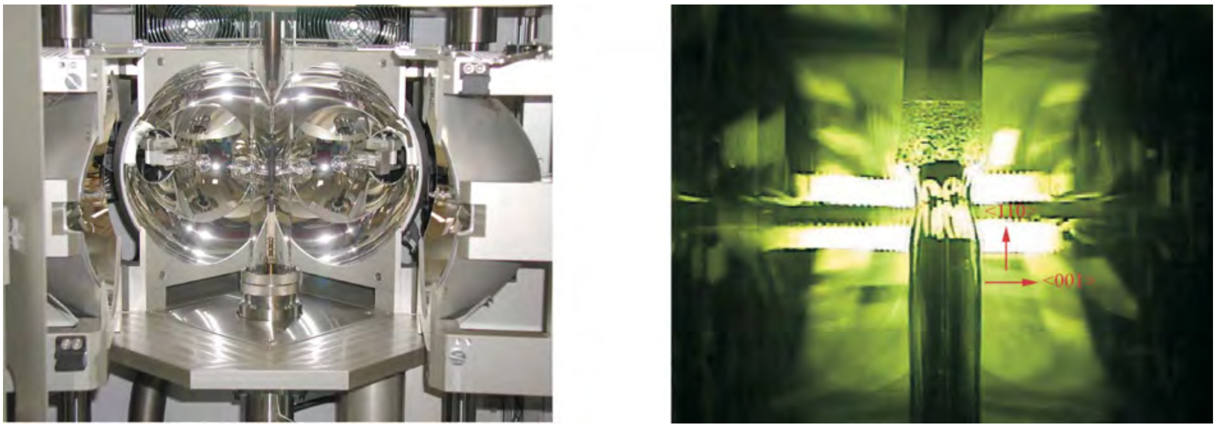

Figure 8: Left: Central part of the image furnace with four elliptical mirrors. In the center one can see the quartz tube with a polycrystalline rod. Right: View on the molten zone of $Pr_{2-x}Ce_xCuO_4$ (melting point: 1280 °C) obtained by a CCD camera.

The X-ray diffraction systems

For X-ray analysis the WMI operates two X-ray diffractometers (Bruker D8 Advance and D8 Discover). The two-circle system is used for powder diffraction. In this system the samples can be heated in oxygen atmosphere up to 1600 °C. It is equipped with a Göbel mirror and an area detector to save measuring time. The second system is a high resolution four-circle diffractometer that can be used for reciprocal space mappings. It is equipped with a Göbel mirror and an asymmetric two-fold Ge monochromator and allows for the texture analysis of thin film heterostructures, superlattices and single crystalline materials. In both systems measurements can be carried out fully computer controlled.

Beside these two Bruker X-ray systems a Laue camera for single crystal analysis and a Debye-Scherrer camera are available.

Figure 9: The two-circle X-ray diffractometer Bruker D8 Advance.

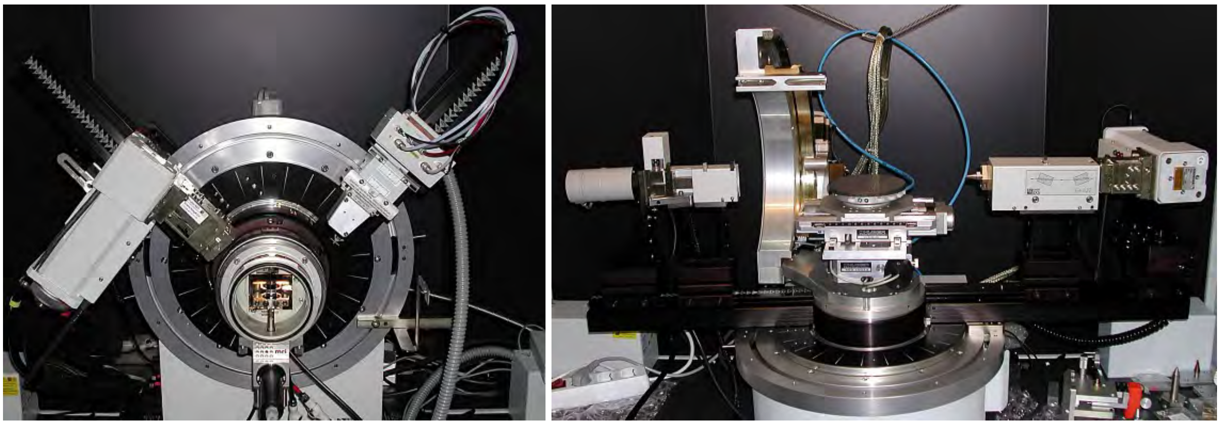

Figure 10: Left: High temperature sample holder of the D8 Advance system. Right: Four-circle high resolution X-ray diffractometer Bruker D8 Discover.

The SQUID magnetometer

Figure 11: Quantum Design SQUID magnetometer.

For the analysis of the magnetic properties of materials, a Quantum Design SQUID magnetometer system (Fig. 11) is operated at the WMI. The SQUID magnetometer allows for measurements in the temperature regime from 1.8 to 400 K and provides excellent sensitivity particularly in the low field regime. Due to the excellent sensitivity of the system, thin film samples with a very small sample volume can be analyzed. The SQUID magnetometer is equipped with a superconducting solenoid allowing for a maximum field of 7 T. At present, the magnetometer is used for the characterization of magnetic and superconducting materials (both in bulk and thin film form). Examples are the cuprate high temperature superconductors, the doped manganites, magnetite, the double perovskites, magnetic semiconductors, or multiferroics.

The High Field Laboratory

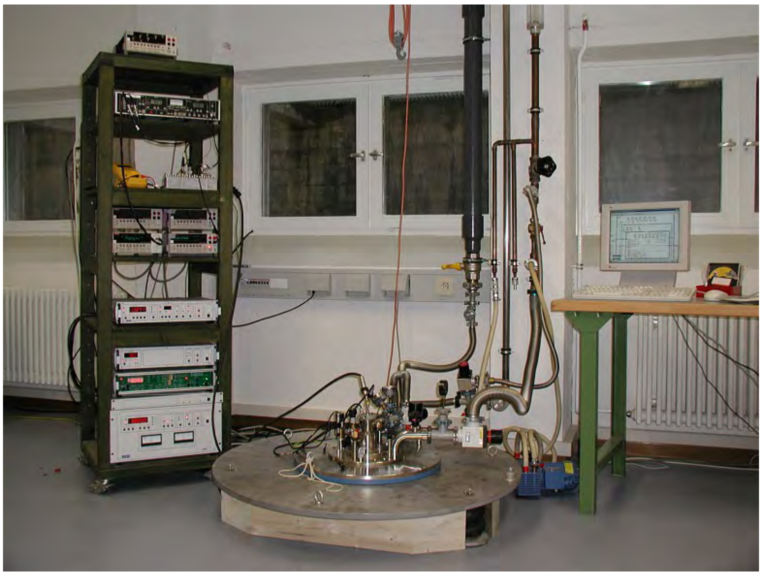

Figure 12: High field laboratory with Oxford 17 T magnet system.

Transport and thermodynamic properties of samples are often studied as a function of the applied magnetic field. For such measurements several superconducting magnets are available at the WMI. Two of them (8/10 and 15/17 Tesla magnet system) are located in the high magnetic field laboratory in the basement of the WMI. The magnet systems are installed below the floor level to facilitate the access to the top flange and the change of the sample sticks. The magnet systems are decoupled from the building to avoid noise due to mechanical vibrations. A variety of sample holders can be mounted allowing for e.g. sample rotation during the measurement. For standard sample holders the accessible temperature regime is $1.5\,\mathrm{K} < T < 300\,\mathrm{K}$. However, also ^{3}He/^{4}He dilution refrigerator inserts ($T > 20\,\mathrm{mK}$) or high temperature units ($T < 700\,\mathrm{K}$) can be mounted. All measurements are fully computer controlled (by the use of the LabView software tool) allowing for remote control and almost continuous measurements.

Since 2012, a 3D vector magnet with variable temperature insert, allowing for 2.5 T in-plane and 6 T out-of-plane magnetic fields is available for thermal and electrical transport experiments. This system has been named “Chaos” cryostat (acronym for “Cold, Hot And Other Secret experiments”). It consists of a ^{4}He flow cryostat with a liquid nitrogen shield and includes a vertically oriented 6 T solenoid combined with two horizontally oriented split coil pairs. The magnet system can be operated in two ways:

- in a single axis mode: up to 6(2.5) T are provided in the vertical (horizontal) direction.
- in a arbitrary axis mode: the flux density vector can be oriented in arbitrary directions and the magnitude of the flux density is limited to 2.5 T.

The magnetic field is controlled by a Mercury IPS superconducting magnet power supply master/slave system. It provides output currents of up to 120 A in bipolar operation for each magnet axis. The control of the system is feasible either directly via touch-screen or remote using a LabView based software.

The Chaos cryostat has a IN100 variable temperature insert (VTI), enabling an operation for temperature setpoints between 1.5 K and 300 K. The temperature control of the sample space inside the VTI can be achieved via an automatic needle valve drive for helium flow control and/or an automatic heater system. The temperature of the VTI is read via a Cernox sensor fitted to the heat exchanger. A remote control of the system is realized by a LabView based software. It provides control of the VTI (heater, needle valve, temperature setpoint) and the IPS (control of the magnetic field setpoints and energizing rates for the three vector components of the field) as well as the display of the actual He and liquid nitrogen levels.

Figure 13: The 3D vector magnet with control electronics in the "CHAOS" Laboratory.

A further 3D vector magnet allowing for 1 T in-plane and 6 T out-of-plane magnetic fields is installed in the WMI Quantum Laboratories as part of a cryogen-free dilution system.

The Clean Room Facility

For the fabrication of nanostructures and quantum circuits including superconducting, spintronic and nanomechanical devices, the WMI operates a class 1000 clean room facility with an area of about 50 m^2. The clean room is subdivided into two parts for optical lithography and electron beam lithography, respectively. The clean room is equipped with the standard tools for optical lithography such as resist coaters, hot plates, wet benches, a Karl Süss MJB3 mask aligner, a direct laser writing system *PicoMaster 200* from 4 PICO, and an optical projection lithography system. The technical infrastructure for the clean room is located in the basement of the WMI directly below the clean room area.

Figure 14: Top: Part of the clean room facility with optical lithography equipment and clean room benches. Bottom: Resist coater and hot plates.

The clean room also is equipped with a reactive ion etching system, Plasmalab 80 Plus with ICP plasma source (Oxford Instruments Plasma Technology).

Electron Beam Lithography

A 100 kV Electron Beam Lithography System nB5 fabricated by NanoBeam Ltd., UK, is installed in the second part of the clean room facility. The nB5 is a round-beam step-and-repeat system oriented towards high-end R&D applications at universities and research institutes. It is designed for nanopatterning and mix-and-match lithography. The innovative design of the electron optics and automation system enhances its throughput and reliability. It is an ideal tool for nano-device research and production. The electron beam lithography is used for the fabrication of nanostructures in metallic and oxide systems required for the study of quantum effects in mesoscopic samples.

Figure 15: 100 kV Electron Beam Lithography System nB5 of NanoBeam Ltd., UK, inside the WMI cleanroom facility.

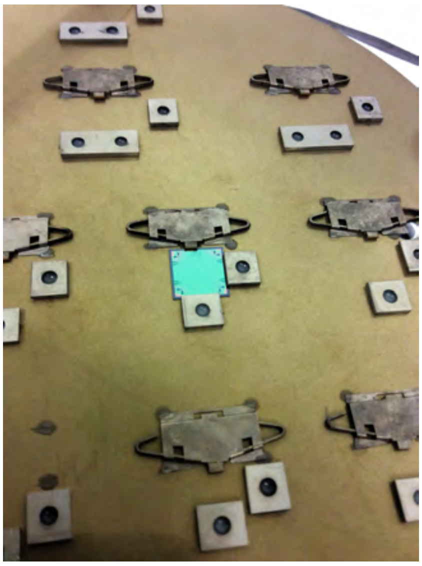

Figure 16: Chuck of the nB5 e-beam lithography system with a mounted $12 \times 12\,\mathrm{mm}^2$ silicon wafer.

The nB5 Electron Beam Lithography System employs low Coulomb-effect electron optics and sophisticated column designs to reduce beam size. The shorter optical column eliminates column bending and reduces system vibration. The modern electronics has low noise and low thermal effects. The perfectly integrated machine structure greatly improves system settling time and total stage move time. The advanced vibration tracking design enables the nB5 system to write on the fly. All these features combined with the fast deflection speed and high data processing rate make the nB5 the highest throughput system available today. Moreover, the nB5 requires undemanding cleanroom conditions, in particular regarding temperature stability, stray field magnitude, and floor vibration level.

The nB5 system is equipped with a thermal field emitter (TFE), an electrostatic lens and magnetic condenser lens, a conjugate beam blanking at < 5 ns slew rate and a dual beam deflection. The latter is used to achieve ultra-high deflection speed for beam writing (clock rate: 55 MHz). The total deflection coverage is combined with the mainfield and the subfield and controlled by two independent deflection sub-systems (field size: $1000\,\mu$m, address resolution: 1 nm). The characteristic performance parameters of the electron optics of the nB5 system are: (i) beam voltage range: 20 kV to 100 kV, (ii) minimum beam current: 0.1 nA, (iii) maximum beam current: 100 nA, (iv) theoretical beam size: 2.3 nm at 100 kV, (v) guaranteed writing beam size: < 5 nm at 2 nA, (vi) beam current drift: $< 0.5\%$/hour at 5 nA, (vii) beam position drift: < 50 nm/hour for 3 nA beam current, including blanking, deflection and stage move.

The XY-stage allows for a traversal distance of 200 mm with a total stage move time of only 150 ms for 1 mm stage movement and a position measurement resolution of 0.3 nm using laser interferometry. The maximum substrate sizes are $2-8$ in for round substrates, $2-5$ for square glass masks up to 3 mm thickness. Finally, the nB5 system has airlock operation with automatic loading robotics with a loading cassette for 6 chucks with a maximum diameter of 8 inch.

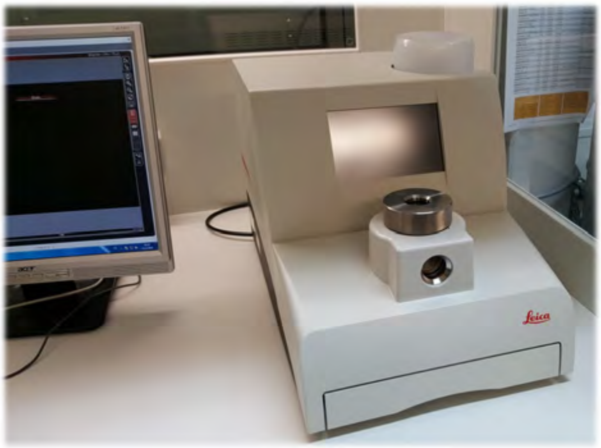

Figure 17: The fully automated Critical Point Dryer Leica EM CPD 300.

Automated Critical Point Dryer Leica EM CPD 300

The fabrication of nanomechanical systems requires the removal of solvent used for wet chemical processing by a critical point dryer. At WMI, we use the Critical Point Dryer Leica EM CPD 300, which allows the fully automated drying of biological specimens such as pollen, tissue, plants, insects etc., as well as NEMS (Nano Electro Mechanical Systems).

To ensure a low CO$_2$ consumption and a very short process time a new filler concept is used in the Leica EM CPD 300. Special attention has been put on safety issues by implementing software controlled cut-off functions and integrating a waste separator.

Optical Lithography

For optical lithography, a Karl Süss MJB 3 maskaligner or a direct laser writing system are used. The maskaligner operates in the 1 : 1 soft or hard contact mode and uses chromium metal masks.

The direct laser writing system *PicoMaster 200* (PM 200) of the company 4 PICO accepts substrate sizes between 5 mm × 5 mm and 200 mm × 200 mm via a turnable chuck. For writing the pattern, it allows for three different spot sizes (300 nm / 600 nm / 900 nm) and a write speed of up to 7.7 mm^2/min. One can choose between two compact writing modules equipped with a 405 nm and a 375 nm laser diode, respectively. The user can easily switch between the two modules within minutes since the full optical path is contained in the modules. Both modules feature automatic focus correction for not too heavily varying resist thickness.

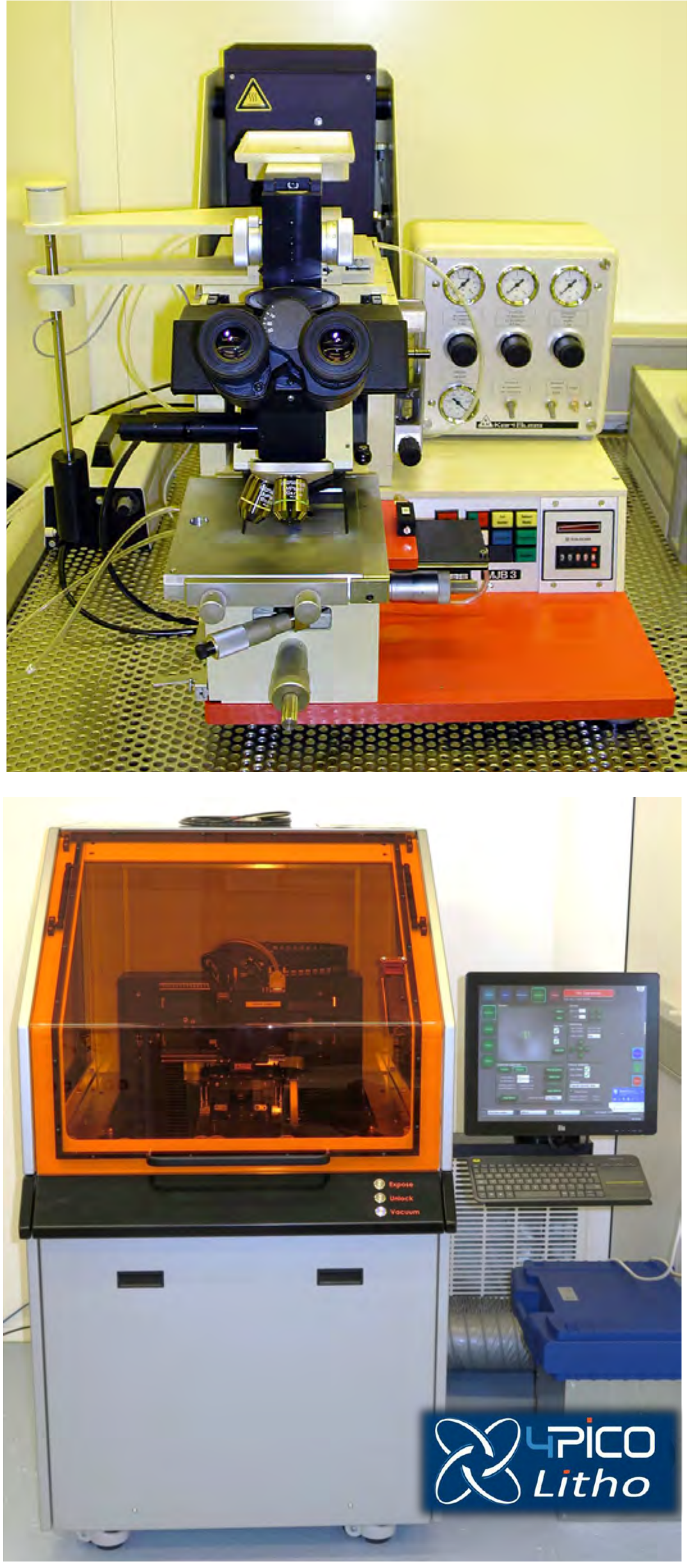

Figure 18: Top: Süss MJB 3 maskaligner for optical lithography. Bottom: Direct laser writing systems *PicoMaster 200*.

Low and Ultra-Low Temperature Facilities

Figure 19: The "dry" dilution refrigerator of the WMI.

Figure 20: Low-temperature unit of a WMI dilution refrigerator ready to go into a cryostat.

At the WMI, we have constructed the first dilution refrigerator with pulse tube pre-cooling for ultra-low temperature experiments. This type of refrigerator works without cryo-liquids, and thus is a lot more practical, more economical and more reliable than cryostats with liquid helium pre-cooling. These days, all major cryo-engineering companies are offering commercial versions of this Millikelvin cooler, and these so-called "dry" refrigerators outsell conventional refrigerators by a wide margin. The general construction concept of most manufacturers is unchanged from our original prototype, where the refrigerator consists of three basic components. The first cooling stage is a commercial pulse tube cryocooler which reaches a base temperature of 2.5 K. The second stage is a Joule-Thomson stage, and the last stage is a dilution refrigeration stage, where the lowest temperature of the cryostat is about 0.01 K (Fig. 19).

Figure 21: Two mixing chamber mounting plates with silver sponges. Those are needed to overcome the thermal resistance (Kapitza resistance) between the liquid ^{3,4}He and the mounting plate of the mixing chamber. To fabricate the mounting of the sponge (square pins embedded in the sponge) a spark erosion technique has been employed.

In many low temperature applications high refrigeration capacities are required. Our design allows for a high circulation rate of ^{3}He which in the end determines the cooling power of a dilution refrigerator. Presently our "dry" fridge reaches a refrigeration capacity of 700 µW at a temperature of the mixing chamber of 0.1 K, seven times the cooling power of the WMI nuclear demagnetization cryostat. Goals of our present work are a further increase of cooling power and a lower base temperature of the dry dilution refrigerator. A smaller version of our cryogen-free fridge has become commercially available later on by *VeriCold Technologies, Ismaning*) which was taken over by *Oxford Instruments* in 2007. It had a refrigeration capacity of 250 µW at a mixing chamber temperature of 0.1 K (Fig. 20).

The WMI also develops and fabricates dilution refrigerator inserts for temperatures down to about 20 mK. The inserts fit into all cryogenic systems (e.g. superconducting magnets) having a two inch bore. They allow fast sample change and rapid cool down cycles of less than five hours. The dilution refrigerator inserts are engineered and fabricated in-house and are also provided to other low temperature laboratories for ultra-low temperature experiments.

Millikelvin Temperatures in Combination with 3D Vector Magnetic-Fields

Figure 22: The dilution refrigerator with the 3D vector magnet located in the Quantum Laboratories.

In one room of the WMI Quantum Laboratories a cryogen-free dilution refrigerator is installed. This system is equipped with a 3D vector magnet allowing for 1 T in-plane and 6 T out-of-plane magnetic fields. Additional microwave coaxial lines allow for the microwave spectroscopy up to 18 GHz under these experimental conditions.

Scientifically, several directions in the field of fundamental light-matter interaction are envisaged:

(i) Circuit quantum electrodynamics (circuit QED), where superconducting qubits form hybrids with microwave resonators. These experiments are time consuming, because quantum effects arise in the limit of low excitation numbers. Hereby, challenging requirements are imposed on the detection systems allowing to detect microwave signals in the attowatt regime.

(ii) Storage of quantum states. One possibility is the transfer of the quantum information contained in photons to long-lived spin states. Additionally, exchange coupled systems or ferromagetic systems come into focus, because the effective coupling strength scales with the square-root of the number of spins contributing. In general, we study the light-matter interaction with long-lived spin systems and integrate them into superconducting quantum circuits.

(iii) Spin systems. Here, our studies are not limited to paramagnetic spin systems, but also involve exchange coupled (ferro- or ferri-) magnetic systems. Hereby, magnetization damping can be investigated as a function of temperature, frequency and magnetic field direction.

(iv) Circuit electro-mechanical hybrid systems consisting of a nano-mechanical element coupled to a superconducting microwave resonator. In this context, sideband cooling of the mechanical system into its ground state and pulsed spectroscopy of hybrid system are performed and will be extended.

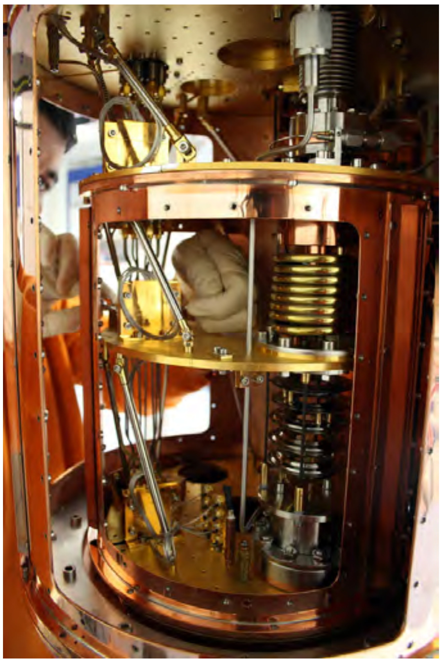

Figure 23: Inside of the dilution system. The windows of the 4 K and the still shield are removed providing access to the low temperature stages.

WMI Millikelvin Facilities for Experiments with Superconducting Quantum Circuits

The research on superconducting quantum circuits at WMI focuses mainly on systems sensitive to externally applied flux (flux qubits), circuit QED systems where flux qubits are coupled to transmission line resonators, squeezing physics in flux driven Josephson parametric amplifiers, and propagating quantum microwaves (e.g., quantum state reconstruction methods). In order to further develop our activities on quantum effects in the microwave regime, additional cryogenic capacities at millikelvin temperatures have been established. In addition to sufficient cooling power, the specifications for these cryostats are mainly dictated by the dimensions (typically a few centimeters in each direction) of bulky microwave components such as circulators or microwave switches.

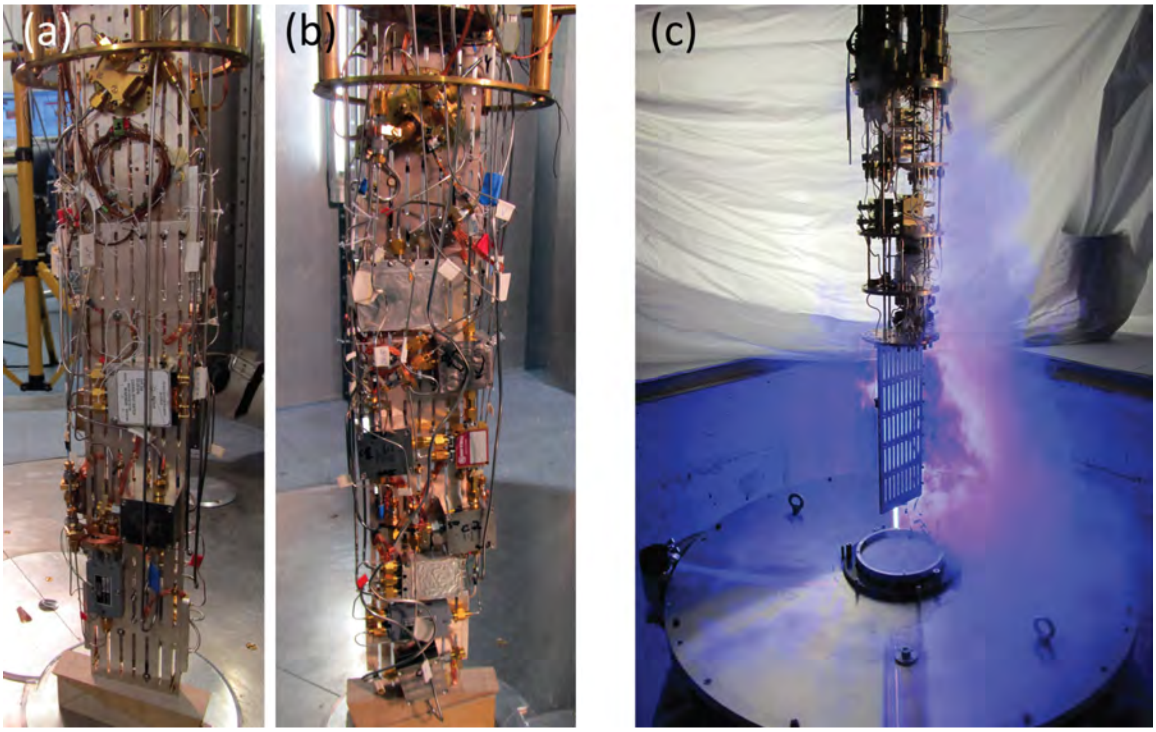

Figure 24: Liquid-helium precooled dilution refrigerators for experiments with superconducting quantum circuits. (a), (b) Back and front sides of the sample stage of the K12-refrigerator equipped with four circuit QED experiments. The height of the silver rod is 50 cm. (c) Sample stage and dewar of the dilution refrigerator in the quantum laboratory K04.

Two liquid-helium precooled dilution refrigerators are available for experiments with superconducting quantum circuits. The dilution refrigerator in laboratory K12 provides a sample space with a cylindrical volume with 11 cm diameter 55 cm height. The refrigerator is equipped with four microwave amplifiers at the 4 K-stage, seven broadband input lines and 80 twisted pair DC lines. This allows for mounting four experiments simultaneously to avoid idle times by interleaved measurements (see Fig. 24(a) and (b)). The base temperature of this refrigerator is 20 mK.

A new liquid-helium precooled dilution refrigerator for experiments with superconducting quantum circuits has been set up in the quantum laboratory K04. To provide enough space at the sample stage we have installed a Cryogenic Ltd. stainless steel dewar with a ^{4}He volume of 89 l. The time between two refills exceeds nine days. The cryostat is equipped with 16 coaxial measurement lines suitable for microwave frequencies down to the mixing chamber stage and low-noise cryogenic high electron mobility transistor (HEMT) amplifiers. Presently up to four samples can be mounted simultaneously to the sample stage. By expanding the number of input lines in the near future a more complex experiment can be set up. The cooling power of the mixing chamber at 100 mK was determined to about 140 µW.

A new cryogen-free dilution refrigerator with a pulse tube refrigerator (PTR) for precooling and with a large sample stage has been set up in room K21 of the WMI Quantum Laboratories using the longstanding experience in dry dilution refrigerators at WMI. This refrigerator features large diameters (tens of centimeters) of all temperature stages providing sufficient space for advanced quantum experiments. The main components of the refrigerator are the PTR, a 1 K-stage and a dilution unit. The two stages of the PTR cool the incoming ^{4}He and the ^{3}He/^{4}He mixture as well as one radiation shield at each stage. To provide sufficiently high cooling power near 1 K to cool microwave components and cables, this refrigerator has been equipped with a 1 K-stage operating in a closed cycle. A refrigeration capacity of the 1 K-stage of up to 100 mW could be reached. The dilution refrigerator is precooled by a dedicated ^{4}He circuit. The minimum base temperature of the refrigerator is below 11 mK. The cooling power at 100 mK was determined to about 300 µW at the maximum ^{3}He flow rate.

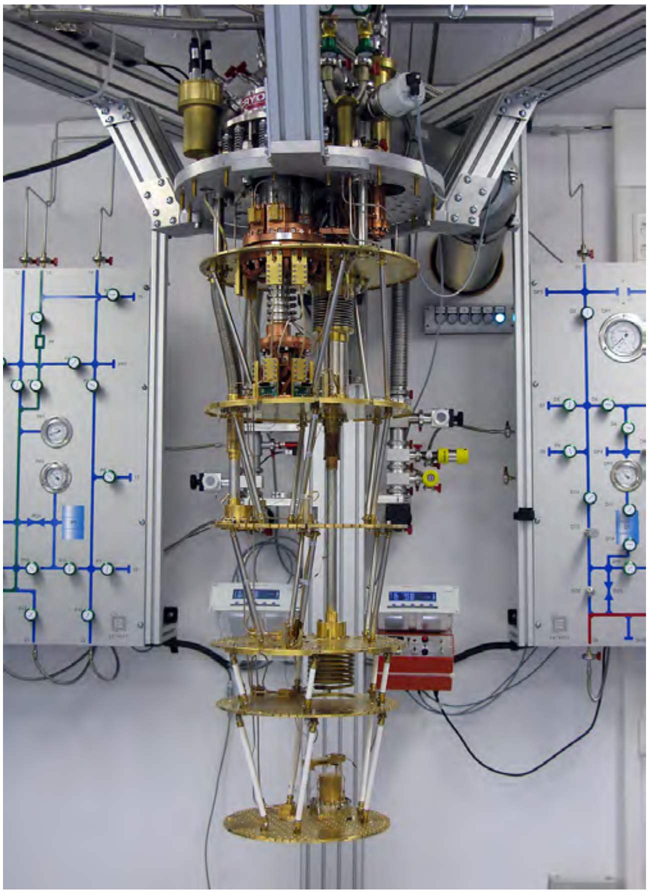

Figure 25: Dry dilution refrigerator with a large sample space.

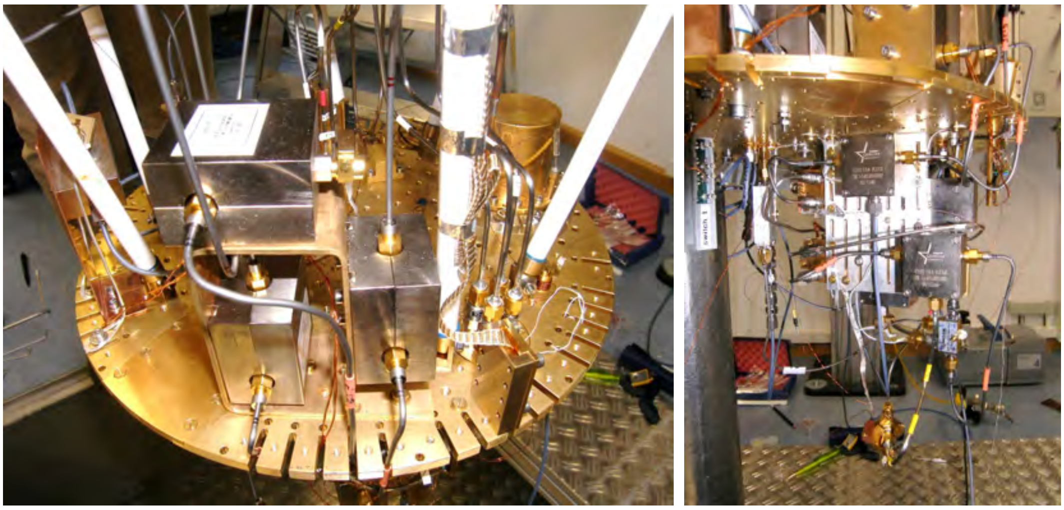

Figure 26: Low temperature platform of K21 dilution refrigerator with experimental setup for circuit QED experiments.

Statistics

Publications

1. **Secure quantum remote state preparation of squeezed microwave states**
S. Pogorzalek, K. G. Fedorov, M. Xu, A. Parra-Rodriguez, M. Sanz, M. Fischer, E. Xie, K. Inomata, Y. Nakamura, E. Solano, A. Marx, F. Deppe, R. Gross
Nature Communications **10**, 2604 (2019)

2. **Spin Transport in a Magnetic Insulator with Zero Effective Damping**
Tobias Wimmer, Matthias Althammer, Lukas Liensberger, Nynke Vlietstra, Stephan Geprägs, Mathias Weiler, Rudolf Gross, Hans Huebl
Physical Review Letters **123**, 257201 (2019)

3. **Magnetoelasticity of $Co_{25}Fe_{75}$ thin films**
Daniel Schwienbacher, Matthias Pernpeintner, Lukas Liensberger, Eric R. J. Edwards, Hans T. Nembach, Justin M. Shaw, Mathias Weiler, Rudolf Gross, Hans Huebl
Journal of Applied Physics **126**, 103902 (2019)

4. **Crossover to strange metal phase: quantum criticality in one unit cell $Bi_2Sr_2CaCu_2O_{8+x}$**
Edoardo Sterpetti, Johan Biscaras, Andreas Erb, Abhay Shukla
J. Phys.: Condens. Matter **32**, 103902 (2020)

5. **Exceptional points in tunable superconducting resonators**
Matti Partanen, Jan Goetz, Kuan Yen Tan, Kassius Kohvakka, Vasilii Sevriuk, Russell E. Lake, Roope Kokkoniemi, Joni Ikonen, Dibyendu Hazra, Akseli Mäkinen, Eric Hyyppä, Leif Grönberg, Visa Vesterinen, Matti Silveri, and Mikko Möttönen
Physical Review B **100**, 134505 (2019)

6. **Anomalous spin Hall angle of a metallic ferromagnet determined by a multiterminal spin injection/detection device**
Tobias Wimmer, Birte Coester, Stephan Geprägs, Rudolf Gross, Sebastian T. B. Goennenwein, Hans Huebl, Matthias Althammer
Applied Physics Letters **115**, 092404 (2019)

7. **Spin-Wave Propagation in Metallic $Co_{25}Fe_{75}$ Films Determined by Microfocused Frequency-Resolved Magneto-Optic Kerr Effect**
Lukas Liensberger, Luis Flacke, David Rogerson, Matthias Althammer, Rudolf Gross, Mathias Weiler
IEEE Magnetics Letters **10**, 5503905 (2019)

8. **High Spin-Wave Propagation Length Consistent with Low Damping in a Metallic Ferromagnet**
Luis Flacke, Lukas Liensberger, Matthias Althammer, Hans Huebl, Stephan Geprägs, Katrin Schultheiss, Aleksandr Buzdakov, Tobias Hula, Helmut Schultheiss, Eric R. J. Edwards, Hans T. Nembach, Justin M. Shaw, Rudolf Gross, Mathias Weiler
Applied Physics Letters **115**, 122402 (2019)

9. **Exchange-Enhanced Ultrastrong Magnon-Magnon Coupling in a Compensated Ferrimagnet**
Lukas Liensberger, Akashdeep Kamra, Hannes Maier-Flaig, Stephan Geprägs, Andreas Erb, Sebastian T. B. Goennenwein, Rudolf Gross, Wolfgang Belzig, Hans Huebl, Mathias Weiler
Physical Review Letters **123**, 117204 (2019)

10. **Role of interface quality for the spin Hall magnetoresistance in nickel ferrite thin films with bulk-like magnetic properties**
Matthias Althammer, Amit Vikam Singh, Tobias Wimmer, Zbigniew Galazka, Hans Huebl, Matthias Opel, Rudolf Gross, Arunava Gupta
Applied Physics Letters **115**, 092403 (2019)

11. **Quantitative Modeling of Superconducting Planar Resonators for Electron Spin Resonance**
Stefan Weichselbaumer, Petio Natzkin, Christoph W. Zollitsch, Mathias Weiler, Rudolf Gross, Hans Huebl

Physical Review Applied **12**, 024021 (2019)

12. **Limits on Dark Matter Effective Field Theory Parameters with CRESST-II**
G. Angloher *et al.*, The CRESST Collaboration
The European Physical Journal C **79**, 43 (2019)

13. **Magnetically Ordered Insulators for Advanced Spintronics**
Matthias Althammer, Sebastian T.B. Goennenwein, Rudolf Gross, et al.
in *Towards Oxide Electronics: a Roadmap*, Applied Surface Science **482**, 48-52 (2019)

14. **T_c and Other Cuprate Properties in Relation to Planar Charges as Measured by NMR**
Michael Jurkutat, Andreas Erb, Jürgen Haase
Condensed Matter **4**(3), 6714 (2019)

15. **Frustrated spin order and stripe fluctuations in FeSe**
A. Baum, H. N. Ruiz, N. Lazarevic, Yao Wang, T. Böhm, R. Hosseinian Ahangharnejhad, P. Adelmann, T. Wolf, Z. V. Popovic, B. Moritz, T. P. Devereaux, and R. Hackl
Communications Physics **2**, 14 (2019)

16. **Printed Thin Diblock Copolymer Films with Dense Magnetic Nanostructure**
Senlin Xia, Lin Song, Wei Chen, Volker Körstgens, Matthias Opel, Matthias Schwartzkopf, Stephan V. Roth, Peter Müller-Buschbaum
ACS Appl. Mater. Interfaces **11**, 21935 (2019)

17. **Spray-Coating Magnetic Thin Hybrid Films of PS-b-PNIPAM and Magnetite Nanoparticles**
Senlin Xia, Lin Song, Nuri Hohn, Kun Wang, Sebastian Grott, Matthias Opel, Matthias Schwartzkopf, Stephan V. Roth, Peter Müller-Buschbaum
Advanced Functional Materials **29**, 1808427 (2019)

18. **First results on sub-GeV spin-dependent dark matter interactions with ^{7}Li**
A. H. Abdelhameed *et al.* (The CRESST Collaboration)
The European Physical Journal C **79**, 630 (2019)

19. **First results from the CRESST-III low-mass dark matter program**
A. H. Abdelhameed *et al.* (The CRESST Collaboration)
Physical Review D **100**, 102002 (2019)

20. **Fermi surface properties of the bifunctional organic metal κ-(BETS)$_2$Mn[N(CN)$_2$]$_3$ near the metal - insulator transition**
V.N. Zverev, W. Biberacher, S. Oberbauer, I. Sheikin, P. Alemany, E. Canadell, and M.V. Kartsovnik
Physical Review B **99**, 125136 (2019)

21. **Challenges in Open-air Microwave Quantum Communication and Sensing**
Mikel Sanz, Kirill G. Fedorov, Frank Deppe, Enrique Solano
IEEE Conference on Antenna Measurements & Applications (CAMA), Västerås, pp. 1-4 (2018)

22. **Crossover to strange metal phase: quantum criticality in one unit cell $Bi_2Sr_2CaCu_2O_{8+x}$**
Edoardo Sterpetti, Johan Biscaras, Andreas Erb, Abhay Shukla
J. Phys.: Condens. Matter **32**, 045601 (2020).

23. **Geant4-based electromagnetic background model for the CRESST dark matter experiment**
A.H. Abdelhameed et al. (The CRESST Collaboration)
The European Physical Journal C **79**, 881 (2019).

24. **Large spin Hall magnetoresistance in antiferromagnetic α-Fe$_2$O$_3$/Pt heterostructures**
Johanna Fischer, Matthias Althammer, Nynke Vlietstra, Hans Huebl, Sebastian T.B. Goennenwein, Rudolf Gross, Stephan Geprägs, Matthias Opel
Physical Review Applied **13**, 014019 (2020).

25. **Quantum Fourier Transform in Oscillating Modes**
Qi-Ming Chen, Frank Deppe, Re-Bing Wu, Luyan Sun, Yu-xi Liu, Yuki Nojiri, Stefan Pogorzalek,

Michael Renger, Matti Partanen, Kirill G. Fedorov, Achim Marx, Rudolf Gross
arXiv:1912.09861, submitted for publication (2019).

26. **Resonant Nanodiffraction X-ray Imaging Reveals Role of Magnetic Domains in Spin Caloritronics**
Paul G. Evans, Samuel D. Marks, Stephan Geprägs, Maxim Dietlein, Yves Joly, Minyi Dai, Jiamian Hu, Laurence Bouchenoire, Paul B. J. Thompson, Tobias U. Schülli, Marie-Ingrid Richard, Rudolf Gross, Dina Carbone, and Danny Mannix
Nature Communications, submitted for publication (2019)

27. **Sideband-resolved resonator electromechanics on the single-photon level based on a nonlinear Josephson inductance**
Philip Schmidt, Mohammad T. Amawi, Stefan Pogorzalek, Frank Deppe, Achim Marx, Rudolf Gross, Hans Huebl
arXiv:1912.08731, submitted for publication (2019).

28. **Fluctuations and pairing in Fe-based superconductors: Light scattering experiments**
N. Lazarević and R. Hackl
arXiv:1909.00173, submitted for publication (2019).

29. **Zeeman spin-orbit coupling and magnetic quantum oscillations in antiferromagnetic conductors**
R. Ramazashvili, P. D. Grigoriev, T. Helm, F. Kollmannsberger, M. Kunz, W. Biberacher, E. Kampert, H. Fujiwara, A. Erb, J. Wosnitza, R. Gross, M. V. Kartsovnik
arXiv:1908.01236, submitted for publication (2019).

30. **Measuring the imaginary time dynamics of quantum materials**
S. Lederer, D. Jost, R. Hackl, E. Berg, S.A. Kivelson
arXiv:1907.10182, submitted for publication (2019).

31. **Description of CRESST-III Data**
A.H. Abdelhameed et al. (The CRESST Collaboration)
arXiv:1905.07335, submitted for publication (2019).

32. **First results from the CRESST-III low-mass dark matter program**
A.H. Abdelhameed et al. (The CRESST Collaboration)
arXiv:1904.00498, submitted for publication (2019).

33. **Emergence of pseudogap from short-range spin-correlations in electron doped cuprates**
F. Boschini, M. Zonno, E. Razzoli, R. P. Day, M. Michiardi, B. Zwartsenberg, P. Nigge, M. Schneider, E. H. da Silva Neto, A. Erb, S. Zhdanovich, A. K. Mills, G. Levy, C. Giannetti, D. J. Jones, A. Damascelli
arXiv:1812.07583, submitted for publication (2018).

34. **Echo trains in pulsed electron spin resonance of a strongly coupled spin ensemble**
Stefan Weichselbaumer, Christoph W. Zollitsch, Martin S. Brandt, Rudolf Gross, Hans Huebl
arXiv:1809.10116, submitted for publication (2018).

35. **Characterizing spin transport: detection of spin accumulation via magnetic stray field**
Matthias Pernpeintner, Akashdeep Kamra, Sebastian T.B. Goennenwein, Hans Huebl
arXiv 1709.01820, submitted for publication (2017).

36. **Perpendicular magnetic anisotropy in insulating ferrimagnetic gadolinium iron garnet thin films**
H. Maier-Flaig, S. Geprägs, Z. Qiu, E. Saitoh, R. Gross, M. Weiler, H. Huebl, S. T. B. Goennenwein
arXiv:1706.08488, submitted for publication (2017).

37. **Non-local magnon transport in the compensated ferrimagnet GdIG**
Kathrin Ganzhorn, Tobias Wimmer, Joseph Barker, Gerrit E. W. Bauer, Zhiyong Qiu, Eiji Saitoh, Nynke Vlietstra, Stephan Geprägs, Rudolf Gross, Hans Huebl, Sebastian T.B. Goennenwein
arXiv:1705.02871, submitted for publication (2017).

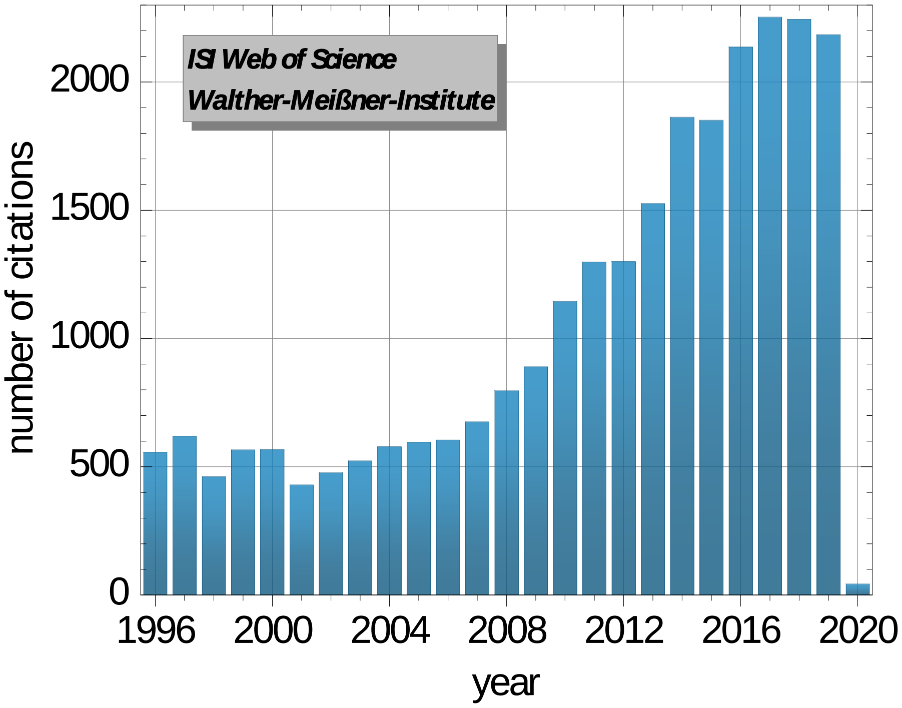

The total number of citations per year of papers published by members of WMI since 1996. This number has about quadrupled within the last twenty years and presently exceeds 2 200.

Bachelor, Master, Doctoral, and Habilitation Theses

A. Completed and Ongoing Habilitation Theses

At present, three postdoctoral researchers – Mathias Weiler, Matthias Althammer and Kirill Fedorov – are passing through the habilitation procedure of the Technical University of Munich. The habilitation serves as the formal assessment tool ascertaining whether or not a candidate is suitable, from an academic and a pedagogical point of view, to be a professor in a particular field at the university level.

The promotion of highly qualified young scholars is a key concern of WMI. The fostering of young scholars goes hand in hand with equipping them to stand on their own in fields that are very competitive on both the national and international scales.

1. Dr. Mathias Weiler

Mathias Weiler started the habilitation process at TUM in June 2015. The research topic of his habilitation project is *Spin-Orbit Interactions in Magnetic Thin Film Systems*. On 2nd November 2017 he successfully passed the intermediate evaluation of his habilitation process. The *Fachmentorat* consisting of Rudolf Gross (TU Munich), Christian Pfleiderer (TU Munich) and Christian Back (TU Munich, formerly University of Regensburg) recommended to finish the habilitation process within 2019. Meanwhile, Mathias Weiler has submitted his habilitation thesis. It has been evaluated by 5 external reviewers. All reports have been very positive and recommended the acceptance of the habilitation thesis by TUM with utmost vigor. The *Fachmentorat* fully supports this judgment and submitted its final report in October 2019. The *Fachbereichsrat* of the Faculty of Physics accepted the habilitation thesis in December 2019.

Mathias Weiler joined WMI in December 2014 after a two-year postdoctoral stay at NIST, Boulder, Colorado, USA, where he worked on spin current transport. His stay abroad was supported by a DAAD fellowship. Besides his successful research work, he took over the lectures on *Magnetism* (winter semester 2015/2016, 2017/2018, and 2019/2020) and *Spin Electronics* (summer semester 2016 and 2018), and contributed to several WMI seminars. His lectures attracted a large number of students and received very good marks from the students. In winter semester 2018/19, he received the ***Supervisory Award*** of the TUM Physics Department. This award was presented to Mathias Weiler by the PhD students of the Faculty Graduate Center for his outstanding performance in advising PhD students.

2. Dr. Matthias Althammer

Matthias Althammer joined WMI in December 2013 after a postdoctoral stay (10/2012 – 11/2013) at the Center for Materials for Information Technology, University of Alabama, Tuscaloosa, USA, where he worked on oxide based spintronics. From 05/2014 to 02/2015 he was on leave from WMI to acquire experience in industry as an Engineering Consultant at Esprit Engineering GmbH, Munich.

Matthias Althammer was accepted as a *"Habilitand"* by the Faculty of Physics of TU Munich in January 2016. In his case, Rudolf Gross (TU Munich), Martin Brandt (TU Munich) and Arunava Gupta (MINT Center, University of Alabama) form the *Fachmentorat*. The research topic of his habilitation project is the *"Experimental Study of Spin-dependent Transport Phenomena"*. On 14th June 2018 he successfully passed the intermediate evaluation of his habilitation process. The *Fachmentorat* appreciated that most of the goals fixed in 2016 have been perfectly achieved. The target agreement has been extended for the second two-year phase of the habilitation procedure and the *Fachmentorat* recommended him to finish the habilitation process until autumn 2020.

3. Dr. Kirill Fedorov

Kirill Fedorov studied physics in Russia (Institute for Physics of Microstructures, Russian Academy of Sciences, Nizhny Novgorod), where he received his master degree in 2008. He then joined the group of Prof. Alexey Ustinov at the Karlsruhe Institute of Technology as a PhD student. He finished his PhD thesis entitled *Fluxon readout for superconducting flux qubits* in 2013 and then joined Walther-Meißner-Institute as a postdoctoral researcher in December 2013. His key research topic is the realization of seminal quantum experiments based on propagating quantum microwaves.

Kirill Fedorov was accepted as a *"Habilitand"* by the Faculty of Physics of TU Munich in September 2016. In his case, Rudolf Gross (TU Munich), Jonathan Finley (TU Munich/Walter Schottky Institute) and Enrique Solano (Universidad del País Vasco and Ikerbasque Foundation, Bilbao, Spain) form the *Fachmentorat*. The midterm evaluation of his habilitation process took place on 18th January 2019, when Kirill Fedorov gave a talk within the Colloquium on Solid-State Physics of the Faculty of Physics entitled *Quantum communication with squeezed microwaves*. Kirill Fedorov successfully passed the intermediate evaluation and the *Fachmentorat* extended the target agreement for the second two-year phase of his habilitation.

B. Completed and Ongoing Ph.D. Theses

Completed Ph.D. Theses:

1. **Magnetization Dynamics in Coupled Magnetic Systems**
   Stefan Horst Klingler, Technical University of Munich, March 2019.
2. **A Scalable 3D Quantum Memory**
   Edwar Xie, Technical University of Munich, November 2019.
3. **Cooper Pairing and Fluctuations in Fe-Based Superconductors**
   Daniel Jost, Technical University of Munich, December 2019.

The Ph.D. students of the Walther-Meißner-Institute finishing their Ph.D. theses in 2019.

Ongoing Ph.D. Theses:

1. **Chains of Nonlinear and Tunable Superconducting Resonators**
   Michael Fischer, Technical University of Munich, since January 2015.
2. **Nanomechanical Quantum Systems**
   Philip Schmidt, Technical University of Munich, since October 2015.
3. **Magnetic Resonance at Millikelvin Temperatures**
   Stefan Weichselbaumer, Technical University of Munich, since December 2015.
4. **Untersuchung des Wärmetransports in porösen Pulvermedien zur Entwicklung einer ökonomischen Hochtemperatur-Vakuumsuperisolation auf Perlitbasis für Anwendungen in Wärmespeichern bis zu 700°C**
   Matthias Johannes Demharter, Technical University of Munich, since February 2016.

5. **Nanoelectromechanics: from magnon phonon coupling to circuit quantum bits**
   Daniel Schwienbacher, Technical University of Munich, since October 2015.
6. **Quantum Gates with Continuous Variable Microwaves**
   Stefan Pogorzalek, Technical University of Munich, since March 2016.
7. **Spin Currents in Magnetic Heterostructures**
   Tobias Wimmer, Technical University of Munich, since January 2017.
8. **ReBCO-Schichten auf ISD biaxial texturierten Substraten für supraleitende Bandleiterder 2. Generation**
   Oleksiy Troshyn, Technical University of Munich, since August 2016.
9. **Direct and Inverse Spin-Orbit Torques**
   Lukas Liensberger, Technical University of Munich, since January 2018.
10. **Evaluierung und Neuentwicklung durch Nutzung von Supraleitern in einer zirkularen Anordnung zur quasi verlustfreien kontaktlosen Energieübertragung für sehr hohe Leistungen**
    Christoph Utschick, Technical University of Munich, since June 2018.
11. **Spatially and Momentum Resolved Raman Studies of Unconventional Superconductors**
    Gabriele Rager, Technical University of Munich, since March 2018.
12. **Spin Dynamics of Hybrid Skyrmion-Magnon Solitons**
    Luis Flacke, Technical University of Munich, since September 2018.
13. **Correlation Measurements in Coupled Nonlinear Resonators**
    Qiming Chen, Technical University of Munich, since October 2018.
14. **Quantum Microwave Communication**
    Michael Renger, Technical University of Munich, since November 2018.
15. **Pure Spin Currents in Epitaxial All Oxide Heterostructures**
    Janine Gückelhorn, Technical University of Munich, since March 2019.
16. **Hybride Solid State Quantum Systems**
    Thomas Luschmann, Technical University of Munich, since September 2019.
17. **Coherent Adiabatic Quantum Annealer Based on Superconducting Quantum Circuits**
    Yuki Nojiri, Technical University of Munich, since September 2019.
18. **Spin Phenomena in Superconductor/Ferromagnet Heterostructures**
    Manuel Müller, Technical University of Munich, starting from March 2020.

C. Completed and Ongoing Bachelor and Master Theses

Completed Master Theses:

1. **A Study of the Non-Linear Susceptibility and Ultrasound Velocity in Quantum Materials**
   Ludwig Friedrich Wilhelm Holleis, Master Thesis, Technical University of Munich, June 2019.
2. **Coherent Coupling Between Superconducting Quantum Circuits and Ferrimagnetic Magnons**
   Mohammad T. Amawi, Master Thesis, Technical University of Munich, April 2019.
3. **Magnetic Fast Wafer Level Reliability (fWLR)**
   Thai Phi Long Pham, Master Thesis, Technical University of Munich, October 2019.
4. **FPGA-based Tomography of Propagating Quantum Microwaves**
   Robert Neagu, Master Thesis, Technical University of Munich, October 2019.
5. **Fabrication and Characterization of Josephson Traveling Wave Parametric Amplifiers**
   Daniel Singh, Master Thesis, Technical University of Munich, November 2019.
6. **Superconductor/Ferromagnet Heterostructures for Superconducting Spintronics**
   Manuel Müller, Master Thesis, Technical University of Munich, November 2019.
7. **Origin of the Nematic Fluctuations in Iron-Based Superconductors**
   Leander Peis, Master Thesis, Technical University of Munich, December 2019.
8. **Acoustically Driven Spin Wave Resonance**
   Adrían Gómez Pardo, Master Thesis, Technical University of Munich, December 2019.
9. **Optimierung supraleitender Schichten aus Niob, Niobnitrid und Niobtitannitrid für den Einsatz in Mikrowellenresonatoren**
   Andreas Faltermeier, Master Thesis, Technical University of Munich, December 2019.

Completed Bachelor Theses:

1. **Implementierung adiabatischer Pulse in supraleitenden Resonatoren für Elektronenspinresonanz**
   Daniela Lutz, Technical University of Munich (2019)
2. **Quantensimulation mit supraleitenden Schaltkreisen**
   Stefanie Grotowski, Technical University of Munich (2019)
3. **Fluctuations and Frustrated Magnetism in Sulphur Substituted Iron Selenide**
   Ramona Stumberger, Technical University of Munich (2019).
4. **Spin Hall Magnetoresistance in Yttrium Iron Garnet | Tungsten Heterostructures**
   Johannes Schirk, Technical University of Munich (2019).
5. **All Electrical Magnon Transport in Magnetically Ordered Insulators**
   Thomas Narr, Technical University of Munich (2019).
6. **Schnelles thermisches Tempern von Pt|$Y_3Fe_5O_{12}$ Heterostrukturen**
   Philipp Schwenke, Bachelor Thesis, Technical University of Munich (2019).
7. **Einfluss epitaxialer Verspannung auf die physikalischen Eigenschaften von dünnen Sr_2IrO_4 Schichten**
   Monika Scheufele, Bachelor Thesis, Technical University of Munich (2019).
8. **All-Electrical Spin Wave Spectroscopy**
   Anastasia Golovin, Bachelor Thesis, Technical University of Munich (2019).

9. **Spinwellenpropagation in Kobalt-Eisen-Keilen**
   Leonhard Hölscher, Bachelor Thesis, Technical University of Munich (2019).
10. **STM- und Raman-Untersuchungen an Festkörperproben und Kohlenstoffnanoröhrchen**
   Robert Steinbinder, Technical University of Munich (2019)
11. **Design and Simulation of a Light Field Display**
   Andreas Straßer, Technical University of Munich (2019).
12. **Untersuchung induktiv gekoppelter supraleitender Mikrowellenresonatoren**
   Niklas Bruckmoser, Technical University of Munich (2019)

Ongoing Master Theses:

1. **Spin Seebeck Effect as a Probe of Magnon Properties**
   Maxim Dietlein, Master Thesis, Technical University of Munich, since January 2019.
2. **Quantum Memory mit Optimal Control / Quantum Memory with Optimal Control**
   Stephan Trattnig, Master Thesis, Technical University of Munich, since February 2019.
3. **A Low Noise Laser System for High Fidelity Rydberg Atom Manipulation**
   Joop Age Harm Adema, Master Thesis, Technical University of Munich, since February 2019.
4. **Oxidische Heterostrukturen für Experimenten mit reinen Spinströmen / Oxide Heterostructures für Pure Spin Current Experiments**
   Raffael Ferdigg, Master Thesis, Technical University of Munich, since March 2019.
5. **Spin Torque Excitation**
   Carolina Lüthi, Master Thesis, Technical University of Munich, since June 2019
6. **Experimentelle Realisierung eines Quantenschlüsseltauschs mit gequetschten Mikrowellenzuständen / Experimental implementation of a quantum key distribution with squeezed microwaves**
   Florian Fesquet, Master Thesis, Technical University of Munich, since October 2019
7. **Optimized Geometry for a Compact 3D Quantum Memory**
   Julia Lamprich, Master Thesis, Technical University of Munich, since October 2019
8. **All-electrical magnon transport and manipulation in magnetically ordered insulators**
   Emir Karadza, Master Thesis, Technical University of Munich, since November 2019
9. **Improved Fabrication Process for Transmon Qubits**
   Christoph Scheuer, Master Thesis, Technical University of Munich, since November 2019
10. **Tunnel- und Raman-Spektroskopie an Kuprat-Supraleitern / Tunneling- und Raman spectroscopy in Cuprate Superconductors**
   Minghao Zhang, Master Thesis, Technical University of Munich, since November 2019

Ongoing Bachelor Theses:

1. **Superconducting Cables for Quantum Microwave Communication**
   Meike Pfeiffer, Technical University of Munich (2019)

Research Projects

A large number of our research projects are benefiting from the collaboration with external groups in coordinated research projects, as well as from individual collaborations, exchange programs and visitors. Most collaborations are based on joint projects, which are funded by different research organizations (see list below). A considerable number of collaborations also exists with universities, other research institutions and industry without direct financial support.

A. German Research Foundation: Excellence Initiative & Strategy

Cluster of Excellence *«Munich Center for Quantum Science and Technology» (MCQST)*

The new Cluster of Excellence has been granted in September 2018 within Germany's Excellence Strategy and started in January 2019. Together with Immanuel Bloch of LMU Munich and Ignacio Cirac of Max Planck Institute of Quantum Optics, Rudolf Gross of Walther-Meißner-Institute is one of the three spokespersons of MCQST.

1. Research Unit C: *Quantum Computing*
   Principal Investigators: F. Deppe, R. Gross
   Contributing Researchers: K. Fedorov, A. Marx, M. Partanen
2. Research Unit D: *Quantum Communication*
   Principal Investigators: F. Deppe, R. Gross
   Contributing Researchers: K. Fedorov, A. Marx, M. Partanen
3. Research Unit E: *Quantum Sensing*
   Principal Investigators: F. Deppe, H. Hübl, R. Gross
   Contributing Researchers: K. Fedorov, A. Marx
4. Research Unit F: *Quantum Matter*
   Principal Investigators: H. Hübl, R. Gross
   Contributing Researchers: M. Althammer, S. Geprägs, M. Weiler

Cluster of Excellence *«Nanosystems Initiative Munich» (NIM)*

The Cluster of Excellence ***«Nanosystems Initiative Munich» (NIM)*** started in October 2006 within Germany's Excellence Initiative and came to an end in October 2019 after 13 highly successful years.

1. Research Area I: *Quantum Nanophysics*
   Principal Investigators: R. Gross, H. Hübl
   Contributing Researchers: F. Deppe, K. Fedorov, A. Marx
2. Research Area II: *Hybrid Nanosystems*
   Principal Investigators: R. Gross, H. Hübl
   Contributing Researchers: M. Althammer, S. Geprägs, A. Marx, M. Weiler

B. German Research Foundation: Collaborative Research Centers

Transregional Collaborative Research Center TRR 80: *«From Electronic Correlations to Functionality»*

1. Project A2: *Spatially and Momentum Resolved Raman Studies of Correlated Systems*
   R. Hackl

C. German Research Foundation: Priority Programs

1. Spin Dynamics of Hybrid Skyrmion-Magnon Solitons
   within the DFG Priority Program 2137 *Skyrmionics: Topological Spin Phenomena in Real-Space for Applications*
   M. Weiler, R. Gross (Az. WE 5386/5-1)
2. Pulsed Electron Paramagnetic Resonance at Millikelvin Temperatures
   within the DFG Priority Program 1601 *New frontiers in sensitivity for EPR spectroscopy: from biological cells to nano materials*
   H. Huebl (Az. HU 1896/2-1)

D. German Research Foundation: Research Projects

1. Project: *Fluctuations and Novel Phases in Systems with Spin, Charge and Orbital Correlations*
   R. Hackl (Az. HA 2071/12-1)
2. Project: *Pure Spin Currents in Oxide-Based Epitaxial Heterostructures*
   M. Althammer, R. Gross (Az. AL 211012-1)
3. Project: *Direct and Inverse Spin-Orbit Torques*
   M. Weiler (Az. WE 5386/14-1)
4. Project: *Correlated Quantum Microwaves: Continuous-Variables for Remote State Preparation and Quantum Illumination*
   K.G. Fedorov (Az. FE 1564/1-1)

E. European Union

1. EU Collaborative Project (call identifier H2020-FETFLAG-2018-2020), project title *Quantum Microwave Communication and Sensing – QMiCS*
   F. Deppe, K. Fedorov, A. Marx, R. Gross, Grant Agreement No. 820505
   project coordination: Walther-Meißner-Institute, partners: several European Universities, research facilities and companies.
2. EU Collaborative Project (call identifier H2020-FETOPEN-1-2016-2017), project title *Magnetomechanical Platforms for Quantum Experiments and Quantum Enabled Sensing Technologies – MaQSens*
   H. Huebl, R. Gross, Grant Agreement No. 736943
   partners: several European Universities and research facilities.

F. Free State of Bavaria

1. International PhD Programme of Excellence *Exploring Quantum Matter (ExQM)* within the Elite Network of Bavaria, Project No. K-NW-2013-231
   R. Gross, A. Marx, F. Deppe, K. Fedorov
   Jointly with 12 quantum physics research groups at the TU Munich, the LMU Munich, and the Max Planck Institute of Quantum Optics.

G. Max Planck Society

1. International Max Plank Research School for *Quantum Science and Technology (IMPRS-QST)*, spokesperson: Prof. Dr. J. Ignacio Cirac
   R. Gross, A. Marx, F. Deppe, K. Fedorov
   With several partners from the Max Planck Institute of Quantum Optics, the Ludwig-Maximilians-Universität Munich and the Technical University of Munich.

H. Bavaria California Technology Center (BaCaTeC)

1. Project: *Bypassing the Analytic Continuation: A New Approach to the Analysis of Spectroscopic Data* (No. 21 [2016-2])
   R. Hackl,
   Partners: Profs. Thomas Devereaux, Steve Kivelson, and Sri Raghu (Stanford University)

I. German Academic Exchange Service

1. Project-based Personnel Exchange Programme (PPP) with Serbia, project 57449106: *Fluctuations, Magnetic Frustration, and Sub-Dominant Pairing in Fe-Based Compounds*, collaboration with the Institute of Physics, University of Belgrade (Dr. Z. V. Popovic)
   R. Hackl
2. Project-based Personnel Exchange Programme (PPP) with Serbia, project 57335339: *Spin and Charge Instabilities in Sulfur-substituted FeSe*, collaboration with the Institute of Physics, University of Belgrade (Dr. Z.V. Popovic).
   R. Hackl
3. Project-based Personnel Exchange Programme (PPP) with India, project 57452943: *Spin Current Transport Across Antiferromagnetic/Metallic Oxide Interfaces*, collaboration with the IIT Madras, Chennai (Prof. Dr. M. S. Ramachandra Rao).
   R. Gross

J. Scientific Instrumentation

1. UHV Electron Beam Deposition System including Sputter Deposition Chamber, Plassys MEB550S4-I,
   DFG, Excellence Strategy, EXC-2111-390814868
2. Cryogen-Free Dilution Refrigerator System, Bluefors Model BF-XLD400,
   DFG, Excellence Strategy, EXC-2111-390814868

Conferences, Workshops, Public Engagement

The Walther-Meißner-Institute has organized/co-organized several conferences, workshops and symposia in 2019. It also was participating in several public outreach events aiming at making science accessible to the public.

A. 686. WE-Heraeus-Seminar «Spin Based Information Processing» (07 – 09 January 2019, Physikzentrum Bad Honnef, Germany)

WILHELM UND ELSE HERAEUS-STIFTUNG

The *686. WE-Heraeus-Seminar* was organized by Hans Hübl (WMI) together with Ulrike Ritzmann (Uppsala University, Sweden), and Evangelos Papaioannou (TU Kaiserslautern). It was addressing questions related to the development and innovation of today's information technology. Important topics have been (i) energy consumption and (ii) enhanced, or highly efficient computing concepts. In particular, the fact that the information and communication technologies (without television) presently consume 920 TWh or about 5% of the annual electricity produced in 2012 was addressed, demonstrating the importance for innovations in this sector. Complementary approaches have been intensely discussed during the workshop, in particular, how spin electronics or in a broader sense logic circuits based on magnetic systems can contribute to these global challenges.

The workshop brought together the areas of information processing with magnetic textures, neuromorphic computing, logic based on magnetic order, ultrafast magnetization control as well as spin based quantum information processing, to discuss the opportunities and challenges of the individual subfields as well as potential overlap between these fields.

B. Focus Session on «Insulator Spintronics» Spring Meeting of the Condensed Matter Section of DPG, 04 April 2019

The Focus Session on «Insulator Spintronics» was organized by Matthias Althammer of WMI to discuss recent results from experimental and theoretical studies on spin currents, spin dynamics and spin textures in insulating magnetic materials. The Focus Session was addressing these fascinating topics within invited talks of leading international experts (Sebastian Diaz, Burkard Hillebrands, Niklas Rohling, Jing Liu, Timo Kuschel, Mathias Kläui).

Within the symposium, also two PhD students of WMI (Lukas Liensberger, Tobias Wimmer) were presenting their research on the hybridization of ferro- and antiferromagnetic magnon modes in GdIG and the all-electrical control of spin transport in a three-terminal yttrium iron garnet/platinum nanostructure, respectively.

C. PhD Workshop of Priority Program 1601 on «Insulator Spintronics» (06 – 08 May 2019, Munich Residence, Germany)

Stefan Weichselbaumer (WMI) co-organized the «Young Researchers Workshop» of the *DFG Priority Program 1601*. The workshop took place in the rooms of BAdW at the Munich Residence. About 25 young researchers working in projects of the priority program were invited to present and discuss their results among peers. Invited guests were Jens Anders (Stuttgart), Patrice Bertet (Paris) and Daniella Goldfarb (Rehovot).

D. Munich Conference on «Quantum Science and Technology» (08 – 09 July 2019, German Science Museum, Munich, Germany)

The *Munich Conference on Quantum Science and Technology* was hosted at the Center for New Technologies (ZNT) of the German Science Museum. The conference brought together MCQST members, selected international guests and industry representatives to exchange ideas and discuss advancements in the fields of quantum science and technology. The primary goal was to strengthen the MCQST network.

The event consisted of selected scientific talks on various topics, poster presentations, and a panel discussion with industry representatives from Google, Huawei, Microsoft, and NVision, all designed to explore the frontiers of quantum science and technology. Additionally, MCQST was teaming up with Microsoft to organise a Quantum Science Slam at the Microsoft Atrium, aiming to bring quantum science into focus of public in an entertaining way.

E. International Workshop on «Spin Waves and Interactions» (03 – 05 September 2019, Greifswald, Germany)

Hans Hübl (WMI) was one of the co-organizers of the *International Workshop on «Spin Waves and Interactions»*. The two-day workshop was supported by the Alfried Krupp Wissenschaftskolleg. Renowned speakers presented recent advancements in spin wave physics and provided insights into topical problems as well as technological paths for future applications.

F. Course 3 of the Ferienakademie: «Physics and Electronics in Everyday Life» (22 September – 04 October 2019, Sarntal, Italy)

As in the previous years, WMI co-organized the course on *«Physics and Electronics in Everyday Life»* of the ***Ferienakademie***. The Ferienakademie is jointly organized by the Technical University of Munich, the University of Erlangen-Nuremberg, and the University of Stuttgart to motivate and foster highly talented students. It takes place annually at Sarntal in the Italian Alps. The course was held by Rudolf Gross (WMI) together with Gert Denninger (University of Stuttgart), supported by Vojislav Krstic (University of Erlangen-Nuremberg) and Sebastian Loth (University of Stuttgart) as guest lecturers.

A relaxing and inspiring atmosphere at the Ferienakademie is provided by a varied supporting program (mountain hiking, excursions to Bozen, table tennis and chess tournament, Törgelen, etc.). Moreover, within the Ferienakademie the students have the opportunity to meet leaders from industry, politics and science. In 2019, an evening talk was presented by Prof. Dr. Günther Leugering, Vice President Research of the University of Erlangen-Nuremberg.

Within the course 3 on *«Physics and Electronics in Everyday Life»* of the Ferienakademie the students prepare presentations on physical phenomena and problems which play an important role in our everyday-life, but usually are poorly understood. Besides the seminar talks there are intensive discussions with the professors and members of other courses. A particular emphasis of course 3 of Ferienakademie is put on hands-on experiments. They aim at providing students an in-depth insight into physical phenomena by performing experiments by themselves. WMI contributes with a variety of experiments on superconductivity, magnetism and low temperature properties of solids. In 2019, the students were building GPS receivers. After the tedious soldering and assembling of the receivers, the students could test them during the mountain hikes. Taking data with three different GPS receivers they could compare the measurement precision of the devices.

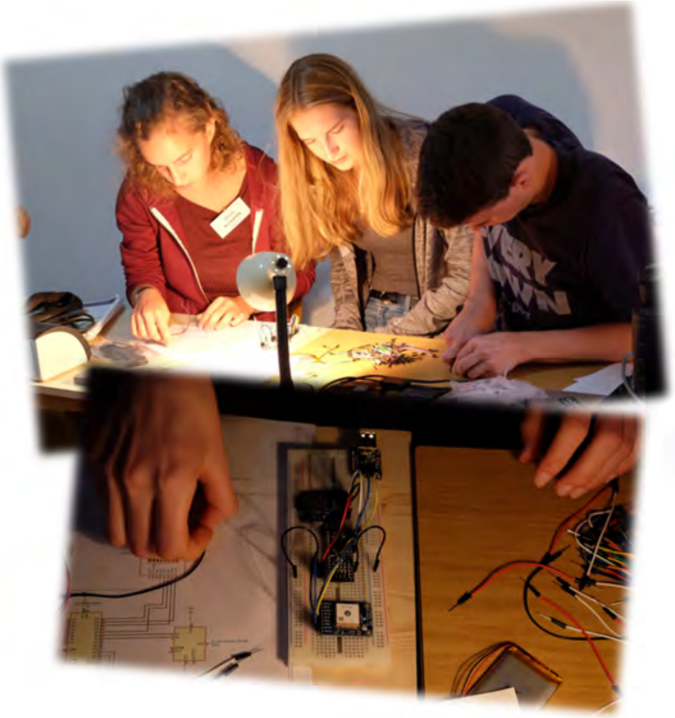

Students of course 3 working on the assembly of a GPS receiver.

G. Training Courses for Teachers

23 – 25 September 2019, Akademie für Lehrerfortbildung, Dillingen, Germany.
18 – 22 October 2019, DPG-Lehrerfortbildung, Bad Honnef, Germany.

Rudolf Gross and Frank Deppe provided lectures for training courses for physics teachers. Rudolf Gross was giving a tutorial lecture on the continuum description of solids within the teacher training program of the German Physical Society at Bad Honnef. Frank Deppe was providing an introduction into quantum computing within the Edgar–Lüscher Lectures at the Akademie für Lehrerfortbildung, Dillingen.

H. Guided Tours, Days of Open House, etc.

Wissenschaft als Show

OsterHASE bringt Vorträge und Show-Experimente ans Humboldt-Gymnasium Vaterstetten

Matthias Opel experimentierte mit flüssigem Stickstoff. Foto:se
Ebersberger & Grafinger Anzeiger, 24. April 2019

The WMI regularly participates in the Days of Open House on the Garching Research Campus. In 2019, we also contributed to the Day of Open House (May 4, 2019) of the Faculty of Physics of LMU, where the presentation of the new clusters of excellence was a key focus. Frank Deppe of WMI contributed with a talk on «*Quantencomputing und Quantenkommunikation mit supraleitenden Schaltkreisen*».

WMI also offers guided tours for school classes and other interested groups. For example, in 2019 Matthias Opel gave tours for the staff of the Leibniz Computing Center and a group of about 35 pupils of the gymnasium Fränkische Schweiz at Ebermannstadt.

Matthias Opel also visited the Humboldt-Gymnasium at Vaterstetten and presented some low temperature experiments there. His low temperature physics show found broad attention in the local press.

Cooperations

Other collaborations without direct project funding involve:

- Stanford University, Stanford, USA (T.P. Devereaux, I. Fisher, B. Moritz, H.N. Ruiz, S.A. Kivelson)
- Universidad del País Vasco and Ikerbasque Foundation, Bilbao, Spain (E. Solano, M. Sanz, L. Lamata)
- Instituto de Física Fundamental, CSIC, Madrid, Spain (J.J. Garcia-Ripoll)
- Instituto de Ciencia de Materials de Barcelona, CSIC, Spain (E. Canadell)
- Osaka Prefecture University, Osaka, Japan (H. Fujiwara)
- Green Innovation Research Laboratories, NEC Corporation, Japan (J.S. Tsai, K. Inomata, T. Yamamoto)
- University of Tohoku, Sendai, Japan (G.E.W. Bauer, E. Saitoh, J. Barker)
- Japan Science and Technology Agency, Sendai, Japan (H. Adachi, S. Maekawa)
- University of Tokyo, Tokyo, Japan (Y. Nakamura)
- European Synchrotron Radiation Facility (ESRF), Grenoble (H. Müller, F. Wilhelm, K. Ollefs, A. Rogalev)
- Lund University, Lund, Sweden (D. Mannix)
- Materials Science Research Centre, IIT Madras, India (M.S. Ramachandra Rao, J. Mukherjee, T.S. Suraj)
- ETH-Zurich, Switzerland (A. Wallraff, L. Degiorgi, R. Monnier, Dr. M. Lavagnini)
- University of Geneva, Geneva, Switzerland (I. Maggio-Aprile)
- Chalmers University of Technology Gothenburg, Sweden (P. Delsing, G. Wendin)
- University of Alabama, MINT Center, Tuscaloosa, USA (A. Gupta)
- Helsinki University of Technology, Materials Physics Laboratory, Finland (T. Heikkilä)
- Delft University of Technology, Kavli Institute of NanoScience, Delft, The Netherlands (T.M. Klapwijk, G.E.W. Bauer)
- B. Verkin Institute for Low Temperature Research and Engineering, Kharkov, Ukraine (V.G. Peschansky)
- Landau Institute for Theoretical Physics, Chernogolovka, Russia (P. Grigoriev)
- University of Oxford, Clarendon Laboratory, England (A. Karenowska)
- Institute of Solid State Physics, Chernogolovka, Russia (V. Zverev)
- Russian Academy of Sciences, Chernogolovka, Russia (N. Kushch, E. Yagubskii)
- High Magnetic Field Laboratory, Dresden (E. Kampert, J. Wosnitza, T. Helm)
- High-Magnetic-Field Laboratory, Grenoble, France (I. Sheikin, D. LeBoeuf)
- High Magnetic Field Laboratory, Toulouse, France (C. Proust, D. Vignolles)
- National High Magnetic Field Laboratory, Tallahassee, USA (J. Brooks)
- University of British Columbia, Vancouver, Canada (D. Bonn, A. Damascelli)
- Université de Toulouse, Laboratoire de Physique Théorique, Toulouse, France (R. Ramazashvili)
- Lawrence Berkeley National Laboratory, Berkeley, USA (A. F. Kemper)
- University of Belgrade, Belgrade, Serbia (Z. Popovic, N. Lazarevic, D. U. Ralevic, R. Gajic)
- University of Aveiro, Portugal (N. A. Sobolev)

- Macquarie University, MQ Research Centre for Quantum Science and Technology, Australia (J. Twamley)
- Hungarian Academy of Sciences, Research Institute for Solid State Physics and Optics, Budapest, Hungary (I. Tüttö)
- University of Rome "La Sapienza", Rome, Italy (S. Caprara, C. Di Castro, M. Grilli)
- Budapest University of Technology and Economics, Budapest, Hungary (A. Virosztek, G. Mihály)
- University of New South Wales, Sydney, Australia (M. Simmons, A. Morello, J. Pla)
- McMaster University, Hamilton, Canada (J.P. Carbotte)
- Technical University of Graz, Austria (E. Schachinger)
- University of Vienna, Austria (M. Aspelmeyer, S. Rotter)
- Johannes-Kepler University of Linz, Institute for Semiconductor and Solid State Physics, Austria (A. Ney)
- National Institute of Standards and Technology, Boulder, USA (H. Nembach, J. Shaw, T.J. Silva, E. Edwards)
- University of Florida, Gainesville, Florida, USA (P.J. Hirschfeld, S. Maiti)
- University of California, Santa Barbara, USA (D.J. Scalapino)
- University of Manitoba, Winnipeg, Canada (C.-M. Hu)
- Kyoto University, Japan (M. Shiraishi)
- Norwegian University of Science and Technology, Trondheim, Norway (A. Kamra)
- Universität Erlangen-Nürnberg (M. Hartmann, F. Marquardt)
- Universidad Nacional de Colombia, Colombia (O. Moran)
- University of Birmingham, UK (E.M. Forgan)
- University of Groningen, The Netherlands (T. Palstra, M. Mostovoy, A. Aqeel)
- IFW Dresden, Germany (B. Büchner, J. Fink, S.V. Borisenko, M. Knupfer, A. Thomas)
- Max-Planck-Institut für Festkörperforschung, Stuttgart (B. Keimer, L. Boeri)
- University of Tübingen, Germany (R. Kleiner, D. Kölle)
- University of Würzburg, Germany (W. Hanke, F. Assaad, C. Honerkamp, M. Potthoff, R. Thomale)
- University of Augsburg, Germany (P. Hänggi, A. Wixforth, A. Kampf, A. Loidl, J. Deisenhofer, V. Tsurkan)
- University of Hamburg, Germany (G. Meier, W. Wurth)
- University of Leipzig, Germany (J. Haase)
- University of Ulm, Abt. Halbleiterphysik, Germany (W. Limmer, M. Abdi)
- RWTH Aachen, Germany (G. Güntherodt, B. Beschoten)
- Ernst-Moritz-Arndt Universität Greifswald, Germany (M. Münzenberg)
- Martin-Luther-Universität Halle, Germany (G. Woltersdorf, G. Schmidt)
- Universität Bielefeld, Germany (G. Reiss, T. Kuschel M. Meinert)
- Free University of Berlin, Berlin, Germany (R. Di Candia)
- Technical University of Munich, Physics Department, Germany (Ch. Back, P. Böni, Ch. Pfleiderer, M. Poot, F.C. Simmel, P. Müller-Buschbaum)
- Technical University of Munich, Walter Schottky Institute, Germany (M. Stutzmann, J. Finley, M. Brandt, A. Holleitner)
- Technical University of Munich, Electrical Engineering (M. Becherer)

- LMU Munich, Physics Department, Germany (J. von Delft, E. Frey, J. Rädler, A. Högele)
- LMU Munich, Chemistry Department, Germany (H. Ebert, D. Ködderitzsch)
- University of Konstanz (A. Leitenstorfer, E. Weig, J. Demsar, A. Pashkin, W. Belzig)
- Jülich Centre for Neutron Science JCNS, Garching, Germany (S. Pütter)
- Goethe University, Frankfurt, Germany (S. Winter, M. Lang)
- Technical University of Braunschweig, Germany (D. Menzel, S. Süllow)
- Technical University of Dresden, Germany (S.T.B. Gönnenwein)
- Fritz Haber Institut Berlin, Germany (T. Seifert, T. Kampfrath)
- Technical University of Dortmund, Germany (M. Müller)
- Johannes-Gutenberg University, Mainz, Germany (C. Cramer, M. Kläui, O. Gomomay)
- Universität Potsdam, Potsdam, Germany (A.v. Reppert, M. Bargheer)
- Saarland University, Saarbrücken (F.K. Wilhelm-Mauch)
- Innovent Technologieentwicklung Jena, Germany (C. Dubs, O. Surzhenko)
- BMW Group, Munich, Germany (J. Schnagl, W. Stadlbauer, G. Steinhoff)
- Attocube, Munich, Germany (K. Karrai, D. Andres, E. Hoffmann)
- THEVA Dünnschichttechnik, Ismaning, Germany (W. Prusseit)

Stays abroad

Extended visits of members of the Walther-Meißner-Institute at foreign research laboratories:

1. **Stephan Geprägs**
   Diamond Light Source, Didcot, UK
   26. 02. - 02. 03. 2019
   20. 11. - 26. 11. 2019
2. **Stephan Geprägs**
   Institut Laue-Langevin, Grenoble, France
   21. 07. - 26. 07. 2019
   02. 09. - 06. 09. 2019
3. **Mark Kartsovnik**
   High Magnetic Field Laboratory, Grenoble, France
   21. 05. - 29. 05. 2019
4. **Mark Kartsovnik**
   Institute of Solid State Physics, Russian Academy of Science, Chernogolovka, Russia
   07. 07. - 17. 07. 2019
5. **Rudi Hackl**
   Institute of Physics Belgrade, Belgrade, Serbia
   03. 10. - 15. 10. 2019

Conference Talks and Seminar Lectures

Matthias Althammer

1. **All-electrical control of spin conductance in magnetically ordered insulators**
   Invited Talk, 686th WE Heraeus Seminar, Bad Honnef, Germany
   08. 01. 2019
2. **Spin transport in a charge current induced magnon Bose-Einstein condensate at room temperature**
   Invited Talk, Spin Caloritronics X Conference, Groningen, The Netherland
   20. 05. 2019
3. **Electrical control of spin transport in yttrium iron garnet thin films**
   Invited Talk, University of Göttingen, Göttingen, Germany
   24. 06. 2019
4. **Carge current control of angular momentum transport**
   Invited Talk, Technical University of Kaiserslautern, Kaiserslautern, Germany
   12. 08. 2019
5. **Spin transport in a magnetic insulator with charge current induced zero effective damping**
   Annual Conference on Magnetism and Magnetic Materials, Las Vegas, USA
   08. 11. 2019
6. **Electrical control of spin transport in jttrium iron garnet thin films**
   Invited Talk, University of Bielefeld, Bielefeld, Germany
   02. 12. 2019

Andreas Baum

1. **Interplay of lattice and electronic and spin degrees of freedom in de-twinned $BaFe_2As_2$: a Raman scattering study**
   Spring Meeting of the German Physical Society, Regensburg, Germany
   31. 03. - 05. 04. 2019
2. **Nematic fluctuations in iron-based systems**
   The 20th Symposium on Condensed Matter Physics SCMP, Belgrade, Serbia
   07. - 11. 10. 2019

Frank Deppe

1. **Introduction of Science Board Member WMI**
   Invited Talk, Kick-off Meeting of the EU Quantum Flagship Project, OpenSuperQ, Bad Honnef, Germany
   17. - 18. 01. 2019
2. **Quantencomputing und Quantenkommunikation mit supraleitenden Schaltkreisen**
   Invited Talk, Open House Day of the LMU Physics Faculty, Munich, Germany
   04. 05. 2019
3. **Secure remote state preparation of squeezed microwave states**
   Invited Talk, 20th Anniversary of Superconducting Qubits Conference, Tsukuba, Japan
   13. - 15. 05. 2019
4. **How to make (your own) somebody else´s quantum state**
   Invited Talk, Physikalisches Kolloquium, Universität Rostock, Rostock, Germany
   23. 05. 2019
5. **Quantum microwave: Secure communication, cryogenic LAN cables, and illumination**
   Invited Talk, Munich Conference on Quantum Science and Technology, Munich, Germany
   08. - 09. 07. 2019
6. **Quantencomputing**
   Invited Talk, High school teacher education, Akademie für Lehrerfortbildung, Dillingen, Germany
   23. - 25. 09. 2019
7. **Optimal control in a 3D compact quantum memory**
   Invited Talk, Quantum Simulation and Computation 2019 Conference, Madrid, Spain
   14. - 18. 10. 2019

8. **Towards frequency-degenerate quantum illumination with continuous variables**
   Invited Talk, The IQC Workshop on Quantum Illumination: From Theory to Practice, Waterloo, Canada
   02. - 03. 12. 2019

Andreas Erb

1. **Single crystal growth of various oxide materials for basic research and applications**
   Invited Talk, 3rd Floating zone technique workshop, Oriel College, University of Oxford, Oxford, UK
   18. 09. 2019

Kirill Fedorov

1. **Quantum discord in squeezed microwaves**
   Spring Meeting of the American Physical Society (APS), Boston, USA
   04. 03. 2019
2. **Quantum communication with squeezed microwaves**
   Invited Talk, Department of Physics, Saarland University, Saarbrücken, Germany
   27. 05. 2019
3. **Quantum discord in squeezed microwaves**
   Invited Talk, International Conference on Quantum Technologies, ICQT, Moscow, Russia
   18. 06. 2019
4. **Quantum discord in squeezed microwaves**
   DPG Fall Meeting, Freiburg, Germany
   26. 09. 2019
5. **Quantum communication with squeezed microwaves**
   Invited Talk, Physikalisches Institut, Karlsruhe Institute of Technology, Karlsruhe, Germany
   29. 10. 2019

Rudolf Gross

1. **Quantencomputing**
   Public Evening Lecture, Humboldt-Gymnasium Vaterstetten, Germany.
   13. 03. 2019
2. **Quantentechnologie – 100 Mio. Euro für Garching**
   Garchinger Gespräche zu Wissenschaft und Weltgeschehen, Bürgerhaus, Garching, Germany.
   10. 07. 2019
3. **Superconducting Quantum Circuits: Memories & Microwave Communication**
   Invited Tutorial, IMPRS-MPHQ Summer School, Bad Aibling, Germany
   22 – 27 July 2019
4. **Kontinuumsbeschreibung von Festkörpern**
   Invited Lecture, DPG-Lehrerfortbildung «Festkörperphysik», Bad Honnef, Germany.
   18 – 22 October 2019
5. **Engineering Quantum States with Superconducting Quantum Circuits**
   Invited Talk, The 20th Symposium on Condensed Matter Physics SCMP, Belgrade, Serbia
   07 – 11 October 2019
6. **Quantum Science, Technology, and Engineering @ Munich**
   Invited Talk, Bavarian Quantum Computing Exchange, Garching, Germany
   13. 11. 2019

Rudolf Hackl

1. **Orbital selective magnetism, nematicity, and fluctuations in FeSe**
   Invited Talk, Spring Meeting of the American Physical Society (APS), Boston, USA
   04. - 08. 03. 2019
2. **A light-scattering study of magnetism and gap excitations in pnictide and chalcogenide superconductors**
   Invited Talk, International Conference on Study of Matter at Extreme Conditions (SMEC 2019), Miami, Florida, USA
   31.03. - 06. 04. 2019

3. **Bardasis-Schrieffer modes as a probe of anisotropic Cooper pairing in iron-based superconductors**
   Colloquium in honor of Alfréd Zawadowski, Budapest, Hungary
   13. - 18. 06. 2019
4. **From weak-to strong-coupling magnetism in Fe-based compounds**
   Invited Talk, International Conference Superstripes 2019, Ischia, Italy
   24. - 29. 06. 2019

Hans Hübl

1. **Controlling magnons: transport properties & magnon-phonon hybridzation**
   Invited Talk, Physics Colloquium, University of Konstanz, Konstanz, Germany
   11. - 13. 02. 2019
2. **All-electrical control of spin transport in a three-terminal yttrium iron garnet/platinum nanotructures**
   Spring Meeting of the American Physical Society (APS), Boston, USA
   02. 03. - 09. 03. 2019
3. **Controlling magnons: transport properties & magnon-phonon hybridization**
   Invited Talk, Optomagnonics Conference, Cambridge, UK
   09. - 10. 09. 2019
4. **Controlling magnons: transport properties & magnon-phonon hybridization**
   Invited Talk, QuSpin-Center Trondheim, Trondheim, Norway
   25. - 26. 09. 2019
5. **Spin Photon Hybrids**
   Invited Talk, Colloquium on Quantum Technology, Technische Akademie Esslingen, Esslingen, Germany
   08. - 09. 10. 2019

Daniel Jost

1. **Evolution of Pairing Interactions in Fe-Based Superconductors**
   Spring Meeting of the American Physical Society (APS), Boston, USA
   04. 03. - 08. 03. 2019

Mark Kartsovnik

1. **Evolution of the electronic system near the Mott transition probed by magnetic quantum oscillations**
   Invited Talk, 3rd International Symposium on Novel States in Correlated Matter, Bad Neuenahr, Germany
   18. - 20. 03. 2019
2. **Electronic system of an organic superconductor near the Mott transition**
   Invited Talk, Seminar on Superconductivity dedicated to the 90th anniversary of Prof. Shchegolev, Institute of Solid State Physics, Chernogolovka, Russia
   16. 10. 2019
3. **Charge Carriers and Electronic Correlations Near the Mott Transition Probed by Magnetic Quantum Oscillations**
   13th International Symposium on Crystalline Organic Metals, Superconductors, Ferromagnets, ISCOM 2019, Tomar, Portugal
   22. - 27. 09. 2019

Lukas Liensberger

1. **Hybridization of Ferro- and Antiferromagnetic Magnon Modes in GdIG**
   Invited Talk, Focus Session on «Insulator Spintronics», Spring Meeting of the German Physical Society, Regensburg, Germany
   31. 03. - 05. 04. 2019

Matthias Opel

1. **Tiefe Temperaturen, Supraleitung und Spinelektronik**
   Invited Talk, MINT-Berufsinformationstag im Rahmen der "Humboldt Academy of Science and

Engineering”, Humboldt-Gymnasium Vaterstetten, Germany
12. 04. 2019

2. **Spin Hall magnetoresistance (SMR) in antiferromagnetic NiO/Pt bilayers**
   Joint European Magnetic Symposia, JEMS 2019, Uppsala, Sweden
   26. 08. 2019

Mathias Weiler

1. **Direct and inverse spin-orbit torques**
   Invited Talk, Ultrafast Spin Dynamics (TRR 227) Retreat, Berlin, Germany
   18. 11. 2019
2. **Hybrid magnon dynamics**
   Invited Talk, Sonderseminar, Technical University of Kaiserlautern, Kaiserslautern, Germany
   28. 08. 2019
3. **Helimagnon resonances in a natural magnonic crystal**
   Skyrmionics (SPP 2137) Retreat, Munich, Germany
   27. 02. 2019

Tobias Wimmer

1. **All-electrical control of spin transport in a three-terminal yttrium iron garnet/platinum nanostructure**
   Invited Talk, Focus Session on «Insulator Spintronics», Spring Meeting of the German Physical Society, Regensburg, Germany
   31. 03. - 05. 04. 2019

Honors and Awards

Most of our PhD and master students give several oral and poster presentations at national and international conferences over the year. We are very happy that they are regularly receiving awards for their presentations. Louis Flacke of WMI was particularly successful in this respect in 2019 by collecting four best poster awards.

IEEE MAGNETICS
VCU College of Engineering

IEEE Magnetics Society Summer School Poster Award

THIS ACKNOWLEDGES THAT

Luis Flacke

HAS BEEN RECOGNIZED FOR SECOND PLACE

JUNE 7, 2019

CHAIR, EDUCATION COMMITTEE
IEEE MAGNETICS SOCIETY

Certificate

Best Poster Prize for

Louis Flacke

Participant at the 686. WE-Heraeus-Seminar on

Spin Based Information Processing

January 7 - 9, 2019
at the Physikzentrum Bad Honnef (Germany)

Scientific Organization:
Dr. Ulrike Ritzmann, Uppsala University/SWE
PD Dr. Hans Hübl, Bayerische Akademie der Wissenschaften/GER
Prof. Evangelos Papaioannou, Technische Universität Kaiserslautern/GER

Bad Honnef, January 2019

Prof. Dr. J. Treusch Ursula Heraeus Prof. Dr. J. Mlynek

Board of Directors of the Wilhelm and Else Heraeus Foundation

The WE-Heraeus Foundation supports research and education in science, especially in physics. German physicists recognize it as the most important private funding institution in their fields.

WILHELM UND ELSE
HERAEUS-STIFTUNG

2019 Magnonics

Best Poster Award
1st place

is awarded to

Luis Flacke

Walther-Meißner-Institut, Garching Munich, Germany

for the poster entitled

Spin pumping and spin wave damping in low damping $Co_{25}Fe_{75}$ heterostructures

presented at the Conference Magnonics 2019
July 28th - August 1st, 2019 – Carovigno (BR), Italy

The Conference Chairs
Prof. Mario Carpentieri Dr. Gianluca Gubbiotti

URKUND

30. Edgar Lüscher Seminar 2019
Hotel Sport / Klosters Schweiz

2. Platz

„Microseminar“

Luis Flacke

Klosters, 05.02.2019

In winter semester 2018/19, Mathias Weiler of WMI received the ***Supervisory Award*** of the TUM Physics Department. This award was presented to him by the PhD students of the Faculty Graduate Center for his outstanding performance in advising PhD students.

Membership in Advisory Boards, Committees, etc.

1. **Frank Deppe** is Coordinator of the European Quantum Technology Flagship Project *Quantum Microwaves for Communication and Sensing (QMiCS)*.
2. **Frank Deppe** is associate member of the Cluster of Excellence *Nanosystems Initiative Munich (NIM)*.
3. **Frank Deppe** is member and principal investigator of the Cluster of Excellence *Munich Center for Quantum Science and Technology (MCQST)*.
4. **Andreas Erb** is spokesmen of the "Arbeitskreis Intermetallische und oxydische Systeme mit Spin- und Ladungskorrelationen" of the *Deutsche Gesellschaft für Kristallzüchtung und Kristallwachstum (DGKK)*.
5. **Rudolf Gross** is member of the Scientific Advisory Board of the Bayerisches Geoinstitut, Bayreuth, Germany.
6. **Rudolf Gross** is member of the Scientific Advisory Board of the Institut de Ciència de Materials de Barcelona, Spain.
7. **Rudolf Gross** is member of the Advisory Board of the permanent exhibition on *Matter and Light* of the German Science Museum.
8. **Rudolf Gross** is member of the committee for the allocation of Alexander von Humboldt Foundation Research Awards.
9. **Rudolf Gross** is member of the Appointment and Tenure Board of the Technical University of Munich.
10. **Rudolf Gross** is spokesperson (together with Immanuel Bloch and Ignacio Cirac) of the Cluster of Excellence *Munich Center for Quantum Science and Technology (MCQST)* and coordinator of the Research Unit C on *Quantum Computing*.
11. **Rudolf Gross** is member of the Executive Board of the Cluster of Excellence *Nanosystems Initiative Munich (NIM)* and coordinator of the Research Area 1 on *Quantum Nanosystems*.
12. **Rudolf Gross** is member of the *Munich Quantum Center (MQC)*.
13. **Rudolf Gross** is course leader at the Ferienakademie of the Universities Munich (TU), Stuttgart and Erlangen-Nürnberg since 2005.
14. **Rudolf Hackl** is member of the evaluation board of the neutron source Heinz Maier-Leibnitz (FRM II).
15. **Hans Hübl** is member and principal investigator of the Cluster of Excellence *Nanosystems Initiative Munich (NIM)*.
16. **Hans Hübl** is member and principal investigator of the Cluster of Excellence *Munich Center for Quantum Science and Technology (MCQST)*.
17. **Mark Kartsovnik** is member of the Selection Committee of EMFL (European Magnetic Field Laboratories).
18. **Mark Kartsovnik** is member of the International Advisory Committee of the 13th International Symposium on Crystalline Organic Metals Superconductors and Ferromagnets (ISCOM 2019).
19. **Matthias Opel** is one of the four elected members of the Speaker Council for the scien-

tists of the Bavarian Academy of Sciences and Humanities.

20. **Mathias Weiler** is member of the Editorial Review Board of IEEE Magnetics Letters.

Teaching

Lectures, Courses and other Teaching Activities

Several members of the Walther-Meißner-Institute give lectures and seminars at the Technical University of Munich.

Matthias Althammer

WS 2018/2019

- Magnetismus (Magnetism)
- Übungen zu Magnetismus (Magnetism, Problem Sessions)
- Seminar: Spin Caloritronics and Spin Pumping (with H. Hübl, M. Weiler)
- Seminar: Advances in Solid-State Physics (with R. Gross, H. Hübl, A. Marx, M. Opel, M. Weiler)
- Seminar: Topical Issues in Magneto- and Spin Electronics (with H. Hübl, M. S. Brandt, M. Weiler)

SS 2019

- Spin Elektronik (Spin Electronics)
- Übungen zu Spin Elektronik (Spin Electronics, Problem Sessions)
- Seminar: Spin Caloritronics and Spin Pumbing (with H. Hübl, M. Weiler)
- Seminar: Topical Issues in Magneto- and Spin Electronics (with M. Brandt, H. Hübl, M. Weiler)
- Seminar: Advances in Solid-State Physics (with R. Gross, H. Hübl, A. Marx, M. Opel, M. Weiler)

WS 2019/2020

- Seminar: Spin Currents and Skyrmionics (with H. Huebl, M. Weiler)
- Seminar: Advances in Solid-State Physics (with R. Gross, H. Hübl, A. Marx, M. Opel)
- Seminar: Topical Issues in Magneto- and Spin Electronics (with H. Hübl, M. S. Brandt, M. Weiler)

Frank Deppe

WS 2018/2019

- Seminar: Superconducting Quantum Circuits (with R. Gross, A. Marx, K. Fedorov)

SS 2019

- Seminar: Superconducting Quantum Circuits (with R. Gross, A. Marx, K. Fedorov)

WS 2019/2020

- Seminar: Superconducting Quantum Circuits (with R. Gross, A. Marx, K. Fedorov)

Dietrich Einzel

WS 2018/2019

- Mathematische Methoden der Physik I (Mathematical Methods of Physics I)
- Übungen zu Mathematische Methoden der Physik I (Mathematical Methods of Physics I, Problem Sessions)

SS 2019

- Mathematische Methoden der Physik II (Mathematical Methods of Physics II)
- Übungen zu Mathematische Methoden der Physik II (Mathematical Methods of Physics II, Problem Sessions)

WS 2019/2020

- Mathematische Methoden der Physik I (Mathematical Methods of Physics I)
- Übungen zu Mathematische Methoden der Physik I (Mathematical Methods of Physics I, Problem Sessions)

Kirill Fedorov

WS 2018/2019
- Seminar: Superconducting Quantum Circuits (with F. Deppe, R. Gross, A. Marx)

SS 2019
- Angewandte Supraleitung: Josephson Effekte, supraleitende Elektronik und supraleitende Quantenschaltkreise (Applied Superconductivity: Josephson Effects, Superconducting Electronics and Superconducting Quantum Circuits, with R. Gross)
- Seminar: Superconducting Quantum Circuits (with F. Deppe, R. Gross, A. Marx)

WS 2019/2020
- Seminar: Superconducting Quantum Circuits (with F. Deppe, R. Gross, A. Marx)

Rudolf Gross

WS 2018/2019
- Physik der Kondensierten Materie I (Condensed Matter Physics I)
- Übungen zu Physik der Kondensierten Materie I (Condensed Matter Physics I, Problem Sessions, with S. Geprägs)
- WMI Seminar on Modern Topics of Low Temperature Solid-State Physics (with M. Althammer, F. Deppe, K. Fedorov, R. Hackl, H. Hübl, A. Marx, M. Opel, M. Weiler)
- Seminar: Advances in Solid-State Physics (with H. Hübl, A. Marx, M. Opel)
- Seminar: Superconducting Quantum Circuits (with F. Deppe, K. Fedorov, A. Marx)
- Festkörperkolloquium (Colloquium on Solid-State Physics, with D. Einzel)

SS 2019
- Physik der Kondensierten Materie II (Condensed Matter Physics II)
- Übungen zu Physik der Kondensierten Materie II (Condensed Matter Physics II, Problem Sessions, with S. Geprägs)
- Seminar: Advances in Solid-State Physics (with H. Hübl, A. Marx, M. Opel)
- WMI Seminar on Modern Topics of Low Temperature Solid-State Physics (with M. Althammer, F. Deppe, K. Fedorov, R. Hackl, H. Hübl, A. Marx, M. Opel, M. Weiler)
- Seminar: Superconducting Quantum Circuits (with F. Deppe, K. Fedorov, A. Marx)
- Festkörperkolloquium (Colloquium on Solid-State Physics, with D. Einzel)
- Ferienakademie: Course 3 «Physics and Electronics in Everyday Life»

WS 2019/2020
- Physik der Kondensierten Materie I (Condensed Matter Physics I)
- Übungen zu Physik der Kondensierten Materie I (Condensed Matter Physics I, Problem Sessions, with S. Geprägs)
- WMI Seminar on Modern Topics of Low Temperature Solid-State Physics (with M. Althammer, F. Deppe, K. Fedorov, R. Hackl, H. Hübl, A. Marx, M. Opel, M. Weiler)
- Seminar: Advances in Solid-State Physics (with H. Hübl, A. Marx, M. Opel)
- Seminar: Superconducting Quantum Circuits (with F. Deppe, K. Fedorov, A. Marx)
- Festkörperkolloquium (Colloquium on Solid-State Physics, with D. Einzel)

Rudi Hackl

WS 2018/2019
- WMI Seminar on Current Topics of Low Temperature Solid-State Physics (with R. Gross, H. Hübl, A. Marx, M. Opel)
- Seminar: Advances in Solid-State Physics (with R. Gross, H. Hübl, A. Marx, M. Opel)

SS 2019

- WMI Seminar on Current Topics of Low Temperature Solid-State Physics (with R. Gross, H. Hübl, A. Marx, M. Opel)
- Seminar: Advances in Solid-State Physics (with R. Gross, H. Hübl, A. Marx, M. Opel)

WS 2019/2020

- Supraleitung und Tieftemperaturphysik I (Superconductivity and Low Temperature Physics I)
- Übungen zu Supraleitung und Tieftemperaturphysik I (Superconductivity and Low Temperature Physics I, Problem Sessions)
- Seminar: Advances in Solid-State Physics (with R. Gross, H. Hübl, A. Marx, M. Opel)
- WMI Seminar on Current Topics of Low Temperature Solid-State Physics (with R. Gross, H. Hübl, A. Marx, M. Opel)

Hans Hübl

WS 2018/2019

- Supraleitung und Tieftemperaturphysik I (Superconductivity and Low Temperature Physics I)
- Übungen zu Supraleitung und Tieftemperaturphysik I (Superconductivity and Low Temperature Physics I, Problem Sessions)
- Seminar: Spin Caloritronics and Spin Pumping (with M. Althammer, M. Weiler)
- Seminar: Advances in Solid-State Physics (with R. Gross, A. Marx, M. Opel)
- WMI Seminar on Current Topics of Low Temperature Solid State Physics (with R. Gross, R. Hackl, A. Marx, M. Opel)
- Seminar: Topical Issues in Magneto- and Spin Electronics (with M. S. Brandt, M. Althammer, M. Weiler, S. Geprägs)

SS 2019

- Supraleitung und Tieftemperaturphysik II (Superconductivity and Low Temperature Physics II)
- Übungen zu Supraleitung und Tieftemperaturphysik II (Superconductivity and Low Temperature Physics II, Problem Sessions)
- Seminar: Spin Currents and Skyrmionics (with M. Althammer, M. Weiler, M. Opel, S. Geprägs)
- Seminar: Advances in Solid-State Physics (with R. Gross, A. Marx, M. Opel)
- WMI Seminar on Current Topics of Low Temperature Solid State Physics (with R. Gross, R. Hackl, A. Marx, M. Opel)
- Seminar: Topical Issues in Magneto- and Spin Electronics (with M. S. Brandt, M. Althammer, M. Weiler, S. Geprägs)

WS 2019/2020

- Seminar: Spin Currents and Skyrmionics (with M. Althammer, M. Weiler, M. Opel, S. Geprägs)
- Seminar: Advances in Solid-State Physics (with R. Gross, A. Marx, M. Opel)
- WMI Seminar on Current Topics of Low Temperature Solid State Physics (with R. Gross, R. Hackl, A. Marx, M. Opel)
- Seminar: Topical Issues in Magneto- and Spin Electronics (with M. S. Brandt, M. Althammer, M. Weiler, S. Geprägs)

Mathias Weiler

WS 2018/2019

- Seminar: Spin Currents and Skyrmionics (with M. Althammer, H. Hübl)
- Seminar: Topical Issues in Magneto- and Spin Electronics (with M. Althammer, H. Hübl, M. S. Brandt)

SS 2019

- Seminar: Spin Currents and Skyrmionics (with M. Althammer, H. Huebl)
- Seminar: Topical Issues in Magneto- and Spin Electronics (with M. Althammer, H. Hübl, M. S. Brandt)

WS 2019/2020

- Magnetismus (Magnetism)
- Übungen zu Magnetismus (Magnetism, Problem Sessions)
- Seminar: Spin Currents and Skyrmionics (with M. Althammer, H. Hübl)
- Seminar: Topical Issues in Magneto- and Spin Electronics (with M. Althammer, H. Hübl, M. S. Brandt)

Seminars and Colloquia

A. Walther-Meißner-Seminar on Modern Topics in Low Temperature Physics WS 2018/2019, SS 2019 and WS 2019/2020

WS 2018/2019:

1. **Charakterisierung von DC-SQUIDs aus granularem Aluminium**
   Felix Friedrich, Physikalisches Institut Karlsruhe, Germany
   13. 11. 2018
2. **Tip-enhanced near-field optical spectroscopy**
   Dr. Kai Braun, Institut für Physikalische und Theoretische Chemie Tübingen, Germany
   07. 12. 2018
3. **Possible proximity effect in a nanoscale-size superconductor-semiconductor ring devices**
   Dr. Michael Stuiber, School of Physics, University of Melbourne, Australia
   14. 12. 2018
4. **Information Theory for Secret Sharing and Identification Problems**
   Prof. Dr. Gerhard Kramer, Dr. Christian Deppe, Roberto Ferrara, Technische Universität München, Lehrstuhl für Nachrichtentechnik, München, Germany
   09.01.2019
5. **Optical spectroscopy of localized excitons in monolayer WSe2 and its heterostructures**
   Janine Gückelhorn, Technische Universität München, Germany
   01. 02. 2019
6. **TmB4-a strongly anisotropic frustrated magnetic system**
   Dr. Karol Flachbart, Institute of Experimental Physics, Slovak Academy of Sciences, Kosice, Slovakia
   05. 02. 2019
7. **The Supermagnonics and Magnon BEC**
   Dr. Yury M. Bunkov, Institute Neel, CNRS, Grenoble, France
   01. 03. 2019
8. **Novel nonequilibrium dynamics in superconductors: Higgs modes and induced superconductivity**
   Dr. Nikolaj Bittner, Department of Physics, Universite de Fribourg, Switzerland
   08.03.2019
9. **A model study of strong correlations in Hund metals**
   Dr. Katharina Stadler, Ludwig-Maximilians-Universität München, Germany
   20. 03. 2019

SS 2019:

10. **Superconducting circuits in tunable environments**
    Dr. Jan Goetz, IQM, Espoo, Finland
    28. 06. 2019
11. **Telecom-Compatible Quantum Digital Signatures**
    Dr. Natalia Korolkova, University of St. Andrews, Scotland, UK
    04. 07. 2019
12. **Relieving YIG from its substrate constraints – YIG resonators on various crystalline substrate materials**
    Prof. Georg Schmidt, Martin-Luther-Universität, Halle-Wittenberg, Halle, Germany
    12. 07. 2019
13. **Large spin Hall conductivity in Pt and NiCu as measured with non contact microwave spectroscopy**
    Dr. Thomas J. Silva, Dr. Mark W. Keller, National Institute of Standards and Technology, Boulder, Colorado, USA
    16. 07. 2019

14. **Ferroelektrische Polymere für flexible Elektronik**
    Dr. Barbara Stadlober, Joanneum Research Forschungsgesellschaft mbH, Weiz, Austria
    26. 07. 2019
15. **Time crystals based on superconducting quantum circuits**
    Dr. Kirill Shulga, RIKEN Center for Emergent Matter Science, Wako, Saitama, Japan
    19. 09. 2019

WS 2019/2020:

16. **Transport Studies in Iridate-Manganite (SrIrO3/LaMnO3) heterostructures**
    T.S. Suraj, Indian Institute of Technology Madras, Chennai, India
    18. 10. 2019
17. **Theory of Higgs spectroscopy of superconductors in non-equilibrium**
    Prof. Dirk Manske, Max Planck Institute for Solid State Research, Stuttgart, Germany
    08. 11. 2019
18. **Strongly correlated spin charge dynamics govern the few-femtosecond magnetic response of ferromagnetic materials**
    Dr. Phoebe Tengdin, Laboratory for Ultrafast Microscopy and Electron Scattering, EPFL, Lausanne, Switzerland
    22. 11. 2019
19. **Superconducting triplet spintronics: why, how and what next**
    Dr. Sol H. Jacobson, Norwegian University of Science and Technology, Trondheim, Norway
    06. 12. 2019
20. **Investigating defects in superconducting qubits with strain and electric fields**
    Dr. Jürgen Lisenfeld, Institute of Technology, Karlsruhe, Germany
    13. 12. 2019

B. Topical Seminar on Advances in Solid State Physics WS 2018/2019, SS 2019 and WS 2019/2020

WS 2018/2019:

1. **Preliminary discussion and assignment of topics**
   R. Gross, Walther-Meißner-Institute (E23), Technical University of Munich and BAdW
   16. 10. 2018 and 23. 10. 2018
2. **Superconductivity at 215 K in lanthanum hydride at high pressures**
   Raffael Ferdigg, Technical University of Munich
   11. 12. 2018
3. **Tunable long-distance spin transport in a crystalline antiferromagnetic iron oxide**
   Thomas Narr, Technical University of Munich
   18. 12. 2018

SS 2019:

4. **Preliminary discussion and assignment of topics**
   R. Gross, Walther-Meißner-Institute (E23), Technical University of Munich and BAdW
   23. 04. 2019 and 30. 04. 2019
5. **Entanglement of bosonic modes through an engineered exchange interaction**
   Tammo Sievers, Technical University of Munich
   14. 05. 2019
6. **Continuous-wave room-temperature diamond maser**
   Niklas Glaser, Technical University of Munich
   21. 05. 2019
7. **The superconducting gravimeter**
   Dominik Kalke, Technical University of Munich
   28. 05. 2019

8. **Terahertz electrical writing speed in an antiferromagnetic memory**
   Andreas Nickl, Technical University of Munich
   04. 06. 2019
9. **Current polarity-dependent manipulation of antiferromagnetic domains**
   Dominik Maier, Technical University of Munich
   18. 06. 2019
10. **Anisotropic electronic and lattice properties in detwinned EuFe2As2**
    Ramona Stumberger, Walther-Meißner-Institute
    23. 07. 2019

WS 2019/2020:

11. **Preliminary discussion and assignment of topics**
    R. Gross, Walther-Meißner-Institute (E23), Technical University of Munich and BAdW
    15. 10. 2019 and 22. 10. 2019
12. **Spin colossal magnetoresistance in an antiferromagnetic insulator**
    Pham Thai Phi-Long, Technical University of Munich
    26. 11. 2019
13. **Superconducting cables for quantum microwave communication**
    Meike Pfeiffer, Technical University of Munich
    03. 12. 2019
14. **Magnetic skyrmion field effect transistors**
    Alexander Jung, Technical University of Munich
    10. 12. 2019
15. **Observation of anisotropic magneto-Peltier effect in nickel**
    Elisabeth Meidinger, Technical University of Munich
    17. 12. 2019
16. **Gated Conditional Displacement Readout of Superconducting Qubits**
    Kexun Luo, Technical University of Munich
    14. 01. 2020

C. Topical Seminar: Spin current and Skyrmionics WS 2018/2019, SS 2019 and WS 2019/2020

WS 2018/2019:

1. **Preliminary discussion and assignment of topics**
   M. Weiler, M. Althammer, S. Geprägs, H. Hübl, Walther-Meißner-Institute (E23), Technical University of Munich and BAdW
   18. 10. 2018 and 25. 10. 2018
2. **Ultra enhanced spin transport in YIG**
   Tobias Wimmer, Walther-Meißner-Institute
   22. 11. 2018
3. **Controlling the magnon transport in YIG**
   Nynke Vlietstra, Walther-Meißner-Institute
   06. 12. 2018
4. **Low damping in a metallic ferromagnet**
   Luis Flacke, Walther-Meißner-Institute
   13. 12. 2018
5. **Spin pumping in superconductor/ferromagnet hybrids**
   Manuell Müller, Walther-Meißner-Institute, Technical University of Munich
   24. 01. 2019
6. **NbN superconducting resonators**
   Andreas Faltermeier, Walther-Meißner-Institute, Technical University of Munich
   31. 01. 2019

7. **Mode hybridization in GdIG**
   Lukas Liensberger, Walther-Meißner-Institute
   07. 02. 2019

SS 2019:

8. **Preliminary discussion and assignment of topics**
   M. Weiler, M. Althammer, S. Geprägs, H. Hübl, Walther-Meißner-Institute (E23), Technical University of Munich and BAdW
   25. 04. 2019 and 02. 05. 2019
9. **High frequency spintronic devices**
   Anastasia Golovin, Walther-Meißner-Institute, Technical University of Munich
   16. 05. 2019
10. **Spinwave propagation in metallic wedges**
    Leonhard Hölscher, Walther-Meißner-Institute, Technical University of Munich
    23. 05. 2019
11. **Ferrimagnet/metal multilayers**
    Philipp Schwenke, Walther-Meißner-Institute, Technical University of Munich
    06. 06. 2019
12. **Optical detection of acoustically driven magnetic resonance**
    Adrian Gomez, Walther-Meißner-Institute, Technical University of Munich
    11. 07. 2019
13. **Magnetic properties of Iridates**
    Monika Scheufele, Walther-Meißner-Institute, Technical University of Munich
    18. 07. 2019
14. **From Kinetic Instability to Bose-Einstein Condensation and Magnon Supercurrents**
    Niklas von Minckwitz, Walther-Meißner-Institute, Technical University of Munich
    25. 07. 2019

WS 2019/2020:

15. **Preliminary discussion and assignment of topics**
    M. Weiler, M. Althammer, S. Geprägs, H. Hübl, Walther-Meißner-Institute (E23), Technical University of Munich and BAdW
    17. 10. 2019 and 24. 10. 2019
16. **Spin orbit torque**
    Mathias Weiler, Walther-Meißner-Institute
    14. 11. 2019
17. **Magnetization dynamics in magnetic bilayers**
    Carolina Lüthi, Walther-Meißner-Institute, Technical University of Munich
    21. 11. 2019
18. **Revealing the origin of the spin Seebeck effect**
    Maxim Dietlein, Walther-Meißner-Institute, Technical University of Munich
    28. 11. 2019
19. **Magnon transport in magnetic insulators**
    Janine Gückelhorn, Walther-Meißner-Institute
    05. 12. 2019
20. **Modulation of magnon spin transport in a magnetic gate transistor**
    Matthias Grammer, Technical University of Munich
    12. 12. 2019
21. **Magnetization dynamics in metallic heterostructures**
    Manuel Müller, Walther-Meißner-Institute, Technical University of Munich
    16. 01. 2020
22. **Nonlinear response in magnetization dynamics**
    Tobias Wimmer, Walther-Meißner-Institute

23. 01. 2020

23. **Magnetic multilayers**
Luis Flacke, Walther-Meißner-Institute
30. 01. 2020

D. Topical Seminar on Superconducting Quantum Circuits WS 2018/2019, SS 2019 and WS 2019/2020

WS 2018/2019:

1. **Preliminary discussion and assignment of topics**
F. Deppe, A. Marx, R. Gross, Walther-Meißner-Institute (E23), Technical University of Munich and BAdW
16. 10. 2018 and 23. 10. 2018
2. **Superradiant emission of color centers in diamond**
Stefan Weichselbaumer, Walther-Meißner-Institute
13. 11. 2018
3. **Programmable interference between two microwave quantum memories**
Edwar Xie, Walther-Meißner-Institute
27. 11. 2018
4. **Control of two non-linear resonators**
Stefanie Grotowski, Walther-Meißner-Institute, Technical University of Munich
04. 12. 2018
5. **Universal Stabilization of a Parametrically Coupled Qubit**
Saibin Zhou, Technical University of Munich
11. 12. 2018
6. **Deterministic quantum state transfer and remote**
Yu Zhu, Technical University of Munich
18. 12. 2018
7. **Programmable interference between two microwave quantum memories**
Jakov Kholodkov, Technical University of Munich
08. 01. 2019
8. **Strong Coupling Cavity QED with Gate-Defined Double Quantum Dots Enabled by a High Impedance Resonator**
Patrick Schnierle, Technical University of Munich
15. 01. 2019
9. **Cavity quantum acoustic device in the multimode strong coupling regime**
Philip Schmidt, Walther-Meißner-Institute
22. 01. 2019
10. **Stroboscopic Qubit Measurements with Squeezed Illumination**
Stefan Pogorzalek, Walther-Meißner-Institute
29. 01. 2019
11. **On-demand quantum state transfer and entanglement between remote microwave cavity memories**
Michael Renger, Walther-Meißner-Institute
05. 02. 2019

SS 2019:

12. **Preliminary discussion and assignment of topics**
F. Deppe, A. Marx, R. Gross, Walther-Meißner-Institute (E23), Technical University of Munich and BAdW
23. 04. 2019 and 30. 04. 2019
13. **From Ginzburg Landau to superconducting qubits**
Alfonso Lamelas, Technical University of Munich

07. 05. 2019

14. **Deterministic bidirectional communication and remote entanglement generation between superconducting qubits**
Stefan Pogorzalek, Walther-Meißner-Institute
14. 05. 2019
15. **Measurement of a superconducting qubit with a microwave photon counter**
Qiming Chen, Walther-Meißner-Institute
21. 05. 2019
16. **Travelling wave parametric amplifiers**
Daniel Singh, Walther-Meißner-Institute, Technical University of Munich
04. 06. 2019
17. **FPGA based reconstruction of quantum microwave signals**
Robert Neagu, Walther-Meißner-Institute, Technical University of Munich
18. 06. 2019
18. **Carbon Nanotube Millikelvin Transport and Nanomechanics**
Daniel Schwienbacher, Walther-Meißner-Institute
25. 06. 2019
19. **An entanglement-based wavelength-multiplexed quantum communication network**
Michael Renger, Walther-Meißner-Institute
02. 07. 2019
20. **Strong spin-photon coupling in silicon**
Stefan Weichselbaumer, Walther-Meißner-Institute
09. 07. 2019
21. **Phonon-Number-Sensitive Electromechanics**
Philip Schmidt, Walther-Meißner-Institute
16. 07. 2019

WS 2019/2020:

22. **Preliminary discussion and assignment of topics**
F. Deppe, A. Marx, R. Gross, Walther-Meißner-Institute (E23), Technical University of Munich and BAdW
15. 10. 2019 and 22. 10. 2019
23. **To catch and reverse a quantum jump mid-flight**
Qiming Chen, Walther-Meißner-Institute
29. 10. 2019
24. **Midterm report: Optimal control of 3D quantum memory**
Stefan Trattnig, Walther-Meißner-Institute, Technical University of Munich
05. 11. 2019
25. **Stabilizing Rabi oscillations in a superconducting qubit using quantum feedback**
Yuki Nojiri, Walther-Meißner-Institute
12. 11. 2019
26. **Phonon-mediated quantum state transfer and remote qubit entanglement**
Gerhard Huber, Technical University of Munich
19. 11. 2019
27. **High-Efficiency Measurement of an Artificial Atom Embedded in a Parametric Amplifier**
Tammo Sievers, Technical University of Munich
26. 11. 2019
28. **Coupling microwave photons to a mechanical resonator using quantum interference**
Philip Schmidt, Walther-Meißner-Institute
03. 12. 2019
29. **Violating Bell´s inequality with remotely connected superconducting qubits**
Michael Renger, Walther-Meißner-Institute
14. 01. 2020

30. **Multiphonon interactions between nitrogen-vacancy centers and nanomechanical resonators**
    Daniel Schwienbacher, Walther-Meißner-Institute
    28. 01. 2020
31. **Solid-state electron spin lifetime limited by phononic vacuum modes**
    Stefan Weichselbaumer, Walther-Meißner-Institute
    04. 02. 2020

E. Solid State Colloquium

The WMI has organized the Solid-State Colloquium of the Faculty of Physics in WS 2018/2019, SS 2019, and WS 2019/2020. The detailed program can be found on the WMI webpage: `http://www.wmi.badw-muenchen.de/teaching/Seminars/fkkoll.html`.

Staff

Staff of the Walther-Meißner-Institute

Director
Prof. Dr. Rudolf Gross

Deputy Director
Priv.-Doz. Dr. habil. Hans Hübl

Technical Director
Dr. Achim Marx

The deputy director, the technical director and the elected representative of the scientific staff (Dr. Matthias Opel) are members of the WMI Executive Committee and support the director in the management of WMI.

Administration/Secretary's Office
Emel Dönertas
Andrea Hamitaga
Carola Siegmayer
Martina Meven

Scientific Staff
Dr. Matthias Althammer
Dr. Andreas Baum
Priv.-Doz. Dr. habil. Frank Deppe
Prof. Dr. Andreas Erb
Dr. Kirill Fedorov
Dr. Stephan Geprägs
Priv.-Doz. Dr. habil. Rudolf Hackl
Dr. Mark Kartsovnik
Dr. Matthias Opel
Dr. Matti Partanen
Dr. Mathias Weiler
M. Sc. Qiming Chen
M. Sc. Luis Flacke
M. Sc. Janine Gückelhorn
M. Sc. Daniel Jost
M. Sc. Lukas Liensberger
M. Sc. Thomas Luschmann
M. Sc. Yuki Nojiri
M. Sc. Stefan Pogorzalek
M. Sc. Gabriele Rager
M. Sc. Michael Renger
M. Sc. Philip Schmidt
M. Sc. Daniel Schwienbacher
M. Sc. Stefan Weichselbaumer
M. Sc. Tobias Wimmer

Technical Staff
Peter Binkert
Thomas Brenninger, M.Sc.
Mario Nodes
Christian Reichlmeier
Alexander Rössl
Andreas Russo
Harald Schwaiger
Jan Naundorf
Georg Nitschke
Dieter Guratzsch
Astrid Habel
Dipl.-Ing. (FH) Josef Höss
Sebastian Kammerer

Assistants
Sybilla Plöderl
Maria Botta

Permanent Guests
Dr. Werner Biberacher
Prof. Dr. Dietrich Einzel
Prof. Dr. B.S. Chandrasekhar
Dr. Kurt Uhlig

y

Guest Researchers

1. Dr. Werner Biberacher
   permanent guest
2. Prof. Dr. B.S. Chandrasekhar
   permanent guest
3. Prof. Dr. Dietrich Einzel
   permanent guest
4. Prof. Dr. Anton Lerf
   permanent guest
5. Dr. Kurt Uhlig
   permanent guest
6. Prof. Karol Flachbart, Slovak Academy of Science, Kosice, Slovakia
   04. 02. - 08. 02. 2019
7. Dr. Akashdeep Kamra, Institutt for Fysikk, Norwegian University of Science and Technology, Trondheim, Norway
   05. 04. - 13. 04. 2019
8. Dr. Nedad Lazarevic, Institute of Physics, University of Belgrade, Belgrade, Serbia
   03. 05. - 18. 05. 2019
   24. 07. - 12. 08. 2019
9. Jasmina Lazarevic, Institute of Physics, University of Belgrade, Belgrade, Serbia
   24. 07. - 12. 08. 2019
10. Sanja Djurdjic-Mijin, Institute of Physics, University of Belgrade, Belgrade, Serbia
    27. 07. - 13. 08. 2019
11. Ei Shigematsu, Department of Electronic Science and Engineering, Kyoto University, Kyoto, Japan
    13. 05. - 25. 05. 2019
12. Prof. Dr. I. Tüttö, Hungarian Academy of Sciences, Budapest, Hungary
    14. 05. - 26. 05. 2019
13. Dr. Brain Moritz, Stanford Institute of Materials and Energy Science (SIMES), Stanford University, Stanford, USA
    06. 06. - 14. 06. 2019
14. Prof. Zoran Popovic, Institute of Physics, University of Belgrade, Belgrade, Serbia
    10. 07. - 25. 07. 2019
15. Dr. Kirill Shulga, RIKEN Center for Emergent Matter Science, Wako, Saitama, Japan
    18. 09. - 21. 09. 2019
16. T. S. Suraj, Materials Science Research Centre, IIT Madras, Chennai, India
    10. 10. - 10. 12. 2019

Scientific Advisory Board & Executive Committee

Scientific Advisory Board

According to the statutes of the Bavarian Academy of Sciences and Humanities (BAdW) the Scientific Advisory Board evaluates the quality of the scientific work of Walther-Meißner-Institute (WMI) and gives advice to its Executive Committee to provide scientific quality assurance. The Scientific Advisory Board regularly reports to the Research Committee of BAdW.

The members of the Scientific Advisory Board include members of BAdW with appropriate scientific background, representatives of the two Munich universities (TUM and LMU), as well as leading national and international scientists. They are appointed by the Section III "Naturwissenschaften, Mathematik, Technikwissenschaften" of BAdW for five years. The director of WMI is a consultive member of the WMI Scientific Advisory Board. The Scientific Advisory Board is headed by a chairperson and deputy chairperson. They are elected by the Section III "Naturwissenschaften, Mathematik, Technikwissenschaften" of BAdW for five years at the suggestion of the members of the WMI Scientific Advisory Board. The chairperson of the Scientific Advisory Board must be a member of BAdW.

The present members of the WMI Scientific Advisory Board are:

- **Vollhardt, Dieter**, chairman (BAdW, University of Augsburg)
- **Abstreiter, Gerhard**, deputy chairman (BAdW, Technical University of Munich)

- **Bloch, Immanuel** (BAdW, LMU Munich and Max-Planck-Institute of Quantum Optics)
- **Bühler-Paschen, Silke** (Technical University of Vienna)
- **Finley, Jonathan** (Technical University of Munich)
- **Gross, Rudolf**, consultive member (BAdW, Technical University of Munich)
- **Hänsch, Theodor** (BAdW, LMU Munich and Max-Planck-Institute of Quantum Optics)
- **Wallraff, Andreas** (ETH Zurich)
- **Weiss, Dieter** (University of Regensburg)
- **Zinth, Wolfgang** (BAdW, LMU Munich)

Executive Committee

The Walther-Meißner-Institute is headed by the scientific director who is responsible for the development and implementation of the research program. He holds a full professor position at one of the Munich universities (TUM or LMU). He is appointed in a joint process of the respective university and BAdW. The director is supported by the deputy director, the technical director and an elected representative of the scientific staff. They are appointed by the Section III "Naturwissenschaften, Mathematik, Technikwissenschaften" of BAdW for five years at the suggestion of the members of the WMI Scientific Advisory Board.

The present members of the WMI Executive Committee are:

- **Gross, Rudolf**, director
- **Hübl, Hans**, deputy director
- **Marx, Achim**, technical director
- **Opel, Matthias**, representative of the scientific staff

Contact:

Walther–Meißner–Institut
Bayerische Akademie der Wissenschaften
Walther–Meißner–Str. 8
D - 85748 Garching
GERMANY

Phone: +49 – (0)89 289 14201
Fax: +49 – (0)89 289 14206
E–mail: Sekretariat@wmi.badw.de

www.wmi.badw.de

Published by:

Walther–Meißner–Institut
Walther–Meißner–Str. 8, D - 85748 Garching
December 2019